



**Politecnico
di Torino**



Politecnico di Torino

MSs in Energy and Nuclear Engineering

Sustainable Nuclear Energy

**Analysis of branching
zero-variance Monte Carlo games
for radiation shielding problems**

Candidate:

Francesco Rossi

Supervisors:

Prof. Sandra Dulla,
Drs. Alexis Jinaphanh,
Davide Mancusi
and Andrea Zoia

Academic Year 2023/24

Abstract

Within the framework of the Monte Carlo variance-reduction techniques lie the so called "zero variance" techniques which, using the solution of the adjoint equation, provide estimates of the sought physical quantities with no error. These techniques are of considerable relevance when the event to be estimated is rare, like in most of the radiation shielding problems. Among this family of methods it is possible to distinguish the "branchless" and "branching" methods based on how the multiplicative phenomena are treated. This work will analyze a set of zero variance branching methods and will compare them with other methods in order to assess their robustness and efficiency.

Contents

1	Introduction	9
2	Background and Theory	11
2.1	Notations	11
2.1.1	Phase space	11
2.1.2	Cross sections	11
2.1.3	Fission and scattering spectra	12
2.2	The Boltzmann's transport equation	12
2.2.1	Neutron flux	12
2.2.2	The Boltzmann equation	13
2.3	Deterministic and stochastic approach	14
2.3.1	Monte Carlo approach	14
3	Zero Variance Monte Carlo	19
3.1	Additional definitions	19
3.1.1	Source, flight and collision kernels	19
3.1.2	Densities	20
3.1.3	Scoring in Monte Carlo games	20
3.2	Type of games	21
3.2.1	Analog	21
3.2.2	Implicit capture	21
3.2.3	Russian roulette	22
3.2.4	Weight windows	23
3.2.5	Exponential transform	23
3.2.6	Forced fission	24
3.3	Zero-variance games	26
3.4	Derivation of the zero-variance games	27
3.4.1	From an analog game	27
3.4.2	From an implicit capture game	30
3.4.3	From a forced fission game	32
3.4.4	On the final variance	32
4	The MGMC code	33
4.1	General description	33
4.2	Population and weighted population tallies	33
4.3	Additions to the input files	34
5	Simulations and results	37
5.1	Case A	37
5.1.1	Analytical results	38
5.1.2	Analog and branchless zero variance	41
5.1.3	Branching zero variance: analog game	44

5.1.4	Branching zero variance: implicit capture game	53
5.1.5	Branching zero variance: forced fission game	57
5.2	Case B	61
5.2.1	Analytical results	61
5.2.2	Analog and branchless zero variance	63
5.2.3	Branching zero variance: analog game	67
5.2.4	Branching zero variance: forced fission game	70
5.3	FOM comparison	73
6	Conclusions	75
A	Analog games derivation of the moments	77
B	Implicit capture games derivation of the moments	81
C	Forced fission games derivation of the moments	87

List of Figures

2.1	Example of the considered packet of neutrons [5]	13
2.2	S-2 model example: after a collision the new direction can only be either "positive" or "negative".	14
3.1	Scheme of an analog game	21
3.2	Scheme of an implicit capture	22
3.3	Scheme of the weight window procedure	23
3.4	Scheme of the exponential transform technique	24
3.5	Scheme of a forced fission game	25
4.1	Routine followed by MGMC with focus on the branching collisions	35
5.1	Case A geometry: the fissile Medium 1, the absorbing Medium 2, as well as the source and the detector are highlighted	37
5.2	Case A: Analytical scalar flux	40
5.3	Case A: Analytical scalar importance	40
5.4	Case A1: scalar neutron flux comparison	43
5.5	Case A1: scalar neutron flux relative variance comparison	43
5.6	Case A1: Student t-test of the scalar neutron flux comparison	44
5.7	Case A1: weighted population evolution comparison	44
5.8	Case A2: scalar neutron flux comparison	45
5.9	Case A2: scalar neutron flux relative variance comparison	45
5.10	Case A2: Student t-test of the scalar neutron flux comparison	46
5.11	Case A2: weighted population evolution comparison	46
5.12	Case A2: simulation times for the branching zero variance and branchless zero variance simulations	49
5.13	Case A2: evolution of the population for the branching zero-variance and branchless zero-variance simulations	49
5.14	Case A2: three-dimensional plot of the maximum value of the population (on the z-axis) with respect to $\Sigma_{f,1}$ (x-axis) and the weight cutoff (y-axis). The red crosses are the numerical datas while the colored surface is obtained interpolating between these datas.	50
5.15	Case A3: q_n generated with a Poisson probability density function	51
5.16	Case A3: comparison of the $\hat{c}_n(P)$ for different fission children probability density functions ($\Sigma_{f,1} = 0.15, \nu_f = 2.25$) in the two direction of flight	51
5.17	Case A3: average number of outgoing particles from the biased collision for different fission children probability density function ($\Sigma_{f,1} = 0.15, \nu_f = 2.25$) in the two direction of flight	52
5.18	Case A3: simulation times for different fission children probability density function ($\Sigma_{f,1} = 0.15, \nu_f = 2.25$)	53
5.19	Case A4: scalar neutron flux comparison	53
5.20	Case A4: scalar neutron flux relative variance comparison	54

5.21	Case A4: Student t-test of the scalar neutron flux comparison	54
5.22	Case A4: weighted population evolution comparison	54
5.23	Case A5: scalar neutron flux comparison	57
5.24	Case A5: scalar neutron flux relative variance comparison	57
5.25	Case A5: Student t-test of the scalar neutron flux comparison	58
5.26	Case A5: weighted population evolution comparison	58
5.27	Case A5: maximum of the population comparison (some values were extrapolated)	58
5.28	Case A5: simulation times comparison (some values were extrapolated)	59
5.29	Case B geometry: the fissile Medium 1, the absorbing Medium 2, as well as the source and the detector are highlighted	61
5.30	Case B: Analytical scalar flux	62
5.31	Case B: Analytical scalar importance	63
5.32	Case B1: scalar neutron flux comparison	64
5.33	Case B1: scalar neutron flux relative variance comparison	64
5.34	Case B1: Student t-test of the scalar neutron flux comparison	65
5.35	Case B1: weighted population evolution comparison	65
5.36	Case B2: scalar neutron flux comparison	67
5.37	Case B2: scalar neutron flux relative variance comparison	67
5.38	Case B2: Student t-test of the scalar neutron flux comparison	68
5.39	Case B2: weighted population evolution comparison	68
5.40	Case B3: scalar neutron flux relative variance comparison	70
5.41	Case B3: Student t-test of the scalar neutron flux comparison	70
5.42	Case B3: maximum of the population comparison	71
5.43	Case B3: simulation time comparison	71
5.44	FOM comparison for Case A	73
5.45	FOM comparison for Case B	73

List of Tables

5.1	Case A physical parameters	41
5.2	Case A k_{eff} of the system in the different simulations	41
5.3	Case A1: Detector error and Student t-test of the detector response for the zero variance branchless simulations. In red are highlighted the first run in which the test fails and eventually some extra runs.	42
5.4	2-bins branching scheme fission children probabilities	45
5.5	Case A2: Detector error and Student t-test of the detector response for the zero variance branching simulations. In red are highlighted the first run in which the test fails and eventually some extra runs.	47
5.6	3-bins-low branching scheme fission children probabilities	50
5.7	3-bins-high branching scheme fission children probabilities	50
5.8	Case A3: Detector error and Student t-test of the detector response for the zero variance branching simulations with different fission children probability density functions	52
5.9	Case A4: Detector error and Student t-test of the detector response for the implicit capture zero variance branching simulations. In red are highlighted the first run in which the test fails and eventually some extra runs.	56
5.10	Case A5: Detector error and Student t-test of the detector response for the forced fission zero variance branching simulations. In red are highlighted the first run in which the test fails and eventually some extra runs.	60
5.11	Case B physical parameters	63
5.12	Case B k_{eff} of the system in the different simulations	63
5.13	Case B1: Detector error and Student t-test of the detector response for the zero variance branchless simulations. In red are highlighted the first run in which the test fails and eventually some extra runs.	66
5.14	Case B2: Detector error and Student t-test of the detector response for the zero variance branching analog simulations. In red are highlighted the first run in which the test fails and eventually some extra runs.	69
5.15	Case B3: Detector error and Student t-test of the detector response for the zero variance branching forced fission simulations. In red are highlighted the first run in which the test fails and eventually some extra runs.	72

Chapter 1

Introduction

It is widely known that Monte Carlo simulations applied to the Boltzmann equation represent the *golden standard* in neutronics and particle transport calculations. By applying a Monte Carlo approach to the Boltzmann equations, in fact, it is possible to sample a given number of particle histories, each of which represents contribution to the sought phenomena to be analyzed. Nevertheless, although they are usually preferred to the deterministic codes because of their capability to avoid the discretization of the phase space, Monte Carlo methods are affected by statistical uncertainty, by construction. To reduce this statistical uncertainty the most straightforward way is to increase the number of simulated particles histories: thanks to the well-known *Central Limit Theorem*, the statistical error will decrease with the increasing number of particles as $1/\sqrt{N}$. This approach makes the Monte Carlo simulations rather long, since to reach satisfactory results N tends to be very large. Especially for problems where the sought estimate is related to a *rare event*, the number of needed histories can become quite burdening. The term rare event is used to indicate a statistical event that has very small probability of occurrence, like the response of a detector placed behind a radiation shield: the number of neutrons that can pass through the shield and reach the detector is so small that the estimate of the detector response will be characterized by a considerable statistical uncertainty.

One way to solve this problem is the implementation of variance reduction techniques. These techniques are able to bias the sampling procedure of the Monte Carlo game in such a way that the variance will be lower with respect to the original game. Then, in order to obtain the same final score (connected to the first order moment) of the simulation, appropriate correction are used. In fact, since the sampling has been biased toward some target result, it is necessary to adjust the particle contribution to the average. In variance reduction Monte Carlo every particle is characterized by a weight that can be decreased or increased depending on the implemented biasing scheme. The number of such biasing techniques is extremely large, and the choice of a specific method is typically imposed by the specific problem at hand.

Among the different types of variance reduction techniques there are two different families called the *branchless* and *branching* techniques: the main difference lies in how these two families of schemes tackle the multiplicative phenomena that may happen. As the name suggests the *branching* schemes allow for branching particle histories, so from a single particle multiple particles can be born and new histories will start. On the other hand the *branchless* schemes follow a sort of *1-in-1-out* kind of approach and do not allow the creation of new branches. The statistical weight of the outgoing particle is adjusted accordingly.

An ideal class of variance-reduction techniques is at the center of this work and allows providing estimates with zero statistical error. Such *zero variance* schemes were investigated by Lux and Koblinger [1], by Hoogenboom [2], by Booth [3] in their respective works. As shown in the following, zero-variance Monte Carlo games require the knowledge of the solution of the adjoint equation, the importance function χ^\dagger . In other words to get to the solution with zero error it is needed to know the exact solution beforehand. This may appear as massive drawback to the practical use of these schemes in real life application. Nevertheless, they provide the theoretical foundations to guide effective importance-sampling schemes such as the Consistent Adjoint-Driven Importance Sampling (CADIS) strategy, which is nowadays available in most Monte Carlo simulation codes.

This work aims at developing a better understanding of the *zero variance branching* methods and to compare their performance in different simulation setups with respect to *zero variance branchless* methods. The focus will be in particular on the class of neutron transport problems simultaneously involving radiation shielding and multiplication, as occurring for instance for ex-core detector monitoring during reactor start-up. For these configurations, Monte Carlo simulations have to take care of two competing goals: pushing the neutrons towards the detector and exploring the fissile regions that are responsible for the source amplifications. Recent investigations have shown that approximate zero-variance techniques like the aforementioned CADIS might fail in this case [4], which motivates the investigations discussed in this manuscript, focusing on zero-variance Monte Carlo games in the presence of neutron multiplication.

The work described in this manuscript is part of a six-month internship performed at the Service d'étude des réacteurs et de mathématiques appliquées (SERMA) of the CEA Paris-Saclay, under the supervision of Drs. A. Jinaphanh, D. Mancusi and A. Zoia. Additionally, I gratefully acknowledge the informal supervision of Ms. T. Gomes-Ferreira, PhD student in the same R&D unit, whose thesis subject concerns zero-variance games.

Some of the results obtained for branching zero-variance games will appear in the paper "T. Gomes Ferreira, F. Rossi, A. Jinaphanh, D. Mancusi, A. Zoia, Comparison of Branching and Branchless Zero-Variance Games", in the proceedings of the M&C2025 conference.

Chapter 2

Background and Theory

2.1 Notations

2.1.1 Phase space

In most of the nuclear engineering applications the study of the neutron population is of outmost importance. Due to the large numbers of particles present in most of the real-life relevant problems, tracking each one of them and describing its history is by no means a trivial matter. For this purpose it is usually preferred to define some average quantities over the stochastic particle histories. By doing so it is possible to look at these average quantities and infer the physical properties. The outcome of this strategy is the Boltzmann's Transport Equation, which will be the object of this Chapter. It is possible to define the phase space of interest using 6 coordinates:

- 3 spatial coordinates $\rightarrow (x, y, z)$, also denoted \vec{r}
- 2 angular coordinates $\rightarrow (\mu, \varphi)$, also denoted $\vec{\Omega}$
- 1 energy coordinate $\rightarrow (E)$

Each point in the phase space is uniquely defined by a combination of these six variables. In this work the six coordinates are condensed under a single letter that will be associated to a point in the phase space:

$$(x, y, z, \mu, \varphi, E) \rightarrow (\vec{r}, \vec{\Omega}, E) \rightarrow P \quad (2.1)$$

$$(x', y', z', \mu', \varphi', E') \rightarrow (\vec{r}', \vec{\Omega}', E') \rightarrow P' \quad (2.2)$$

2.1.2 Cross sections

Now consider a neutron flying around in a non-void medium: at some point the particle's flight path will intercept one of these nuclei, creating a collision. The collision types can be very different, but the most relevant can be summarized as:

- Scattering: the neutron collides with an atomic nucleus and it is scattered with possibly different direction and energy. Scattering can be elastic or inelastic.
- Capture: the neutron collides with the nucleus and is absorbed.
- Multiplicative event: like for the capture case the neutron is absorbed inside the collided nucleus which becomes in this case unstable and expels a given number of outgoing particles.

Regarding the multiplicative events, probably one of the most interesting is the fission event: during a fission event the unstable atomic nucleus tries to regain its former stability by expelling a certain amount of neutrons and by splitting itself in lighter nuclei.

Each collision event can happen with a given probability, that depends on the position and energy of the incident neutron. These probabilities are expressed using the macroscopic cross sections and are indicated with the symbol $\Sigma_i(P)$. Depending on the atomic density of the media where the collision takes place, the collision can happen more or less often. Macroscopic cross sections can be decomposed into:

$$\Sigma_i(x, y, z, E) = \sigma_i(E)N_i(x, y, z) \quad (2.3)$$

The macroscopic cross section represents the probability per unit path that a particle having a certain position and energy interacts inducing the reaction i .

Summing all the possible collision types that a particle can experience it is possible to define the total microscopic and macroscopic cross sections:

$$\Sigma_t(\vec{r}, E) = \Sigma_s(\vec{r}, E) + \Sigma_c(\vec{r}, E) + \Sigma_f(\vec{r}, E) \quad (2.4)$$

It is also useful to group together the fission and capture event in what is usually called an absorption event:

$$\Sigma_a(\vec{r}, E) = \Sigma_c(\vec{r}, E) + \Sigma_f(\vec{r}, E) \quad (2.5)$$

2.1.3 Fission and scattering spectra

In case of fission or scattering where some particles can actually come out from a collision it is also needed to define the outgoing direction and energy of those particles. This outgoing direction and energy take different values according to a probability density function (see also Sec. 2.3.1). The so called "fission spectrum",

$$\chi(E)dE \quad (2.6)$$

is defined as the probability that an outgoing neutron generated from a fission event is emitted with energy dE around E . The emission of the fission neutron is usually an isotropic process. It can additionally be noted that the fission spectra do not depend on the incoming neutron energy and direction. The scattering probability density function depends on both the energy and direction:

$$f_s(\vec{r}, \vec{\Omega} \rightarrow \vec{\Omega}', E \rightarrow E') \quad (2.7)$$

The factor above defines the probability that a neutron undergoing scattering in \vec{r} and colliding with the nucleus with direction $\vec{\Omega}$ and energy E is re-emitted after the collision with direction $\vec{\Omega}'$ and energy E' .

2.2 The Boltzmann's transport equation

2.2.1 Neutron flux

The average number of neutrons per unit volume is denoted by:

$$N(\vec{r}, \vec{\Omega}, E)d\vec{r}d\vec{\Omega}dE \quad (2.8)$$

or more simply $N(P)dP$, where $N(P)$ is the neutron angular density. This expression represents the (expected) number of neutrons around \vec{r} about $d\vec{r}$, flying with direction around $\vec{\Omega}$ about $d\vec{\Omega}$ and with energy around E about dE . Then the neutron flux is defined as the product between the neutron density and the neutron velocity.

$$\phi(\vec{r}, \vec{\Omega}, E) = v(E)N(\vec{r}, \vec{\Omega}, E) \quad (2.9)$$

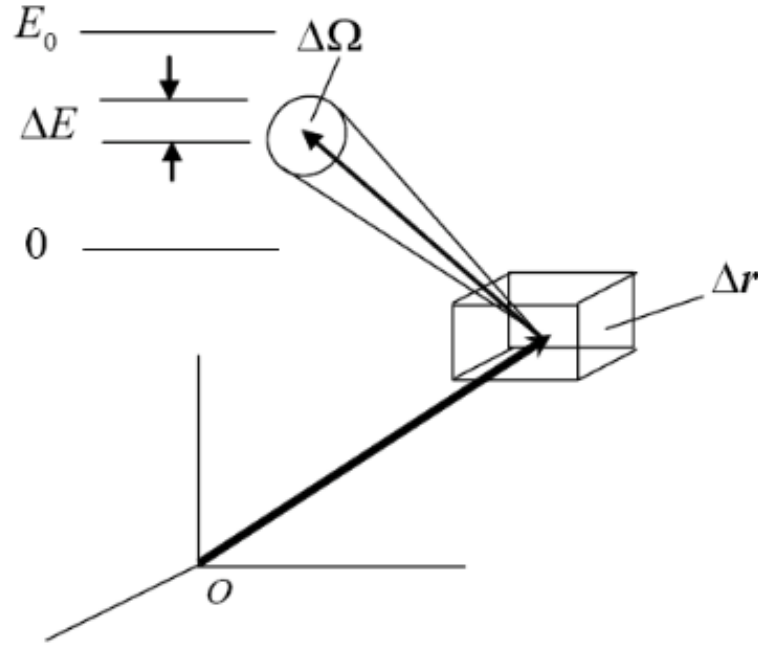


Figure 2.1: Example of the considered packet of neutrons [5]

2.2.2 The Boltzmann equation

It is possible to show that the neutron flux satisfies the linear Boltzmann equation [6]:

$$\begin{aligned} \vec{\Omega} \cdot \nabla \phi(\vec{r}, \vec{\Omega}, E) + \Sigma_t(\vec{r}, E) \phi(\vec{r}, \vec{\Omega}, E) = \\ \int d\vec{\Omega}' \int dE' \Sigma_s(\vec{r}, E') f_s(\vec{r}, \vec{\Omega}' \rightarrow \vec{\Omega}, E' \rightarrow E) \phi(\vec{r}, \vec{\Omega}', E') + \\ \frac{\chi(\vec{r}, E)}{4\pi} \int d\vec{\Omega}' \int dE' \nu(\vec{r}, E') \Sigma_f(\vec{r}, E') \phi(\vec{r}, \vec{\Omega}', E') + \\ Q(\vec{r}, \vec{\Omega}, E) \end{aligned} \quad (2.10)$$

The equation was derived from a balance of the exiting and disappearing the domain of the phase space considered and the neutrons entering and appearing in the same phase space domain. The equation above is nothing else than a balance between all the possible ways a neutron can enter the small region of phase space under consideration and all the possible way a neutron can disappear from the said region.

The term $\vec{\Omega} \cdot \nabla \phi(\vec{r}, \vec{\Omega}, E)$ represents the leakage out of the considered element; it is also called the "streaming term".

The term $\Sigma_t(\vec{r}, E) \phi(\vec{r}, \vec{\Omega}, E)$ represents the disappearance of the neutrons due to some interaction that takes place inside the phase space domain of interest.

On the right-hand side of the equation lies the effect of the scattering and fission events, which acts as sources of neutrons with phase space coordinates P . Looking specifically at the first term it can be read as: all the incoming neutrons with energy E' and direction $\vec{\Omega}'$ which undergo a scattering in \vec{r} about $d\vec{r}$ and which are re-emitted with energy and direction respectively E and $\vec{\Omega}$, integrated over all the possible incoming energy and direction. Something similar can be said about the fission term that appears after this scattering term.

The last term is the contribution of an external source.

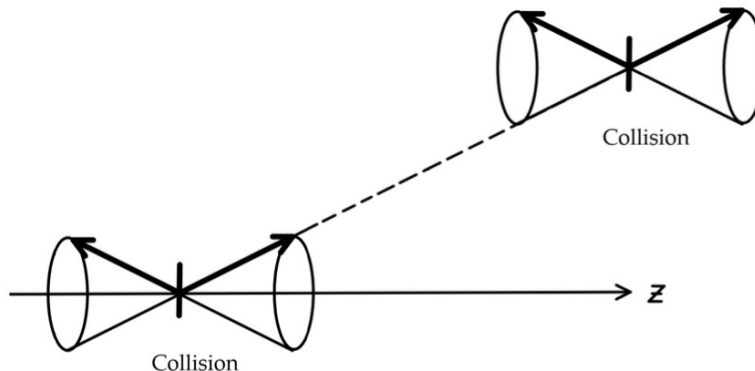


Figure 2.2: S-2 model example: after a collision the new direction can only be either "positive" or "negative".

2.3 Deterministic and stochastic approach

Solving analytically the Boltzmann's transport equation is de facto impossible but for extremely simple cases, so two main numerical approaches are used instead:

- Deterministic approach: discretize the phase space using suitable simplifications in order to reduce the number of unknowns, and then find a solution on the discretized mesh by standard numerical methods. Some useful deterministic methods are:
 - P-N method,
 - S-N method (see Figure 2.2 for an example),
 - Diffusion model.
- Stochastic approach (also called Monte Carlo) : sample neutron histories, from the source to death by absorption or leakage; record the events of interest, ie the contributions to a given "detector"; finally, take the ensemble averages over the simulated histories, in order to have an estimate of the sought observable.

2.3.1 Monte Carlo approach

The other way to solve the Boltzmann transport equation is the Monte Carlo approach which relies on the statistical aspects related to the neutron transport: as mentioned, in fact, all the cross sections Σ_i that governs the physical phenomenon of interest represent probabilities per unit path. The key point to understand the stochastic approach is that the average behavior of the whole neutron population can be predicted by looking at the statistical laws. The same reasoning can be applied to a coin toss: it is not possible to predict *a priori* if a tossed coin will land on head or tail but it is known that tossing the same coin over and over will result in half of the results being head and the other half being tail. This type of reasoning is the basis of the Monte Carlo simulations for neutron transport that will be used in this work to solve the Boltzmann equation.

Probability notations

At the basis of this work and at the basis of every Monte Carlo simulation lies the theory of probability. It is possible to give the axiomatic definition of probability stating that probability is an application that goes from the event space (space where all the possible outcomes of a phenomenon lie) to the real axis in the interval $[0,1]$. This definition is based on 3 axioms [7]:

- The probability of any event is equal or larger than 0.
- The probability of the whole sample space is 1.
- Given E_j with $j = 1, 2, \dots$ events such that $E_i \cap E_j = \emptyset$ if $i \neq j$ (the events are *mutually exclusives*), the probability of their union is the sum of their probabilities.

From this definition the concept of probability is derived and to indicate the probability that a certain phenomenon x happens, the writing $P[x]$ is used.

Then it is possible to give the definition of "random variable" which will be used later on: a random variable ξ is application from the sample space to a real number between 0 and 1 [7]. It is also possible to define the "cumulative density function" as:

$$F_\xi(t) = P[\xi \leq t] \quad (2.11)$$

and this function is such that:

$$\begin{cases} \lim_{t \rightarrow -\infty} F_\xi(t) = 0 \\ \lim_{t \rightarrow +\infty} F_\xi(t) = 1 \\ \lim_{t \rightarrow t_0^+} F_\xi(t) = F_\xi(t_0) \\ \textit{it is a monotonic increasing function} \end{cases} \quad (2.12)$$

Lastly the "probability density function" is:

$$f_\xi(t) = \frac{dF_\xi(t)}{dt} \quad (2.13)$$

An example of probability density function is the "normal distribution" which has the form of:

$$f_\xi(t) = \frac{1}{\sqrt{2\pi\sigma^2}} \exp \left[-\frac{(t - \mu)^2}{2\sigma^2} \right] \quad (2.14)$$

where μ is the mean value and σ^2 is the variance of the distribution.

Central limit theorem and its applications

To know the mean value of a statistical phenomenon a series of experiments should be performed in order to get a set of random variables ξ_i with $i = 1, 2, \dots, N$. Each ξ_i is *statistically independent*, so the values they assume do not depend on the values the others, and *identically distributed*, since they are connected to the same statistics. We define then the "sample average" as:

$$\bar{\xi}^{(N)} = \frac{1}{N} \sum_{i=1}^N \xi_i \quad (2.15)$$

The sample average $\bar{\xi}^{(N)}$ is an approximation of the mean value of the phenomenon which we will indicate by $M_1[x]$, ie the first order moment of the phenomenon.

From the Tchebycheff inequality it can be demonstrated that the probability that the absolute difference between the mean value of a statistical phenomenon and the result

of the statistical of the said phenomenon has an upper bound which depends on some tolerance. In other words:

$$P \left[|\xi - M_1[x]| \geq k \right] \leq \frac{\sigma^2[x]}{k^2} \quad (2.16)$$

Applying this theorem to the sample average it is possible to obtain the following:

$$P \left[|\bar{\xi}^{(N)} - M_1[x]| \geq k \right] \leq \frac{\sigma^2[x]}{N \cdot k^2} \quad (2.17)$$

From the previous equation it follows directly that by increasing the number of experiments it is less and less likely that the sample average $\bar{\xi}^{(N)}$ is far from the expected value. Also:

$$P \left[|\bar{\xi}^{(N)} - \mu| \geq k \right] = P \left[\bar{\xi}^{(N)} \geq \mu + k \right] + P \left[\bar{\xi}^{(N)} \leq \mu - k \right] \quad (2.18)$$

$$= F_{\bar{\xi}^{(N)}}(\mu + k) - F_{\bar{\xi}^{(N)}}(\mu - k) \quad (2.19)$$

Where $F_{\bar{\xi}^{(N)}}(y)$ is the cumulative function calculated in y . Calling now the mean value and variance of the phenomenon as:

$$M_1[x] = \mu \quad (2.20)$$

$$\sigma^2[x] = \sigma^2 \quad (2.21)$$

it is possible to apply the "Central Limit Theorem" which states that given a statistical phenomenon for which it exists a mean value μ and a variance σ^2 and given a set of random variables ξ_i that are generated according to it and that can be used to define the sample average $\bar{\xi}^{(N)}$, then if the number of experiments N is large enough the said sample average is normally distributed and the variance of the mean scales as $\frac{\sigma^2}{N}$. Applying this theorem to the relations derived from the Tchebycheff Inequality it can be demonstrated that:

$$P \left[\left| \frac{\bar{\xi}^{(N)} - \mu}{\frac{\sigma}{\sqrt{N}}} \right| \leq 1 \right] \approx 0.68 \quad (2.22)$$

$$P \left[\left| \frac{\bar{\xi}^{(N)} - \mu}{\frac{\sigma}{\sqrt{N}}} \right| \leq 2 \right] \approx 0.95 \quad (2.23)$$

$$P \left[\left| \frac{\bar{\xi}^{(N)} - \mu}{\frac{\sigma}{\sqrt{N}}} \right| \leq 3 \right] \approx 0.99 \quad (2.24)$$

So, taking an interval wide 3σ around the sample average assures that the real solution is inside that interval with a confidence of 99%.

Random walks

The application of basic probability and statistics concepts to neutron transport is now considered, with the aim of obtaining estimates of the quantity of interest via Monte Carlo simulations. The first element to define is the concept of *random walks*, which represent random transitions between points in the phase space. To ensure that these random walks accurately reflect the underlying physical phenomena, it is necessary to impose the condition that, on average, the mean value of the physical statistical phenomenon aligns with the estimate derived from the random walks. The process begins with a simple example focusing solely on neutron flight. The probability that a neutron can move from a point $P = (\vec{r}, \vec{\Omega}, E)$ to a point $P' = (\vec{r}', \vec{\Omega}', E)$ with a free flight is composed of two parts: the probability that the free flight ends in P' and the probability that the particle

can move from P to P' without interactions. Knowing also that the probability of having an interaction of any kind in a specific point is proportional to $\Sigma_t(P)$ and supposing a purely homogeneous medium (so that the macroscopic cross section does not depend on the position), it is possible to write the following probability density function for the neutron free flight:

$$f_{flight}(|\vec{r} - \vec{r}'|, E) = \Sigma_t(E) e^{-(|\vec{r} - \vec{r}'|)\Sigma_t(E)} \quad (2.25)$$

Then by definition the cumulative of this probability density function is:

$$F_{flight}(|\vec{r} - \vec{r}'|, E) = 1 - e^{-(|\vec{r} - \vec{r}'|)\Sigma_t(E)} \quad (2.26)$$

Once the cumulative function is known, the *inverse transform method* can be employed to sample random values distributed according to it. This method is applicable only when the analytical expression of the cumulative function is available. If the statistical phenomenon is complex and the derivation of the cumulative function is difficult, alternative approaches may be more suitable. The method is based on the following algorithm:

- generation of a random number $\rho \in [0, 1]$ with any method;
- setting of $F_{flight}(s, E) = \rho$;
- inversion of the relation to find $s = F_{flight}^{-1}(\rho)$.

For simplicity the substitution $s = (|\vec{r} - \vec{r}'|)$ was used. For our example the inversion is rather simple and yields:

$$s = -\frac{1}{\Sigma_t(E)} \log(1 - \rho) \quad (2.27)$$

In this way it was possible to generate free flights for the neutron that on average respect the physical laws imposed by the Boltzmann transport equation.

Chapter 3

Zero Variance Monte Carlo

The approach used to simulate the neutron flight and interaction is the same as the one used by Lux and Koblinger in their book [1]. Like the two authors did, it is useful to identify three main steps, which are:

- the sampling from the source, connected to the *source kernel* Q ;
- the sampling of the flight length, connected to the *flight kernel* T ;
- the sampling of the reaction channel, connected to the *collision kernel* C .

3.1 Additional definitions

3.1.1 Source, flight and collision kernels

Any particle source can be characterized by the source density:

$$Q(\vec{r}, \vec{\Omega}, E) = Q(P) \quad (3.1)$$

The sampling process from the source depends on the type of the source (ie isotropic, collimated, mono-energetic...).

How the particle can travel from a point in space to another is defined by the flight kernel, namely:

$$T(P', P) = \Sigma_t(\vec{r}', E) \exp \left[- \int_0^{|\vec{r} - \vec{r}'|} ds' \Sigma_t(\vec{r}' + s' \vec{\Omega}) \right] \frac{\delta \left(\vec{\Omega} - \frac{\vec{r} - \vec{r}'}{|\vec{r} - \vec{r}'|} \right)}{(|\vec{r} - \vec{r}'|)^2} \delta(\vec{\Omega}' - \vec{\Omega}) \delta(E - E') \quad (3.2)$$

One way to interpret the equation above is the following: the average number of particles having coordinates P given a particle starting a flight with coordinates P' is given by the probability of colliding in ds around \vec{r} multiplied by the probability of not colliding until point \vec{r}' multiplied by the probability the particle has the correct direction and energy.

What the particle does upon reaching the next collision site at the end of its free flight is governed by the collision kernel:

$$C(P', P) = \sum_i \sum_j \frac{\Sigma_{t,i}(\vec{r}', E') \sigma_{i,j}(E')}{\Sigma_t(\vec{r}', E')} \nu_{i,j}(E') f_{i,j}(\vec{\Omega}' \rightarrow \vec{\Omega}, E' \rightarrow E) \delta(\vec{r} - \vec{r}') \quad (3.3)$$

The collision kernel represents the average number of particles with coordinates P given a particle having a collision in P' .

In general, the kernels T and C and the source Q are not normalized. In this case, the sampling can be performed by first normalizing the aforementioned quantities in order to express them as appropriate probability densities. Then, the sampled particle is attributed a weight correction factor equal to the norm of the sampled kernel. Alternatively, the normalization factor can be taken into account in the particle multiplicity at collision event.

3.1.2 Densities

With the help of the kernels above it is possible to define also the so-called "collision densities" $\chi(\vec{r}, \vec{\Omega}, E)$ and $\psi(\vec{r}, \vec{\Omega}, E)$ like:

$$\chi(\vec{r}, \vec{\Omega}, E) = Q(\vec{r}, \vec{\Omega}, E) + \int dE' \int d\Omega' \psi(\vec{r}, \vec{\Omega}, E) C(\vec{\Omega}', E' \rightarrow \vec{\Omega}, E | \vec{r}) \quad (3.4)$$

$$\psi(\vec{r}, \vec{\Omega}, E) = \int d\vec{r}' \chi(\vec{r}', \vec{\Omega}, E) T(\vec{r}' \rightarrow \vec{r} | \vec{\Omega}, E) \quad (3.5)$$

In the first equation the form of the emission density was derived, and it can be interpreted as the average number of particles leaving a collision (or the source) at point P . The second one instead defines the collision density which is the average number of particles going into a collision at point P .

3.1.3 Scoring in Monte Carlo games

In any Monte Carlo simulation, it is necessary to record the relevant information used to estimate average quantities. The standard approach involves utilizing response functions R in conjunction with the appropriate payoff function $f(P)$:

$$R = \int dP f_\chi(P) \chi(P) = \int dP f_\psi(P) \psi(P) \quad (3.6)$$

Since the collision densities can be expanded into a Neumann series, each integral can be evaluated as an infinite sum of integrals, as follows:

$$R = \sum_{i=0}^{\infty} R_{i,\chi} = \sum_{i=0}^{\infty} \int dP f_\chi(P) \chi_i(P) \quad (3.7)$$

$$R = \sum_{i=0}^{\infty} R_{i,\psi} = \sum_{i=0}^{\infty} \int dP f_\psi(P) \psi_i(P) \quad (3.8)$$

Practically, every single contribution of the histories is recorded at each collision and then they are summed up to obtain the total contribution of the history to the score. The weights due to the biased sampling processes also contribute to the final score. The score of a single history is then:

$$\mu_\chi = \sum_{i=0}^{\infty} r_{i,\chi} = \sum_{i=0}^{\infty} f_\chi(P_i) \quad (3.9)$$

$$\mu_\psi = \sum_{i=0}^{\infty} r_{i,\psi} = \sum_{i=0}^{\infty} f_\psi(P_i) \quad (3.10)$$

Then the detector response is given taking the first moment of the score and integrating over the desired phase space.

3.2 Type of games

3.2.1 Analog

The term *analog game* refers to a type of simulation where the particle weight remains fixed at unity, and no weight corrections are applied to bias the statistics. In such simulations, the particle typically follows the natural statistical laws governing the physical phenomenon [3]. The collision kernel for the analog game can be expressed as:

$$C(P', P'') = c_c(P')\delta(P'' - \bar{P}) + c_s(P')C_s(P', P'') + c_f(P') \sum_{n=1}^{\infty} nq_n(P')C_n(P', P'') \quad (3.11)$$

In the equation above, \bar{P} is a point outside the phase space region where the simulation takes place, where both the contribution probabilities and the kernels are zero.

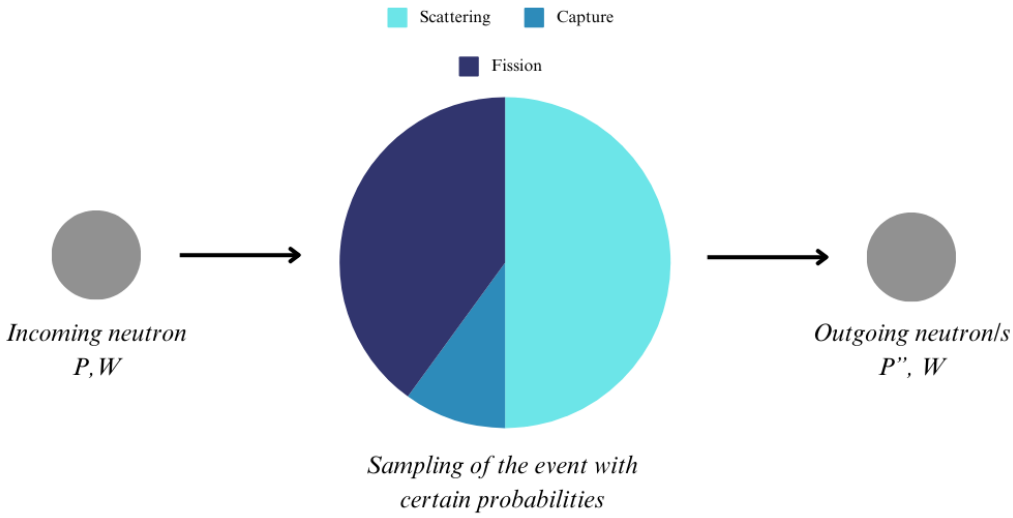


Figure 3.1: Scheme of an analog game

3.2.2 Implicit capture

The implicit capture game represents the first and arguably the simplest extension of the analog game, emerging from a common issue encountered in analog simulations. In traditional analog games, the history of a particle is terminated when a sampled collision results in capture. This limitation becomes apparent in scenarios where, despite simulating a large number of particles to reduce variance, the capture event prematurely halts the particle's trajectory. This issue is particularly important in radiation shielding problems, where simulations often involve media with high attenuation. To mitigate the impact of capture on particle histories, implicit capture games omit the simulation of capture events. Specifically, collisions that would normally result in capture are no longer sampled. However, since a probability density function is still required for Monte Carlo simulations, the scattering and fission probabilities are renormalized to sum to unity. To correct for this modification in the original statistical distribution, the particle's weight is adjusted by a factor equivalent to the capture probability. Conceptually, this can be interpreted as only a fraction of the particle surviving the collision, with the remaining fraction being effectively terminated during the interaction. This perspective clarifies why the weight correction factor corresponds precisely to the capture probability [8].

Using the * symbol to indicate a game with this kind of biasing, the collision kernel for an implicit capture game is then:

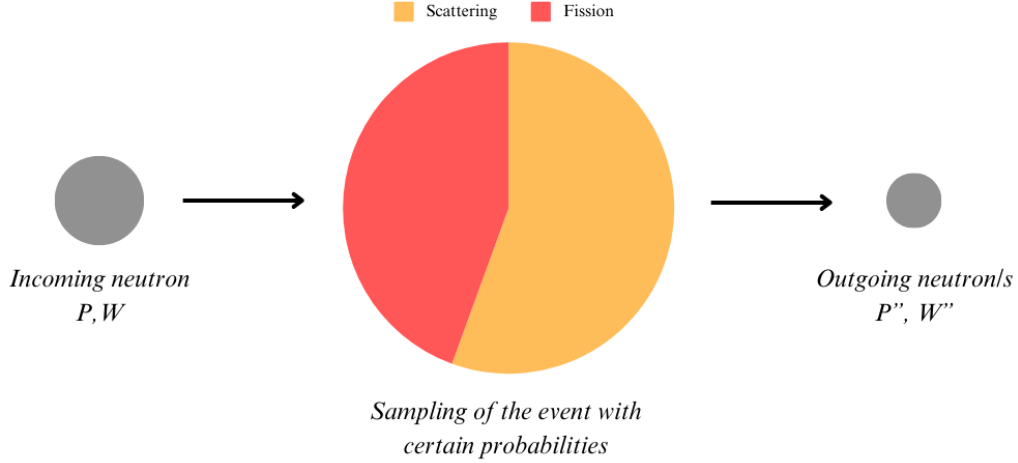


Figure 3.2: Scheme of an implicit capture

$$\begin{aligned}
 C^*(P', P) &= \frac{\sigma_s^*(E')}{\sigma_t^*(E')} \cdot \nu_s(E') \cdot f_s(\Omega', E' \rightarrow \Omega, E) \delta(r - r') \\
 &+ \sum_{n=1}^{\infty} \frac{\sigma_f^*}{\sigma_t^*} \cdot q_n \cdot \nu_{f,n}(E') \cdot f_f(\Omega', E' \rightarrow \Omega, E) \delta(r - r')
 \end{aligned} \tag{3.12}$$

$$\begin{aligned}
 C^*(P', P) &= c_s^*(P') \cdot \nu_s(E') \cdot f_s(\Omega', E' \rightarrow \Omega, E) \delta(r - r') \\
 &+ \sum_{n=1}^{\infty} c_f^*(P') \cdot q_n \cdot \nu_{f,n}(E') \cdot f_f(\Omega', E' \rightarrow \Omega, E) \delta(r - r')
 \end{aligned} \tag{3.13}$$

$$C^*(P', P) = c_s^*(P') C_s^*(P, P') + c_f^*(P') \sum_{n=1}^{\infty} n q_n^*(P') C_n^*(P, P') \tag{3.14}$$

3.2.3 Russian roulette

In an infinite medium without capture we will have *immortal particles* and the simulation will run indefinitely. One of the most commonly used method to terminate a particle history which is used in this type of scenarios is the so called *Russian roulette*. The idea of this method is to try to kill the particle with a small weight that will then contribute in a negligible manner to the score.

To implement this algorithm first it is needed to define a certain weight cutoff and if the particle weight is lower than this cutoff the said particle will undergo Russian roulette. Once inside the roulette a termination probability proportional to the particle weight (and eventually dependent on some other parameters) is defined, and subsequently it is decided if the particle history is terminated or not. If the particle survives the roulette its weight is re-set to a chosen value.

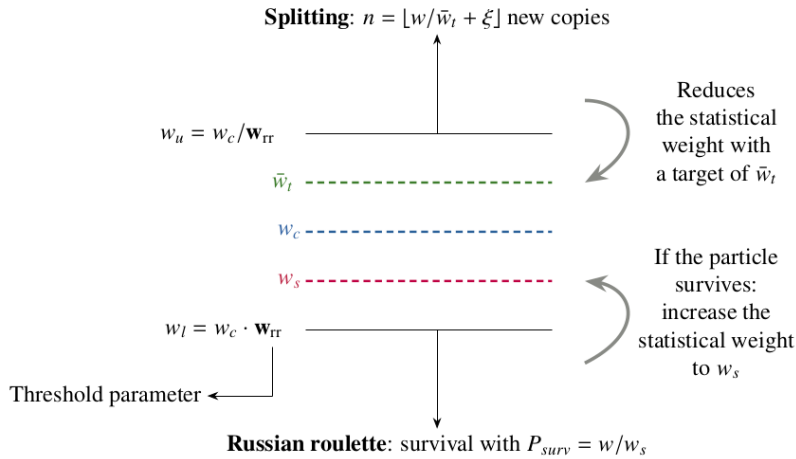


Figure 3.3: Scheme of the weight window procedure

3.2.4 Weight windows

A more complex way to implement the previous population control methods by also adding the information of the importance, derived from the solution of the adjoint Boltzmann equation. First of all, this method combines the Russian roulette previously described with a splitting method in order to define a *window* in which the particle weight can be. If the weight is below the window's lower limit the particle enters a roulette, if it is above the window's upper limit the particle is split in a number of particles such that the weight of each one of them is inside the limits. Once the window's limits have been defined this way, it is possible to enlarge or shrink the window depending on the importance of the point in the phase space where the particle is located. A particle near a region with a higher importance will have a lower chance of being killed by the roulette than a particle with the same weight but in a region with a lower importance. [9]

This method has two advantages: first it forces the particle to move from regions of lower importance to regions with higher importance, second it delays the termination of the particle histories depending on their position. The first advantage is related to the fact that less and less particles can survive in lower importance regions, while a lot more particles will do in the higher importance ones: the result is similar to a biasing of the transport kernel $T(P, P')$ but it is achieved not during the free flight but during the collision. The second advantage is instead related to a problem that can arise when the weight windows do not consider the information of the adjoint flux: in this first version, in fact, the window's limits are the same regardless of the position, then particles that have been doing the same collisions will be killed at the same time. This creates a sort of *oscillating behavior* thanks to which the total population will go down when a lot of particles experience the roulette altogether at the same time. Introducing the importance adds some unique information to each particle so that each window's limits will be different than the others.

A scheme depicting the weight window procedure is presented in Figure 3.3.

3.2.5 Exponential transform

The biasing of the free flight can be implemented using the exponential transform technique. This technique, also called *path length stretching* is designed to increase the efficiency for deep penetration problems, so it fits well in the scope of radiation shielding. It is based on the definition of a *stretching parameter*, used to increase the distance travelled

in directions with higher importance regions and to decrease the same distance in directions with regions of lower importance. The biasing of the free flight length is done by modifying the total cross section as follows:

$$\Sigma_t^* = \Sigma_t(1 - p\mu) \quad (3.15)$$

Where p (with $|p| < 1$) is the exponential transform parameter used to vary the degree of biasing and μ is the cosine of the angle between the preferred direction and the particle's direction. Shorter free flights are associated with a higher frequency of collisions and of instances where the particle can undergo Russian roulette and thus be killed. An example of the exponential transform, or path stretching is presented in Figure 3.4.

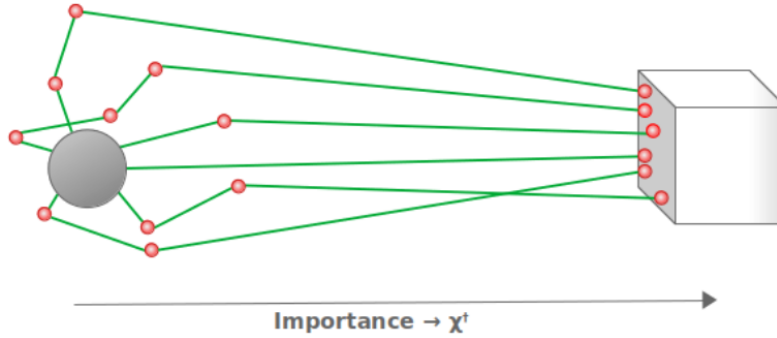


Figure 3.4: Scheme of the exponential transform technique

3.2.6 Forced fission

In a forced fission game, the events that a particle can experience during a collision are fundamentally different from those in the corresponding analog game. In the original analog game, a particle has three possible interactions: it can either scatter, be captured, or undergo fission (according to what was said up until now). In contrast, in the forced fission game, the capture reaction channel is suppressed, so the particle can only scatter and undergo fission, provided that fission is possible, but these events happen during the same collision event. So, since the reaction channel is basically only one, the particle is always forced to take this channel and every collision will always contain both a fission part and a scattering part. In other words:

$$P[\text{fission} + \text{scattering}] = 1 \text{ at every collision}$$

Imaging the collision as a whole unique process it is possible to visualize it as a black box where 1 neutron enters the collision and n neutrons exit the collision. In addition, knowing that scattering will always occur (a particle can always be scattered while it undergoes fission only if inside a multiplicative medium), so the number of outgoing neutrons will not be lower than 1. In other words it exists:

$$\min(n) = m \geq 1 \quad (3.16)$$

The number of outgoing neutrons from a fission event using a forced fission scheme can be sampled as [10]:

$$\hat{\nu} = \lfloor \frac{\nu\sigma_f}{\sigma_t} + \rho \rfloor \quad (3.17)$$

This is not the only way to implement the forced fission scheme but it will be the one used in this work. It is evident how from this sampling approach $\hat{\nu}$ can have only two possible values:

$$\begin{cases} \hat{\nu} = \frac{\nu\sigma_f}{\sigma_t} & \text{with probability } P = 1 - \frac{\nu\sigma_f}{\sigma_t} \\ \hat{\nu} = \frac{\nu\sigma_f}{\sigma_t} + 1 & \text{with probability } P = \frac{\nu\sigma_f}{\sigma_t} \end{cases} \quad (3.18)$$

Then combining the fact that for sure a neutron is coming out from the scattering (and since scattering and fission are not correlated) it is possible to think of the collision in the forced fission scheme as the aforementioned "black-box" where for each incoming neutron, the n number of outgoing neutron is:

$$\min(n) = m = \lfloor \frac{\nu\sigma_f}{\sigma_t} \rfloor + 1 \quad (3.19)$$

$$\begin{cases} n < m \rightarrow c_n(P') = 0 \\ n = m \rightarrow c_n(P') = 1 - \frac{\nu\sigma_f}{\sigma_t} \\ n = m + 1 \rightarrow c_n(P') = \frac{\nu\sigma_f}{\sigma_t} \end{cases} \quad (3.20)$$

Within the fissile media, otherwise the solution is trivial and it corresponds to having only scattering (so $n = 1$) with probability equal to unity.

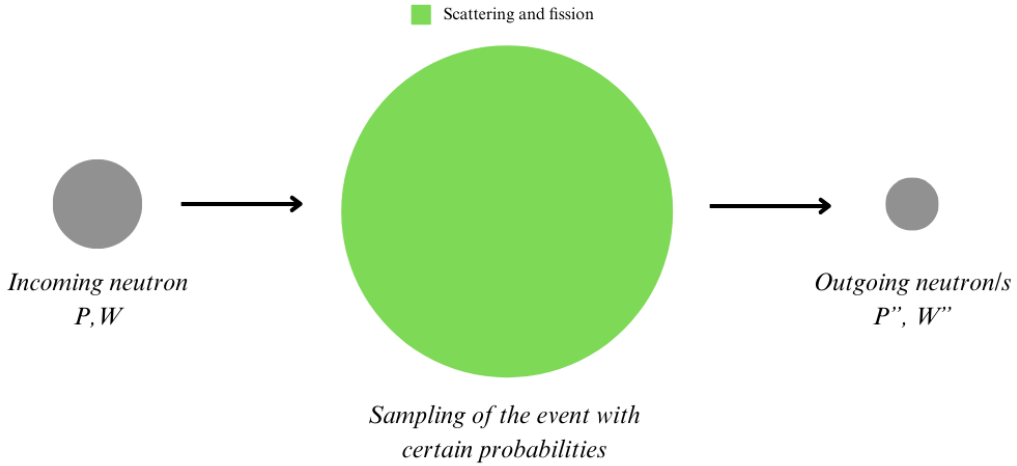


Figure 3.5: Scheme of a forced fission game

Ultimately, in forced fission branching games it is meaningless to talk about reaction channel probabilities, since the outcome of every collision will always be the same. Keeping this in mind it is possible to write the collision kernel for a forced fission game as:

$$C^{FF}(P', P'') = C_s^{FF}(P', P'') + \delta_f(P') \sum_{n=1}^{\infty} n q_n^{FF}(P') C_n^{FF}(P', P'') \quad (3.21)$$

$$\delta_f(P') = \begin{cases} 1 & \text{if } c_f(P') > 0 \\ 0 & \text{if } c_f(P') = 0 \end{cases} \quad (3.22)$$

where the symbol FF was used to indicate that it is a forced fission scheme.

3.3 Zero-variance games

The simple analog game described above can be replaced by a modified (non-analog) game by replacing the source, flight and collision kernels respectively by the modified quantities:

$$\hat{Q}, \hat{T}, \hat{C} \quad (3.23)$$

Then the detector response is:

$$R = \int dP f_\psi(P) \psi(P) = \int dP f_\psi(P) \frac{\psi(P)}{\psi^*(P)} \psi^*(P) \quad (3.24)$$

and the quantity $\frac{\psi(P)}{\psi^*(P)}$ can be interpreted as a weight correction factor that preserves an unbiased average, where $\psi^*(P)$ is given instead as:

$$\psi^*(P) = \int dP' \hat{T}(P, P') \int dP'' \hat{C}(P'', P') \psi^*(P'') + \int dP' \hat{T}(P, P') \hat{Q}(P') \quad (3.25)$$

It is possible to choose the modified \hat{Q}, \hat{T} and \hat{C} in such a way that the variance of the sought response function is exactly zero. The derivation of these zero-variance kernels will become clearer after the formulation of the *moments equations* presented in the following Chapters and in the Appendices of this work. However, the final results can already be presented in simple case of the zero-variance game derived from a purely analog game:

$$\hat{T}(P, P') = T(P, P') \frac{f(P, P') + \int dP'' C(P, P') \chi^*(P'')}{\chi^*(P)} \quad (3.26)$$

$$\hat{C}(P', P'') = C(P', P'') \frac{\chi^*(P'')}{\int dP'' C(P', P'') \chi^*(P'')} \quad (3.27)$$

$$\hat{Q}(P) = Q(P) \frac{\chi^*(P)}{\int dP Q(P) \chi^*(P)} \quad (3.28)$$

By using the new kernels the simulation is biased toward the desired outcome, so to have at the end an unbiased result a system of weights that conserves the average score needs to be implemented. These weights were already introduced in the description of the score at the detector and the corrections of the particle weight can happen:

- After a flight from P to P' the weight correction is W'
- After a scattering from P' to P'' the weight correction is W''
- After a n-fission phenomena from P' to P''_n the weight correction of the n-th outgoing particle is W''_n

It is possible to express \hat{C} by singling out each reaction channel:

$$\hat{C}(P', P'') = \hat{c}_c(P') \delta(P'' - \bar{P}) + \hat{c}_s(P') \hat{C}_s(P', P'') + \hat{c}_f(P') \sum_{n=1}^{\infty} n \hat{q}_n(P') \hat{C}_n(P', P'') \quad (3.29)$$

Where each \hat{c}_j is the probability to choose that specific reaction channel. Considering as multiplicative event a fission where either two or three neutrons can be produced, the previous equation can be simplified as:

$$\hat{C}(P', P'') = 1 \times \left[\hat{c}_s(P') \hat{C}_s(P', P'') \right] + 2 \times \left[\hat{c}_f(P') \hat{q}_2(P') \hat{C}_2(P', P'') \right] + 3 \times \left[\hat{c}_f(P') \hat{q}_3(P') \hat{C}_3(P', P'') \right] \quad (3.30)$$

where each possible reaction channel was divided.

3.4 Derivation of the zero-variance games

The aim of this part of the report is to derive formally the kernels associated with the zero-variance Monte Carlo game and using the strategy of the *moments equation*. The general condition to achieve zero variance is that:

$$\hat{D}(P) = \hat{M}_2(P) - \hat{M}_1^2(P) = 0 \quad (3.31)$$

where $\hat{M}_2(P)$ and $\hat{M}_1(P)$ are the respectively the second and first order moment of a tally associated with the random walk of the particle for a given response function and $\hat{D}(P)$ is the variance of the said tally. From the previous equation, it is evident how to derive the zero variance kernels the expressions for the first and second order moment of the desired estimator are necessary. Here, we present the final formulas of the derivation; the full derivation of the expressions for the moments can be found in the Appendices. The derivation will be shown first for analog game, and then it will be adapted to implicit capture and forced fission game, for which only the final result will be shown in this Chapter. It was decided to not formally derive the zero variance kernels for the branchless games since this kind of work has been already investigated by others [11] [12] and since the focus of this work are the branching games.

3.4.1 From an analog game

The derivation proposed here is the same as the one proposed by Lux and Koblinger [1]. Recalling once again the form of the collision kernel for an analog game but modifying it so that the scattering term and the term with only 1 outgoing neutron from fission are grouped together in the same term:

$$C(P', P'') = c_c \delta(P'' - \bar{P}) + \sum_{n=1}^{\infty} n c_n(P') C_n(P', P'') \quad (3.32)$$

Then let also recall the first moment of the general score estimator $f(P, P')$:

$$M_1(P) = \int dP' T(P, P') f(P, P') + \int dP' T(P, P') \int dP'' C(P', P'') M_1(P'') \quad (3.33)$$

and by substituting the collision kernel:

$$M_1(P) = \int dP' T(P, P') f(P, P') + \int dP' T(P, P') \sum_{n=1}^{\infty} n c_n(P') \int dP'' C_n(P, P'') M_1(P'') \quad (3.34)$$

where the first term on the r.h.s. is the partial score due the particle moving from P to P' and the second term represents the partial score due to all the collided particles. The expression for $M_1(P)$ is formally equal to the adjoint of the emission density $\chi^*(P)$, which can be interpreted as the importance itself. [1]

Now, let us call $\int dP'' C_n(P', P'') M_1(P'')$ as $\bar{m}_n(P')$ and let us add and subtract the term:

$$\int dP' T(P, P') \sum_{n=1}^{\infty} n c_n(P') H(P, P') H_n(P') \bar{m}_n(P') \quad (3.35)$$

where $H(P, P')$ and $H_n(P')$ are for now arbitrary functions. Then it is possible to rewrite the first moment as:

$$\begin{aligned}
M_1(P) &= \int dP' T(P, P') \left\{ f(P, P') + \sum_{n=1}^{\infty} n c_n(P') [1 - H(P, P') H_n(P')] \bar{m}_n(P') \right\} \\
&\quad + \int dP' T(P, P') H(P, P') \sum_{n=1}^{\infty} n c_n H_n(P') \bar{m}_n(P')
\end{aligned} \tag{3.36}$$

The second moment of the general score estimator is instead:

$$\begin{aligned}
M_2(P) &= \int dP' T(P, P') f^2(P, P') + 2 \int dP' T(P, P') f(P, P') \int dP'' C(P', P'') M_1(P'') \\
&\quad + \int dP' T(P, P') \int dP'' C(P', P'') M_2(P'')
\end{aligned} \tag{3.37}$$

Let us now assume to change the game from analog to non-analog with proper weights corrections to ensure the unbiasedness of the modified game:

$$W' = \frac{T(P, P')}{\hat{T}(P, P')} \tag{3.38}$$

$$W_n'' = W' \frac{c_n(P') C_n(P', P'')}{\hat{c}_n(P') \hat{C}_n(P', P'')} \tag{3.39}$$

and the total weight of the particle when in P is simply indicated by W . Thanks to the *moment equations* for a general non-analog game, the first and second moment corresponding to the non-analog game with a particle starting with unit weight at P can be expressed as:

$$\begin{aligned}
W \hat{M}_1(P) &= \int dP' \hat{T}(P, P') [W' \hat{f}(P, P') + c_c(P') W^c \hat{f}_c(P')] \\
&\quad + \hat{c}_s(P') \int dP'' \hat{C}_s(P', P'') W'' \hat{f}_s(P', P'') \\
&\quad + \hat{c}_f(P') \sum_{n=1}^{\infty} \hat{q}_n(P') \sum_{i=1}^n \int dP''_{(i)} \hat{C}_n(P', P''_{(i)}) W''_{n(i)} \hat{f}_n(P', P'') \\
&\quad + \int dP' \hat{T}(P, P') [\hat{c}_s(P') \int dP'' \hat{C}_s(P', P'') W'' \hat{M}_1(P'') \\
&\quad + \hat{c}_f(P') \sum_{n=1}^{\infty} \hat{q}_n(P') \sum_{i=1}^n \int dP''_{(i)} \hat{C}_n(P', P''_{(i)}) W''_{n(i)} \hat{M}_1(P''_{(i)})]
\end{aligned} \tag{3.40}$$

$$\begin{aligned}
\hat{M}_2(P) &= \int dP' \hat{T}(P, P') [(W')^2 f^2(P, P') \\
&\quad + 2W' f(P, P') \sum_{n=1}^{\infty} n \hat{c}_n(P') \int dP'' \hat{C}_n(P', P'') W'' M_1(P'') \\
&\quad + \sum_{n=1}^{\infty} n(n-1) \hat{c}_n(P') (\int dP'' \hat{C}_n(P', P'') W'' M_1(P''))^2] \\
&\quad + \int dP' \hat{T}(P, P') \sum_{n=1}^{\infty} n \hat{c}_n(P') \int dP'' \hat{C}_n(P', P'') (W''_n)^2 \hat{M}_2(P'')
\end{aligned} \tag{3.41}$$

Monte Carlo game will be zero-variance if:

$$\frac{\hat{M}_2(P)}{\hat{M}_1(P)} = \hat{M}_1(P) \quad (3.42)$$

Since the game needs to be unbiased the first moments of the analog and of the general non-analog games need to be equal, so $\hat{M}_1(P) = M_1(P)$. Dividing the equation for the second moment by the first moment $M_1(P)$ and dividing and multiplying in the last term by $\frac{\Theta(P')}{M_1(P')}$, where $\Theta(P')$ is for now an arbitrary function, results in

$$\begin{aligned} \frac{\hat{M}_2(P)}{M_1(P)} &= \int dP' \hat{T}(P, P') \left[(W')^2 f^2(P, P') + 2W' f(P, P') \sum_{n=1}^{\infty} n \hat{c}_n(P') \int dP'' \hat{C}_n(P', P'') W_n'' M_1(P'') \right. \\ &\quad \left. + \sum_{n=1}^{\infty} n(n-1) \hat{c}_n(P') \left(\int dP'' \hat{C}_n(P', P'') W_n'' M_1(P'') \right)^2 \right] / M_1(P) \\ &\quad + \int dP' \hat{T}(P, P') \frac{\Theta(P')}{M_1(P')} \sum_{n=1}^{\infty} n \hat{c}_n(P') \int dP'' \hat{C}_n(P', P'') \frac{M_1(P'')}{\Theta(P')} (W_n'')^2 \frac{\hat{M}_2(P'')}{M_1(P'')} \end{aligned} \quad (3.43)$$

To ensure a zero-variance game the equality of the terms on the r.h.s. of this equation with respect to the two terms on the r.h.s. of $M_1(P)$ is needed. For the second term:

$$\begin{aligned} \hat{T}(P, P') \frac{\Theta(P')}{M_1(P')} \hat{c}_n(P') \hat{C}_n(P', P'') \frac{M_1(P'')}{\Theta(P')} (W_n'')^2 \\ = T(P, P') H(P, P') c_n(P') C_n(P', P'') H_n(P'') \end{aligned} \quad (3.44)$$

which is satisfied for:

$$\begin{cases} \hat{T}(P, P') = \frac{T(P, P') \Theta(P')}{H(P, P') M_1(P)} \\ \hat{c}_n(P') \hat{C}_n(P', P'') = \frac{c_n(P') C_n(P', P'') M_1(P'')}{\Theta(P') H_n(P'')} \\ \frac{\Theta(P')}{H(P, P')} = f(P, P') + \sum_{n=1}^{\infty} n c_n(P') \bar{m}_n(P') \end{cases} \quad (3.45)$$

The last equation was added to satisfy the normalization of $\hat{T}(P, P')$. For what concerns the second term to compare, after some manipulation it can be obtained that the two are equal if the following condition is satisfied:

$$\begin{aligned} f(P, P') + \sum_{n=1}^{\infty} n c_n(P') \bar{m}_n(P') [1 - H(P, P') H_n(P'')] \\ f(P, P') [f(P, P') + \sum_{n=1}^{\infty} n c_n(P') \bar{m}_n(P')] \frac{H(P, P')}{\Theta(P')} \\ + \sum_{n=1}^{\infty} n c_n(P') \bar{m}_n(P') [f(P, P') + (n-1) H_n(P') \Theta(P')] \frac{H(P, P')}{\Theta(P')} \end{aligned} \quad (3.46)$$

Which is true for:

$$\begin{cases} H_n(P') = \frac{\sum_{n=1}^{\infty} n c_n(P') \bar{m}_n(P')}{n \Theta(P')} \\ \sum_{n=1}^{\infty} \hat{c}_n(P') = 1 \end{cases} \quad (3.47)$$

In the zero-variance game the absorption probability is zero, since all the $\hat{c}_n(P')$ are normalized to unity. Lastly, the expressions for the zero-variance kernels that was previously anticipated in Sec. 3.3 can be written.

$$\hat{T}(P, P') = \frac{T(P, P')\Theta(P')}{H(P, P')M_1(P)} \quad (3.48)$$

$$= T(P, P') \frac{f(P, P') + \bar{M}_1(P')}{M_1(P)} \quad (3.49)$$

$$= T(P, P') \frac{f(P, P') + \int dP'' C(P', P'') M_1(P'')}{M_1(P)} \quad (3.50)$$

$$\hat{C}(P', P'') = \hat{c}_c(P')\delta(P'' - \bar{P}) + \sum_{n=1}^{\infty} n\hat{c}_n(P')\hat{C}_n(P', P'') \quad (3.51)$$

$$= \sum_{n=1}^{\infty} \frac{nc_n(P')\bar{m}_n(P')}{\bar{M}_1(P')} \frac{C_n(P', P'')M_1(P'')}{\bar{m}_n(P')} \quad (3.52)$$

$$= \sum_{n=1}^{\infty} nc_n(P')C_n(P', P'') \frac{M_1(P'')}{\int dP'' C(P', P'')M_1(P'')} \quad (3.53)$$

$$= C(P', P'') \frac{M_1(P'')}{\int dP'' C(P', P'')M_1(P'')} \quad (3.54)$$

$$\hat{Q}(P) = Q(P) \frac{M_1(P)}{\int dP Q(P)M_1(P)} \quad (3.55)$$

Using the duality between the adjoint of the emission density and the first order moment of the desired estimator it is possible to retrieve the expressions described in the previous pages.

3.4.2 From an implicit capture game

We sketch now the derivation of a zero-variance MC game based on an underlying implicit capture game. Even if the starting game is not an analog game, the structure of the kernels remains almost unchanged while performing an implicit capture game. For this reason it is expected that the final version of the kernels even in the zero-variance version of this type of game to be similar to the zero-variance games derived from an analog game. In the Appendix B of this work the derivation is discussed and here only the final results are depicted. The first and second order moment of a general estimator in this kind of game were found to be equal to:

$$M_1^*(P) = \int dP' T(P, P') f(P, P') \quad (3.56)$$

$$+ \int dP' T(P, P') \int dP'' \left[c_s(P')C_s(P', P'') + c_f(P') \sum_{n=1}^{\infty} nq_n(P')C_n(P', P'') \right] M_1^*(P'')$$

$$= \int dP' T(P, P') f(P, P') + \int dP' T(P, P') \int dP'' C(P', P'') M_1^*(P'')$$

$$= M_1(P) \quad (3.57)$$

$$\begin{aligned}
M_2^*(P) = & \left[1 \int dP' T(P, P') c_s(P') \int dP'' C_s(P', P'') \frac{f^2(P, P')}{1 - c_c(P')} \right] \\
& + \left[2 \int dP' T(P, P') c_s(P') \int dP'' C_s(P', P'') f(P, P') M_1(P'') \right] \\
& + \left[1 \int dP' T(P, P') c_s(P') \int dP'' C_s(P', P'') (1 - c_c(P')) M_2^*(P'') \right] \\
& + \left[1 \int dP' T(P, P') c_f(P') \sum_{n=1}^{\infty} n q_n \int dP'' C_n(P', P'') \frac{f^2(P, P')}{1 - c_c(P')} \right] \\
& + \left[2 \int dP' T(P, P') c_f(P') \sum_{n=1}^{\infty} n q_n \int dP'' C_n(P', P'') f(P, P') M_1(P'') \right] \\
& + \left[1 \int dP' T(P, P') c_f(P') \sum_{n=1}^{\infty} n q_n \int dP'' C_n(P', P'') (1 - c_c(P')) M_2^*(P'') \right] \\
& + \int dP' T(P, P') c_f(P') \sum_{n=1}^{\infty} n(n-1) q_n (1 - c_c(P')) \left[\int dP'' C_n(P', P'') M_1(P'') \right]^2 \\
& - \int dP' T(P, P') c_f(P') \sum_{n=1}^{\infty} (n-1) q_n \frac{f^2(P, P')}{1 - c_c(P')}
\end{aligned}$$

From the first of the previous two equations it is possible to see that the expected value of the estimator is preserved, making this an unbiased game.

For the derivation of the zero-variance scheme starting from an implicit capture game, an attempt was made into mapping the modified starting rules of the game into the derivation done by Lux and Koblinger [1] and by correcting the weight of the particle in a such a way to have an unbiased way. Practically:

- the implicit capture game is derived
- with the collision kernel of this new game the zero-variance game is derived
- at the end the weight is corrected using the weight correction of both the schemes.

The results are:

$$\hat{T}^*(P, P') = T^*(P, P') \frac{f(P, P') + \int dP'' C^*(P', P'') M_1(P'')}{M_1(P)} \quad (3.58)$$

$$\hat{C}^*(P', P'') = \sum_{n=1}^{\infty} n \hat{c}_n^*(P') \hat{C}_n^*(P', P'') \quad (3.59)$$

$$= \sum_{n=1}^{\infty} n c_n^*(P') C_n^*(P', P'') \frac{M_1(P'')}{\int dP'' C^*(P', P'') M_1(P'')} \quad (3.60)$$

$$\hat{Q}^*(P) = Q(P) \frac{M_1(P)}{\int dP Q(P) M_1(P)} \quad (3.61)$$

And the weight correction after a collision is defined as:

$$W_n'' = W' \frac{c_n^*(P') C_n^*(P', P'')}{\hat{c}_n^*(P') \hat{C}_n^*(P', P'')} \quad (3.62)$$

3.4.3 From a forced fission game

The forced fission game is fundamentally different than any other game, since the event that a particle can experience are not mutually exclusive anymore: it is in fact possible for a particle to undergo scattering and fission at the same collision. The final sampling procedure must take into account also for this difference. To derive the zero-variance scheme for a game of this type it was necessary to derive new expressions for the *moments equations* since the ones used up until now were derived under the assumption of mutually exclusives events (namely scattering, fission and absorption). To the best of our knowledge, this result is novel. It will appear in *Comparison of Branching and Branchless Zero-Variance Games* (T. Gomes Ferreira, F. Rossi, A. Jinaphanh, D. Mancusi, A. Zoia) in Proc. of the M&C2025 conference. The full derivation can be found into the Appendix C of this work, and the final results are:

$$\hat{T}^{FF}(P, P') = T(P, P') \frac{f(P, P') + \int dP'' C^{FF}(P', P'') M_1(P'')}{M_1(P)} \quad (3.63)$$

$$\hat{C}_s^{FF}(P') = C_s(P', P'') \frac{M_1(P'')}{\int dP'' C_s(P', P'') M_1(P'')} \quad (3.64)$$

$$\hat{C}_n^{FF}(P') = C_n(P', P'') \frac{M_1(P'')}{\int dP'' C_n(P', P'') M_1(P'')} \quad (3.65)$$

And the weight correction rules for a collision event are:

$$W'' = W' \frac{c_s(P') C_s(P', P'')}{\hat{C}_s^{FF}(P', P'')} \quad (3.66)$$

$$W''_n = W' \frac{c_f(P') q_n(P') C_n(P', P'')}{\hat{q}_n^{FF}(P') \hat{C}_n^{FF}(P', P'')} \quad (3.67)$$

3.4.4 On the final variance

As seen, the condition for a Monte Carlo game to be zero variance is:

$$\frac{\hat{M}_2(P)}{\hat{M}_1(P)} = \hat{M}_1(P) \quad (3.68)$$

but the first order moment will be conserved regardless of the original game. So it follows that:

$$M_1(P) = M_1^*(P) = M_1^{FF}(P) = \hat{M}_1(P) = \hat{M}_1^*(P) = \hat{M}_1^{FF}(P) \quad (3.69)$$

where we used the symbol * to indicate an implicit capture game, ^{FF} to indicate a forced fission game and ^ to indicate the associated zero variance moment. It follows directly that the second order moment will also be the same, since the zero variance condition is always the same.

$$\hat{M}_2(P) = \hat{M}_2^*(P) = \hat{M}_2^{FF}(P) \quad (3.70)$$

The moment equations and the resulting zero-variance schemes hold true if no population control methods are present: in other words the weight cutoff of the Russian roulette has to be zero. In the case of non-negligible population control, the scheme implemented will not be a zero-variance scheme. Practically speaking, however, population control is highly recommended, or even mandatory when immortal particles can be produced in zero-variance schemes. Thus, the said threshold can be thought as a "convergence" parameter and the different games can have a different "convergence" trend toward the zero-variance regime with respect to the weight cutoff of the Russian roulette [13].

Chapter 4

The MGMC code

4.1 General description

MGMC is the name for a 3D, multi-group Monte Carlo transport code which solves the Boltzmann neutron transport equation for *fixed-source*, *k-eigenvalue*, and *neutron-noise* problems with different particle tracking method like *Surface tracking*, *Delta tracking*, and *Carter tracking*. This code is being developed by the CEA in order to investigate the usefulness of branchless schemes for Monte Carlo simulations. The geometry, the physical parameters and the simulations setup are all controlled by a single *YAML* input file and parsed by the code. Some of the most basic inputs are the number of particles and the number of replicas (or batches) used during the simulation. Various tallies can also be added to the input file to score different physical quantities, such as *neutron flux*, *reaction rates* and more.

It is possible also to use the code in a *parallel thread mode*: using the OpenMP shared memory setting it is possible to use computational threads, then letting all of them run independently and at the end of all the simulations assemble the results. The advantage of doing so lies in the fact that it is possible to run several particle histories in parallel, tracking each one of them and obtain the results faster.

Compared to the branchless simulation which are possible inside MGMC, the branching one require a bit more care for some peculiar aspects. In the next section these aspects will be better investigated without explaining in an excessive way in the coding part, in order to not weight too much this work and to respect the industrial property of the CEA.

4.2 Population and weighted population tallies

The branching Monte Carlo simulations are characterized by an increase in the total population due to the presence of multiplicative phenomena. Even with the thread parallelism added by OpenMP it is very much possible that inside each one of the threads the population can grow so much the total run time increases exponentially to very high numbers. In the following sections the relevance of this aspect will be better explained, but for now it should be understood that tracking the total population evolution is of utmost relevance in this type of games. To do so two new tallies have been implemented: the *population* and *weighted population* tallies which make use of some new attributes added to the particle information. Every particle is in fact characterized by some basic information, like its phase space coordinate, and by some other secondary information, *e.g* the spatial coordinate of the previous collision, the Boolean variable that defines its state. The new secondary information added concern the generation and the death of the particle and they can be summed up as:

- Birth generation: it is the generation in which a particle was born. All the source particle will have a birth generation of 0.
- Type of birth: it is used to determine the type of reaction that generate the particle. Thanks to it is possible to differentiate between a source particle, a particle born from a fission event and a particle born from a splitting event.
- Survived generations: it is the number of collision a particle has survived. Every particle starts with 0 and if they are alive at the end of the collision routine this number is increased.
- Type of death: it is used to determine the type of reaction that terminated the particle history. Thanks to this it was possible to know if a particle was captured, was the parent of a fission reaction or if its history was terminated by a Russian roulette.

With these new information, at the end of every collision routine it is possible to keep track of the particle still alive in two different ways: counting the total absolute number of particle alive (using the *Population tally*) or counting the total weight of the particle alive (using the *Weighted Population tally*). To have a more clear idea of the structure of the routine implemented by MGMC it is possible to look at the Figure 4.1.

4.3 Additions to the input files

With MGMC every aspect of the simulation is controlled by the input file so it necessary to provide all the simulation setups inside it. Some of the already existing inputs are:

- Simulation type
- Number of particles per batch
- Number of batches
- Setups for the Russian roulette
- Setups for the biasing
- Sources and physical media position and properties

In order to be able to control even more aspects of the simulation, some more inputs were implemented:

- Implicit capture input flag: if set to *True* the simulation will use an implicit capture scheme
- Forced fission input flag: if set to *True* the simulation will use an forced fission scheme
- Maximum length of the population tally vector: it is used to pre-allocate the memory for the population and weighted population tallies
- Type of fission children probability density function: by default this function is set to a *2-bins distribution* but it is possible to change it to a *Poisson distribution* or a different one.

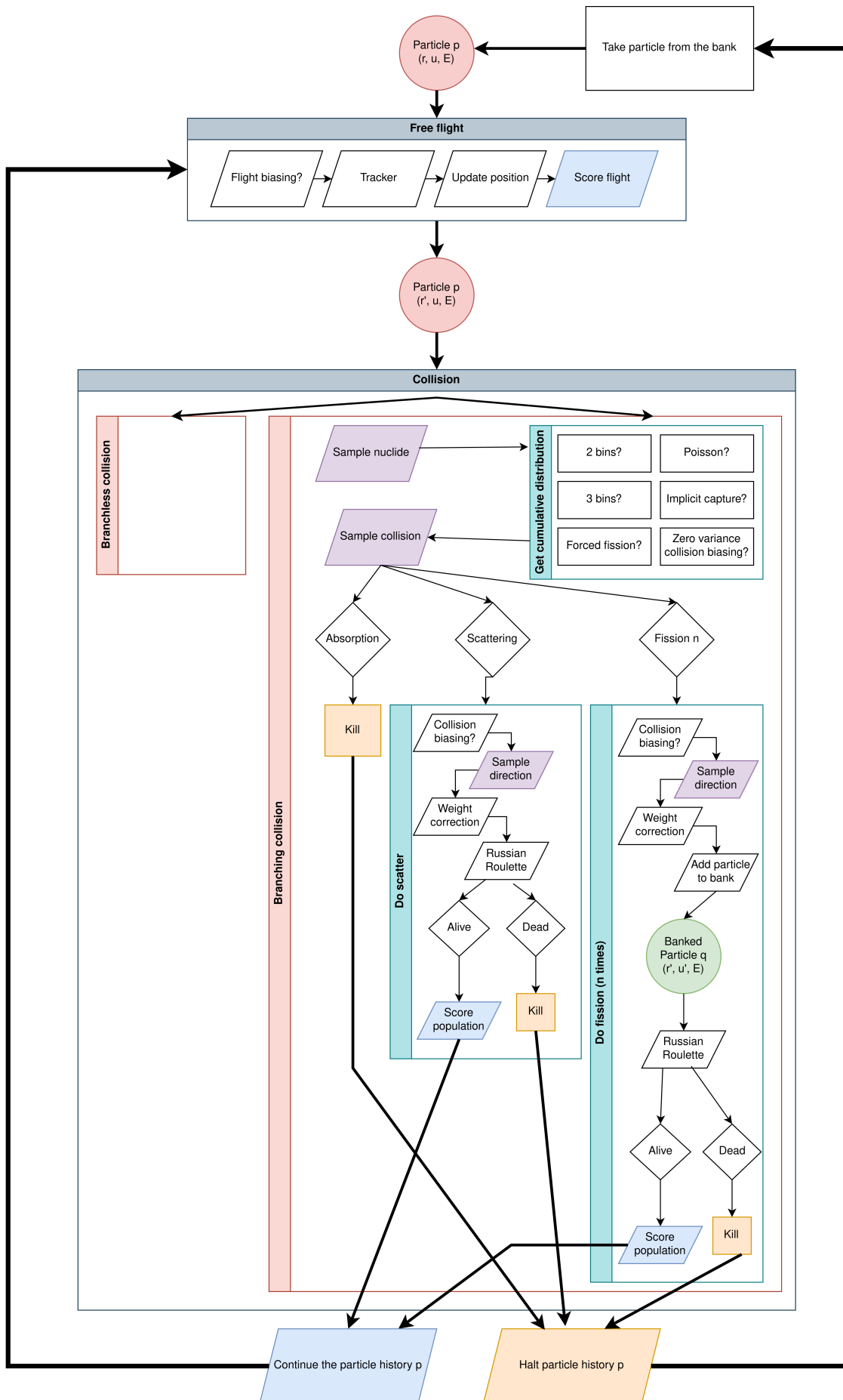


Figure 4.1: Routine followed by MGMC with focus on the branching collisions

Chapter 5

Simulations and results

After implementing the zero-variance branching schemes, we aimed to evaluate their performance across a series of benchmark configurations. This chapter outlines the selected configurations and presents the simulation results obtained for each case.

5.1 Case A

The first geometrical configuration under investigation includes a single fissile medium with a neutron source surrounded on every side by non fissile media. To simplify the derivation of the analytical solutions it was also supposed:

- to have a 1-D bi-directional problem;
- to have a mono-energetic problem;
- to have a stationary problem.

The problem under these assumptions becomes rather simple, but this was done in order to have a straightforward derivation of the analytical solutions, which are necessary both for the zero-variance kernels and as benchmarks for the Monte Carlo results. In the Figure 5.1 the geometrical configuration is depicted.

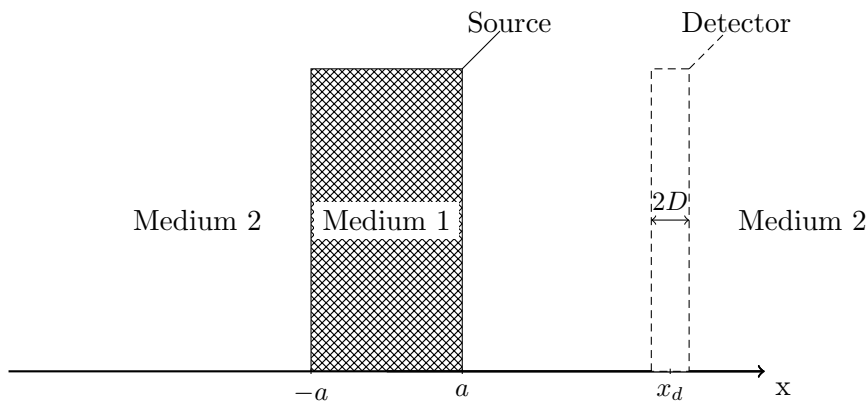


Figure 5.1: Case A geometry: the fissile Medium 1, the absorbing Medium 2, as well as the source and the detector are highlighted

The coordinates of the different planes in the figure are:

- $a = 5 \text{ cm}$;
- $x_d = 15.5 \text{ cm}$;

- $2D = 1 \text{ cm}$

To see the effect of a single physical parameter, in the following simulations, the most relevant ones were changed one at a time keeping the other parameters constant.

5.1.1 Analytical results

The analytical solution is derived with a deterministic method that approximates the direction of flight with two discrete directions, one positive one negative, along the same axis. This simplification allows the total flux to be represented as the sum of the positive and negative angular fluxes, while their difference corresponds to the net neutron current. Although reliant on simplifying assumptions (mono-dimensional, stationary and mono-energetic problem) this solution is able to describe anisotropic scattering processes. Under these assumptions, the Boltzmann equation for the flux $\phi(x, \mu)$ with the two directions being $\mu = \pm 1$ takes the form of:

$$\begin{aligned} \mu \frac{d}{dx} \phi(x, \mu) + \Sigma_t(x) \phi(x, \mu) &= \Sigma_s(x) \sum_{\mu'=(\pm 1)} \phi(x, \mu') f_s(x, \mu' \rightarrow \mu) \\ &+ \nu_f(x) \Sigma_f(x) \sum_{\mu'=(\pm 1)} \phi(x, \mu') f_f(x, \mu' \rightarrow \mu) + Q(x, \mu) \end{aligned} \quad (5.1)$$

Where $\phi(x, \mu)$ is the angular flux.

After some manipulation the equation for the scalar flux $\phi(x)$ is:

$$-\frac{1}{\Sigma_{tr}(x)} \frac{d^2 \phi(x)}{dx^2} + \Sigma_e(x) \phi(x) = q(x) \quad (5.2)$$

where:

$$\Sigma_{tr}(x) = \Sigma_t(x) - \nu_{cd}(x) \hat{\mu}_{cd}(x) \Sigma_{cd}(x) \quad (5.3)$$

$$\nu_{cd}(x) = \frac{\Sigma_s(x) + \nu_f(x) \Sigma_f(x)}{\Sigma_s(x) + \Sigma_f(x)} \quad (5.4)$$

$$\hat{\mu}_{cd}(x) = \frac{\bar{\mu}_s(x) \Sigma_s(x) + \bar{\mu}_f(x) \Sigma_f(x) \nu_f(x)}{\Sigma_s(x) + \nu_f(x) \Sigma_f(x)} \quad (5.5)$$

$$\Sigma_{cd}(x) = \Sigma_s(x) + \Sigma_f(x) \quad (5.6)$$

$$\Sigma_e(x) = \Sigma_t(x) - \nu_{cd}(x) \Sigma_{cd}(x) \quad (5.7)$$

Then the solution can be found using the symmetry of along the x-axis for the multiplicative media and the infinite boundary conditions for the second media. Using the same notation as above, namely:

- $x = -a \rightarrow$ left interface between the two media
- $x = a \rightarrow$ right interface between the two media
- $x = D_{begin} \rightarrow$ left coordinate of the detector
- $x = D_{end} \rightarrow$ right coordinate of the detector

then:

$$\phi(x) = \begin{cases} \frac{1}{2a\Sigma_{e,1}} + C_1 \cos(\beta x) & \text{if } |x| < a \\ C_2 \exp(-\sqrt{\Sigma_{tr,2}\Sigma_{e,2}}|x|) & \text{if } |x| \geq a \end{cases} \quad (5.8)$$

The constants C_1 and C_2 can be found by imposing the continuity of the neutron flux and current at the interface.

The detector response is:

$$R = \int dx \eta_\phi \phi(x) = \int dx \frac{1}{D_{end} - D_{beginning}} \phi(x) \quad (5.9)$$

The expression of the importance equation is:

$$-\frac{1}{\Sigma_{tr}(x)} \frac{d^2 \chi^\dagger(x)}{dx^2} + \Sigma_e(x) \chi^\dagger(x) = \eta_\phi(x) \quad (5.10)$$

$$\chi^\dagger(x) = \begin{cases} B_1 \exp(\sqrt{\Sigma_{tr,2}\Sigma_{e,2}}x) & \text{if } x < -a \\ A_2 \cos(\beta x) + B_2 \sin(\beta x) & \text{if } |x| < a \\ A_3 \exp(-\sqrt{\Sigma_{tr,2}\Sigma_{e,2}}x) + B_3 \exp(\sqrt{\Sigma_{tr,2}\Sigma_{e,2}}x) & \text{if } x > a \wedge x < D_{beginning} \\ \frac{1}{\Sigma_{e,2}(D_{end} - D_{beginning})} + A_4 \exp(-\sqrt{\Sigma_{tr,2}\Sigma_{e,2}}x) \\ \quad + B_4 \exp(\sqrt{\Sigma_{tr,2}\Sigma_{e,2}}x) & \text{if } x > D_{beginning} \wedge x < D_{end} \\ A_5 \exp(-\sqrt{\Sigma_{tr,2}\Sigma_{e,2}}x) & \text{if } x > D_{end} \end{cases} \quad (5.11)$$

In the Figures 5.2 and 5.3 the analytical solutions of the flux and importance for varying fission cross section of the first media are represented. The most remarkable effect of increasing the fission cross section is the increase in the peak of the flux inside the fissile media; increasing the fission cross section has instead a smaller effect for the importance shape primarily because the detector region has such a high importance compared to the fissile media (notice that the importance plot is in log scale).

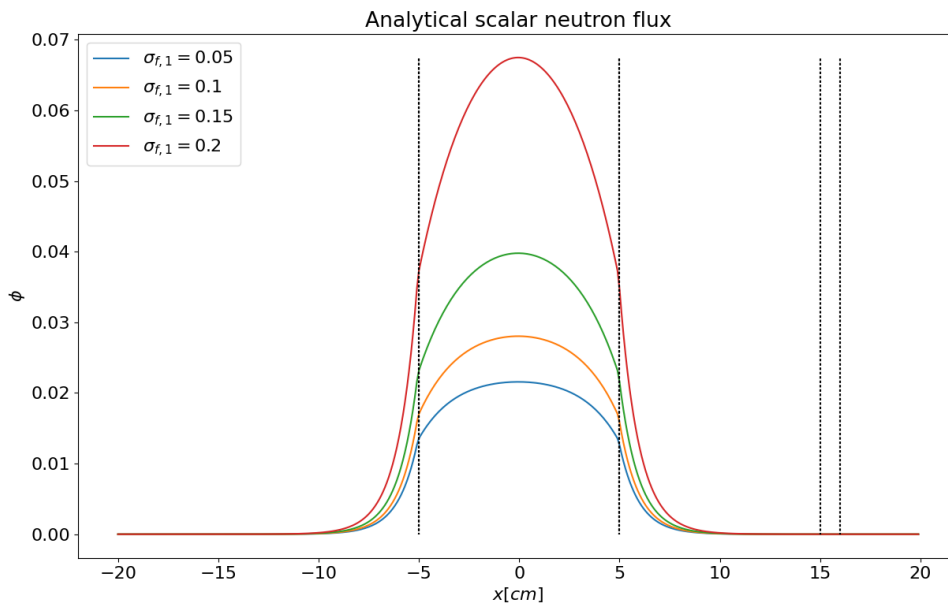


Figure 5.2: Case A: Analytical scalar flux

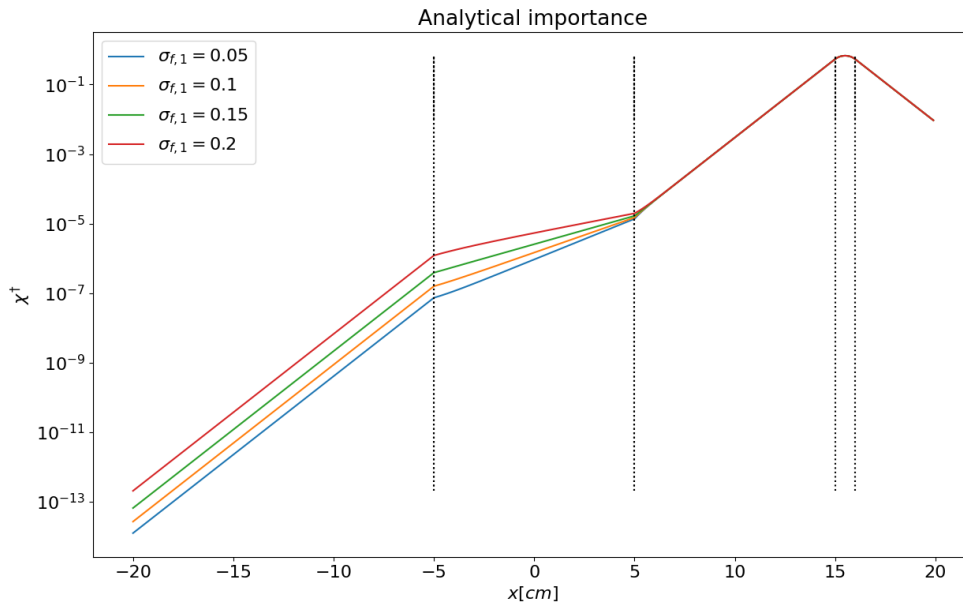


Figure 5.3: Case A: Analytical scalar importance

5.1.2 Analog and branchless zero variance

The purely analog and branchless zero-variance simulations are used as references for the branching zero variance simulations. In Table 5.1 the simulation parameters of *Case A* have been summed up.

	$\Sigma_t[cm^{-1}]$	$\Sigma_s[cm^{-1}]$	$\Sigma_a[cm^{-1}]$	$\Sigma_f[cm^{-1}]$	$\nu_f[-]$	$\nu_s[-]$	$\bar{\mu}_s[-]$	$\bar{\mu}_f[-]$
Medium 1	1.0	0.45	0.55	0.10/0.15/0.20	2.25	1.0	0.75	0.0
Medium 2	3.0	2.4	0.6	0.0	0.0	1.0	0.5	0.0

Table 5.1: Case A physical parameters

Important is to notice that by increasing the fission cross section also the k_{eff} of the system is changing, creating much more particles from fission phenomena and thus moving toward a critical system. As seen later on, the degree of criticality of the system will play a big role in determining the efficiency of the zero variance branching methods. The k_{eff} of the system for the different simulations setups were derived with the same code used, but changing the simulation mode from *fixed source* (or *branchless fixed source* when running the branchless simulations) to *branchless k eigenvalue*. Table 5.2 sums up the values of the k_{eff} of the system in the three different simulation runs considered.

Simulation	$\Sigma_{f,1}[cm^{-1}]$	k_{eff}
Run 1	0.10	0.363942 ± 0.000219
Run 2	0.15	0.545823 ± 0.000285
Run 3	0.20	0.727533 ± 0.000319

Table 5.2: Case A k_{eff} of the system in the different simulations

We now present the results of the simulations aimed at estimating the detector response using the zero-variance branchless approach. Table 5.3 summarizes these results, obtained by varying key parameters such as the number of particles, batches, and cutoff values. For each configuration, three independent runs with three different values of k_{eff} were performed, to better investigate how the schemes behaves when the particle production due to fission is increased. The table reports the Student t-test (STT) values, which evaluate the consistency between runs, and the associated detector error. The Student t-test checks the statistical significance of the results, with values near zero indicating consistency across runs, while deviations outside the acceptable range of ± 3 highlight potential issues in the simulation stability or accuracy [7].

$$STT = \frac{R_{average} - R_{analytical}}{\sigma/\sqrt{N}} \quad (5.12)$$

Red-highlighted rows mark the first cutoff where the test fails, along with additional exploratory runs.

Branchless zero-variance

Cutoff	N° particles			N° batches			STT			Detector error		
	<i>RUN 1</i>	<i>RUN 2</i>	<i>RUN 3</i>	<i>RUN 1</i>	<i>RUN 2</i>	<i>RUN 3</i>	<i>RUN 1</i>	<i>RUN 2</i>	<i>RUN 3</i>	<i>RUN 1</i>	<i>RUN 2</i>	<i>RUN 3</i>
10^{-1}	10000	10000	10000	500	500	500	9.51×10^{-1}	6.30×10^{-1}	-1.40	1.85×10^{-10}	2.25×10^{-10}	3.86×10^{-10}
10^{-2}	10000	10000	10000	500	500	500	6.86×10^{-1}	-7.54×10^{-1}	-1.74	1.66×10^{-11}	2.28×10^{-11}	3.84×10^{-11}
10^{-3}	10000	10000	10000	500	500	500	-8.23×10^{-1}	-5.94×10^{-1}	-3.29×10^{-1}	1.77×10^{-12}	2.43×10^{-12}	3.81×10^{-12}
10^{-4}	10000	10000	10000	500	500	500	-8.26×10^{-1}	-8.64×10^{-1}	-5.96×10^{-1}	1.74×10^{-13}	2.39×10^{-13}	3.80×10^{-13}
10^{-5}	10000	10000	10000	500	500	500	-2.26×10^{-1}	-3.61×10^{-1}	2.59×10^{-2}	1.79×10^{-14}	2.34×10^{-14}	3.65×10^{-14}
10^{-6}	10000	10000	10000	500	500	500	-3.47×10^{-1}	-3.54×10^{-1}	-9.61×10^{-1}	1.79×10^{-15}	2.43×10^{-15}	3.72×10^{-15}
10^{-7}	10000	10000	10000	500	500	500	-1.46	-1.18	1.73×10^{-1}	1.74×10^{-16}	2.52×10^{-16}	3.70×10^{-16}
10^{-8}	10000	10000	10000	500	500	500	-1.52	-5.12×10^{-1}	-4.91×10^{-1}	1.78×10^{-17}	2.35×10^{-17}	3.80×10^{-17}
10^{-9}	10000	10000	10000	500	500	500	1.38×10^{-1}	-3.64×10^{-1}	-9.22×10^{-1}	1.75×10^{-18}	2.32×10^{-18}	3.82×10^{-18}
10^{-10}	10000	10000	10000	500	500	500	-7.66×10^{-1}	-1.07×10^{-2}	2.99×10^{-1}	1.76×10^{-19}	2.38×10^{-19}	3.77×10^{-19}
10^{-11}	10000	10000	10000	500	500	500	-1.30×10^1	-5.89	6.76	1.65×10^{-20}	2.43×10^{-20}	3.71×10^{-20}
10^{-12}	10000	10000	10000	500	500	500	-1.37×10^{-1}	3.80×10^1	2.65	3.10×10^{-21}	4.55×10^{-21}	6.72×10^{-21}
10^{-13}	10000	10000	10000	500	500	500	6.10×10^2	5.88×10^2	6.22×10^2	2.72×10^{-21}	3.89×10^{-21}	5.61×10^{-21}

Table 5.3: Case A1: Detector error and Student t-test of the detector response for the zero variance branchless simulations. In red are highlighted the first run in which the test fails and eventually some extra runs.

It can be observed that by decreasing the weight cutoff in population control algorithms, the detector error effectively reduces to the level of machine precision (approximately 10^{-16} for the system used in these simulations). This precision is achieved with a weight cutoff of at least 10^{-7} . Notably, for the lowest weight cutoffs, the Student's t-test yields values significantly outside the typically accepted range of ± 3 . This anomaly occurs because the denominator in the t-test calculation is the detector response error, which can approach machine precision due to the zero-variance scheme implemented. As the error becomes exceedingly small, the test fails, resulting in excessively large values. This indicates that the zero-variance scheme has been highly effective, limited only by the machine's precision. The following Figures offer a comprehensive view of the scalar neutron flux in the region of interest and the evolution of the total population weight across generations: Figure 5.4 compares the scalar flux from zero-variance branchless schemes with the purely analog and analytical solutions, Figure 5.6 shows the STT values for the Monte Carlo flux estimates across the domain, with an acceptable range of ± 3 , Figure 5.5 illustrates the relative variance of the flux estimates while Figure 5.7 tracks the evolution of the weighted population over generations for each scheme.

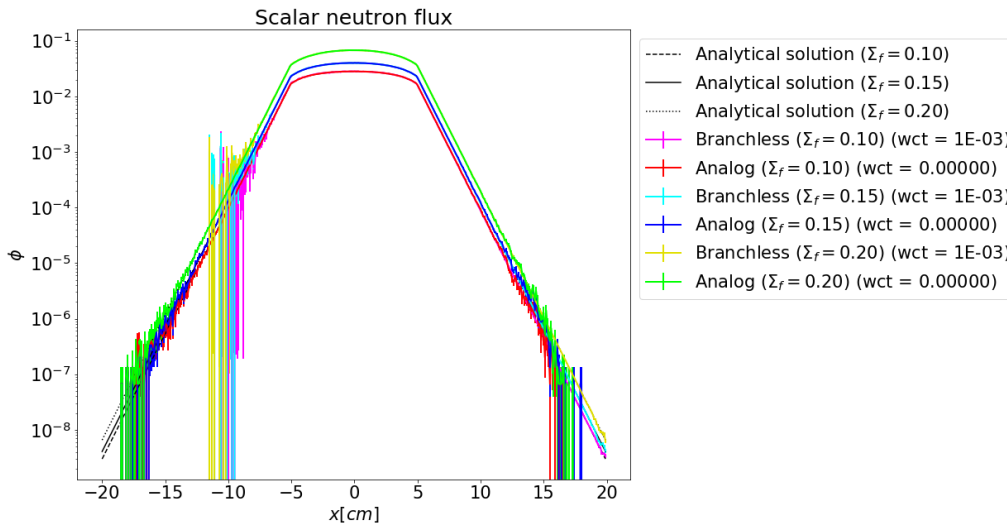


Figure 5.4: Case A1: scalar neutron flux comparison

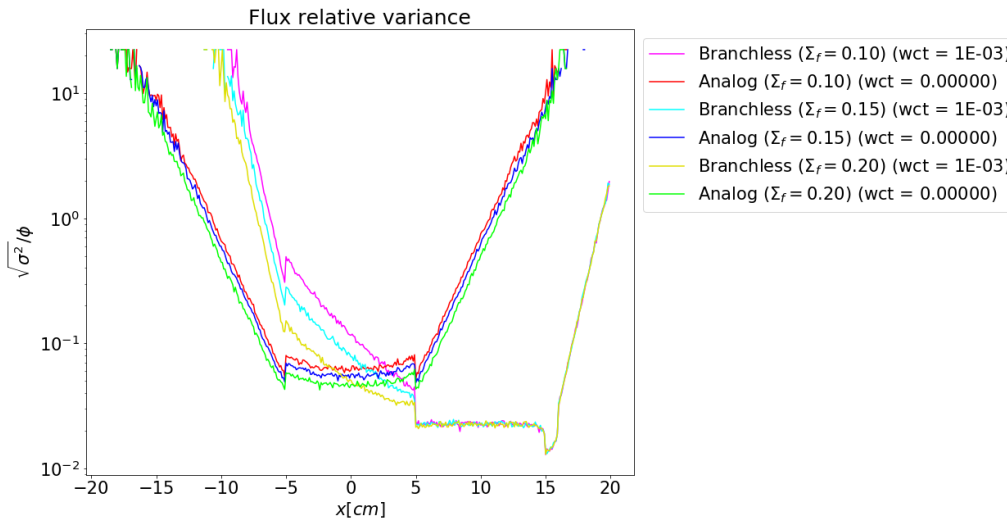


Figure 5.5: Case A1: scalar neutron flux relative variance comparison

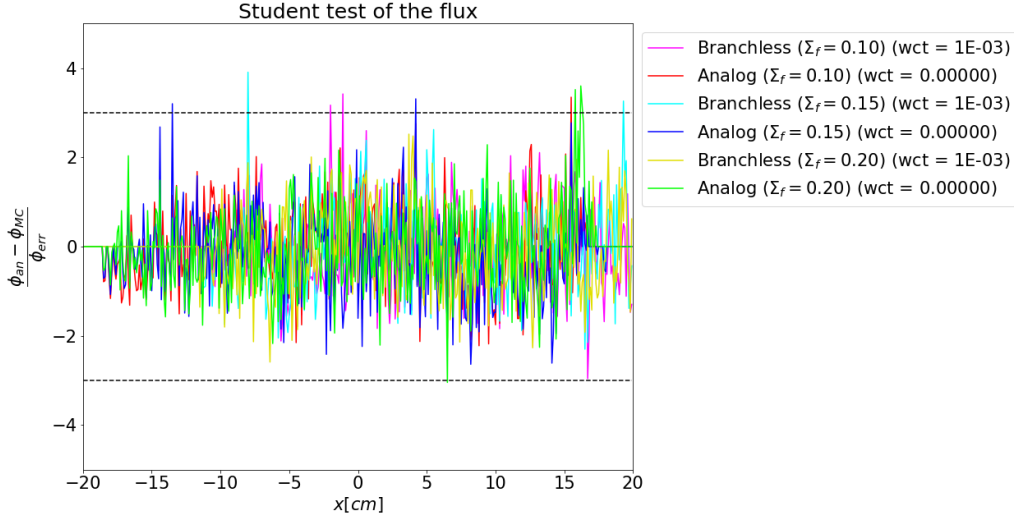


Figure 5.6: Case A1: Student t-test of the scalar neutron flux comparison

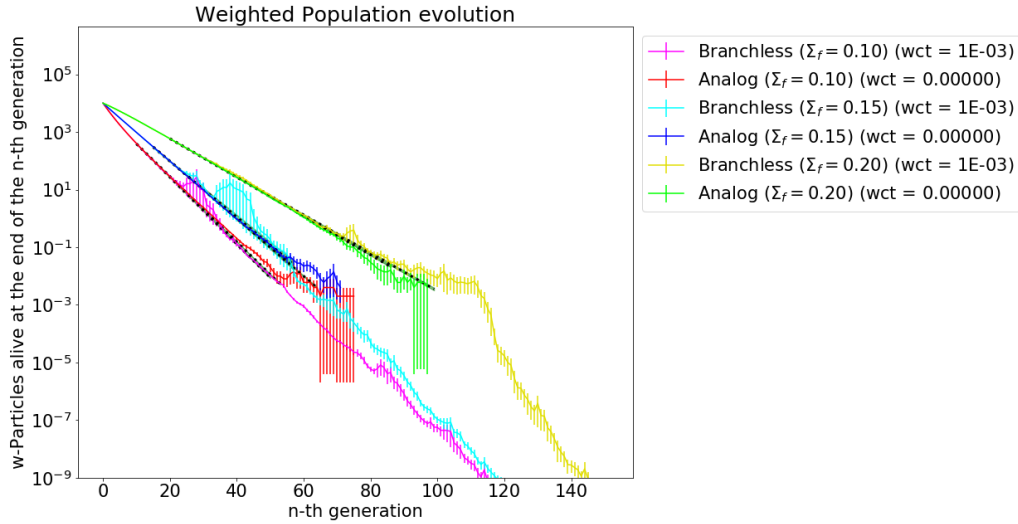


Figure 5.7: Case A1: weighted population evolution comparison

5.1.3 Branching zero variance: analog game

In this section, a comparison is made between the branching zero-variance schemes derived from analog simulations and the reference branchless zero-variance simulations. In the following figures, the branching scheme under investigation is referred to as "*2-bins Branching*". This specification is necessary, as the performance of the branching scheme depends on the fission children probability density function—specifically, the probability of generating n outgoing fission particles (previously denoted by q_n). For the simulations discussed here, the fission children probability density function was constructed in the simplest form as depicted in Table 5.4:

n outgoing particles	q_n
$\lfloor \nu_f \rfloor = 2$	$\lceil \nu_f \rceil - \nu_f = 0.75$
$\lceil \nu_f \rceil = 3$	$\nu_f - \lfloor \nu_f \rfloor = 0.25$

Table 5.4: 2-bins branching scheme fission children probabilities

The advantage of using the integer part of the average number of fission neutrons is that this formulation is valid regardless of the actual numerical value of ν_f . In a similar way to what was done previously for the zero-variance branchless and purely analog simulations, Figures 5.8, 5.9, 5.10 and 5.11 offer a general overview of the scalar neutron flux across the domain and of the evolution of the total weighted population of the system.

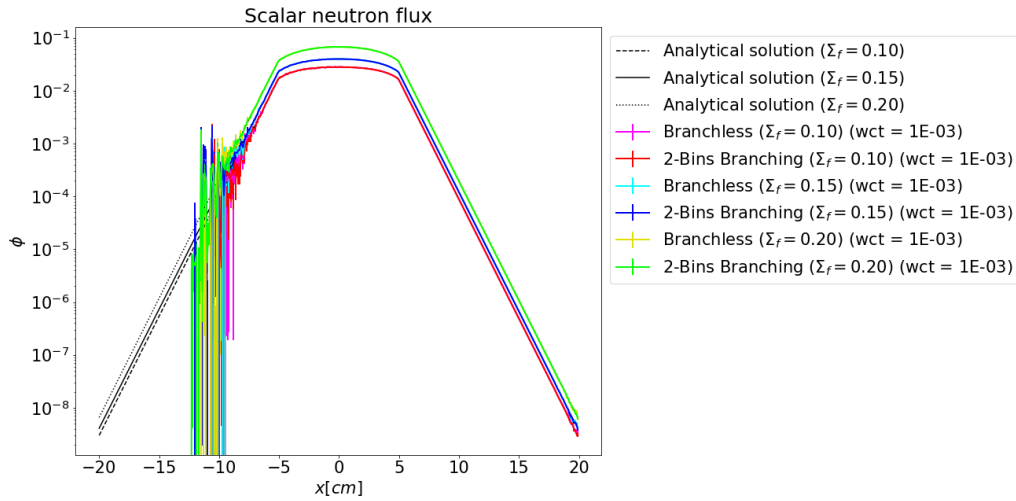


Figure 5.8: Case A2: scalar neutron flux comparison

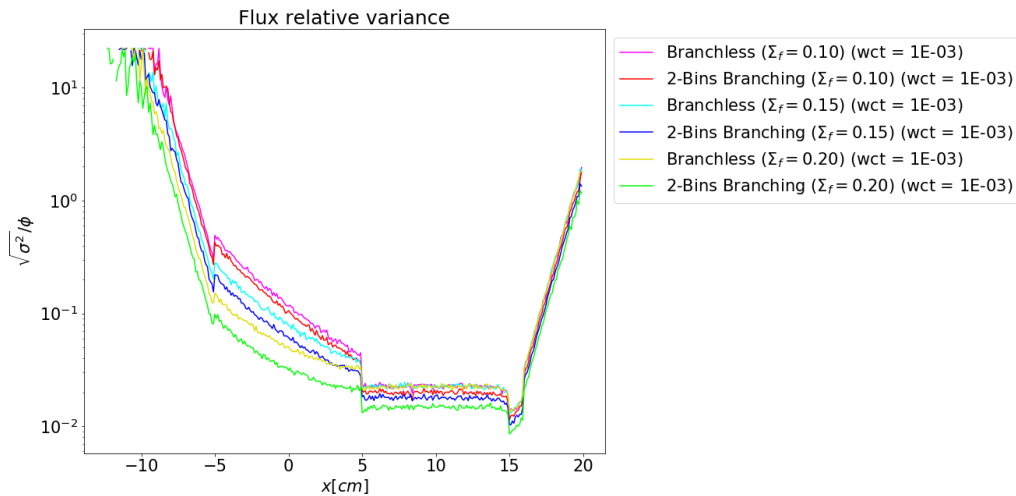


Figure 5.9: Case A2: scalar neutron flux relative variance comparison

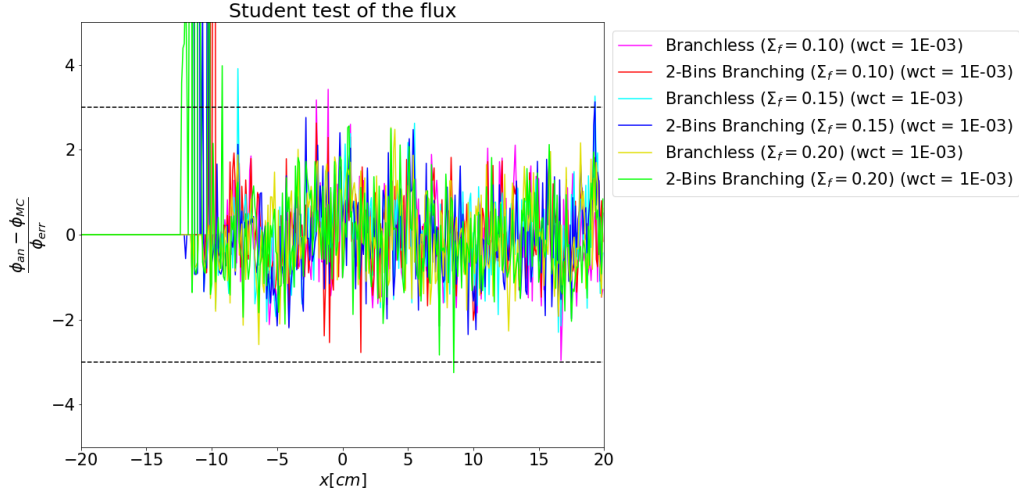


Figure 5.10: Case A2: Student t-test of the scalar neutron flux comparison

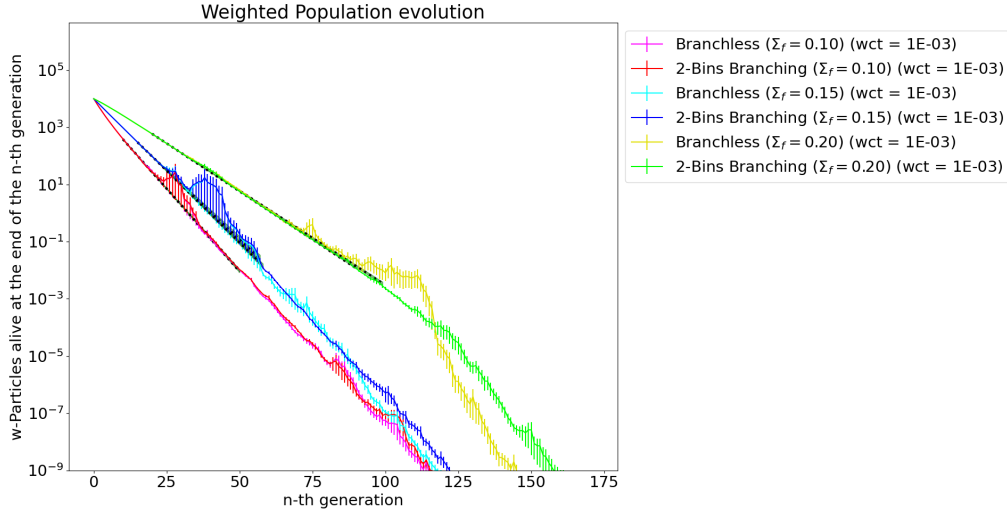


Figure 5.11: Case A2: weighted population evolution comparison

In the simulation called *RUN 3* in order to speed up the calculations, it was decided to reduce the number of particles and batches for the runs with a lower value of weight cutoff. This decision was deemed necessary since the time spent to finish each run grows greatly with the number of particles present in the system, and this effect has proven to be greatly dependent on the k_{eff} of the system. For this reason the results of the second half of the simulations for the *RUN 3* set have a different number of particles and batches. If the games are unbiased, this choice should not affect the Student t-test results but it will affect the detector error trend towards the zero-variance. To account for this practical limitation and to still have a complete trend, even for the simulations with a lower number of source particles and batches it was decided to rescale the error of the detector response to have the same number of starting particles histories. Results of this type will be highlighted with the * symbol in the Table 5.5 which sums up all the results: this Table follows what has been done in Table 5.3 and depicts the detector error trend and the STT trend for the different simulations runs with varying cutoff values.

Branching analog zero-variance

Cutoff	N° particles			N° batches			STT			Detector error		
	<i>RUN 1</i>	<i>RUN 2</i>	<i>RUN 3</i>	<i>RUN 1</i>	<i>RUN 2</i>	<i>RUN 3</i>	<i>RUN 1</i>	<i>RUN 2</i>	<i>RUN 3</i>	<i>RUN 1</i>	<i>RUN 2</i>	<i>RUN 3</i>
10^{-1}	10000	10000	10000	500	500	500	6.66×10^{-1}	-1.33	5.32×10^{-1}	2.66×10^{-10}	4.95×10^{-10}	1.30×10^{-9}
10^{-2}	10000	10000	10000	500	500	500	-1.41×10^{-1}	1.45×10^{-2}	-7.77×10^{-1}	3.01×10^{-11}	7.56×10^{-11}	2.71×10^{-10}
10^{-3}	10000	10000	10000	500	500	500	-1.48	-7.27×10^{-1}	1.78	2.92×10^{-12}	1.06×10^{-11}	5.31×10^{-11}
10^{-4}	10000	10000	10000	500	500	500	2.12×10^{-1}	9.80×10^{-2}	-7.34×10^{-1}	3.20×10^{-13}	1.51×10^{-12}	1.12×10^{-11}
10^{-5}	10000	10000	10000	500	500	500	-6.60×10^{-1}	-1.29	-1.24	3.21×10^{-14}	2.11×10^{-13}	2.61×10^{-12}
10^{-6}	10000	10000	10000	500	500	500	3.03×10^{-1}	-1.46	-8.10×10^{-1}	3.26×10^{-15}	3.03×10^{-14}	6.92×10^{-13}
10^{-7}	10000	10000	10000	500	500	5	-4.47×10^{-2}	7.85×10^{-1}	1.69×10^{-1}	3.29×10^{-16}	3.95×10^{-15}	3.37×10^{-13} *
10^{-8}	10000	10000	10000	500	500	5	-2.36	1.10	3.80×10^{-3}	3.15×10^{-17}	5.63×10^{-16}	1.42×10^{-13} *
10^{-9}	10000	10000	10000	500	500	5	6.66×10^{-1}	9.30×10^{-1}	-2.58×10^{-1}	3.30×10^{-18}	7.87×10^{-17}	5.08×10^{-14} *
10^{-10}	10000	10000	100	500	500	5	6.15×10^{-1}	-7.14	3.46	3.29×10^{-19}	1.12×10^{-17}	8.83×10^{-16} *
10^{-11}	10000	10000	10	500	500	5	-2.47×10^1	-2.77×10^2	1.02	3.38×10^{-20}	2.33×10^{-18}	1.29×10^{-16} *
10^{-12}	10000	10000	1	500	500	5	5.87	9.95×10^1	-2.99×10^{-1}	6.20×10^{-21}	1.57×10^{-17}	3.80×10^{-17} *
10^{-13}	10000	-	-	500	-	-	5.28×10^2	-	-	1.24×10^{-20}	-	-

Table 5.5: Case A2: Detector error and Student t-test of the detector response for the zero variance branching simulations. In red are highlighted the first run in which the test fails and eventually some extra runs.

Preliminary conclusions

It is possible to draw the following conclusions:

- By comparing the relative variance of the flux in Figure 5.5, it is evident that transitioning from the purely analog scheme to the zero-variance scheme leads to a significant change in the variance profile. In the analog simulations, the minimum relative variance is observed in the fissile medium, where source particles originate and new particles are produced. However, in the zero-variance scheme, the minimum relative variance shifts to the region near the detector, as a result of the biasing process that directs particles toward regions of higher importance.
- Comparing the flux estimates in Figure 5.8, both the zero-variance branchless and branching schemes fail to provide accurate solutions in the region $x \in [-15, -10]$ cm and do not provide estimates for $x < -15$ cm. This behavior originates from the importance-based biasing of the physical processes, which directs particles toward regions of higher importance, leaving areas of lower importance sparsely sampled.
- In Figure 5.9, the region with the lowest variance for both the zero-variance branchless and branching schemes is located near the detector, consistent with the observations above. Furthermore, the branching scheme presents a slightly lower variance than the branchless scheme due to the higher number of simulated particles, which increases the overall statistical information.
- The evolution of the weighted particle population, as shown in Figure 5.11, is independent of the scheme employed and is solely influenced by the physical and geometrical parameters of the system.
- A comparison of the detector response errors in Tables 5.3 and 5.5 reveals that achieving zero variance becomes increasingly challenging for zero-variance branching schemes as the fission cross-section increases. Also, the rate at which zero variance is reached appears to be dependent on the system's k_{eff} : in fact, as the criticality increases, the convergence to zero variance slows in relation to the cutoff, while for zero-variance branchless schemes, the "convergence" speed remains nearly unaffected by variations in k_{eff} .
- Finally, the results of the two Student t-tests on the flux and detector response, shown in Figures 5.6, 5.10, and Tables 5.3, 5.5, confirm that the implemented schemes are unbiased, at least in regions of higher importance.

An additional aspect worth considering is the computational time: from all of the previous graphs, the computational cost of the two schemes was mentioned but not deeply analyzed. In general, the branching schemes will always have a higher computational cost than the branchless ones, since more particles to be simulated than the original source particle are added to the system so the number of collisions and free flights will increase exponentially. The total number of interactions will also depend on the k_{eff} of the system and on the sampling strategy for the fission children probability density function. This increase will however face a halt if the system is subcritical, so if $k_{eff} < 1$. The comparison of the simulation times is presented in Figure 5.12 where it is possible to see the almost exponential trend for the time increase of the branching simulations. For the simulations in the *RUN 3* set with a lower amount of source particles and batches, the total simulation time has been rescaled in order to have a more faithful comparison. Doing this it is also possible to see how much time the full simulations would have taken to complete: with a quick calculation, the run with the lowest cutoff of the *RUN 3* would have taken

approximately 31 years if 10000 source particles and 500 batches were simulated (see Figure 5.12).

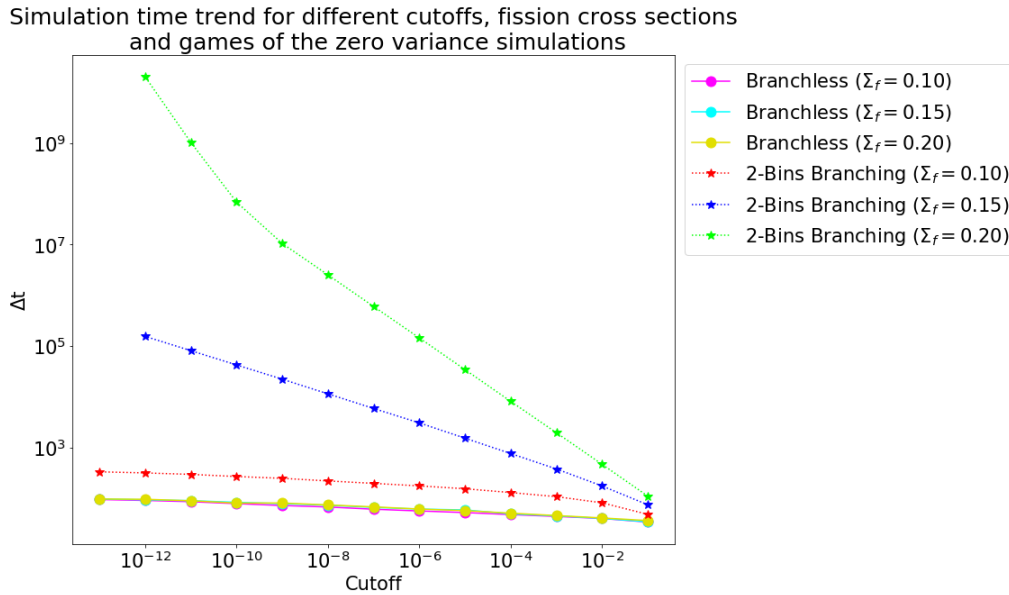


Figure 5.12: Case A2: simulation times for the branching zero variance and branchless zero variance simulations

In Figure 5.13 the population evolution has been depicted for both the zero-variance branchless and branching simulations. While the branching simulations experience an increase in the total population, the branchless ones, precisely because of how they were built, do not see an increase in the population.

It is also interesting to observe how the maximum population value varies across the different branching simulations. For this purpose, the graph in Figure 5.14 was created. With the aid of this Figure the reader can also have a rough idea of the orders of magnitude related to the population sizes: depending on the system configuration it is in fact possible to increase the population from 1000 particles to 10^{11} particles.

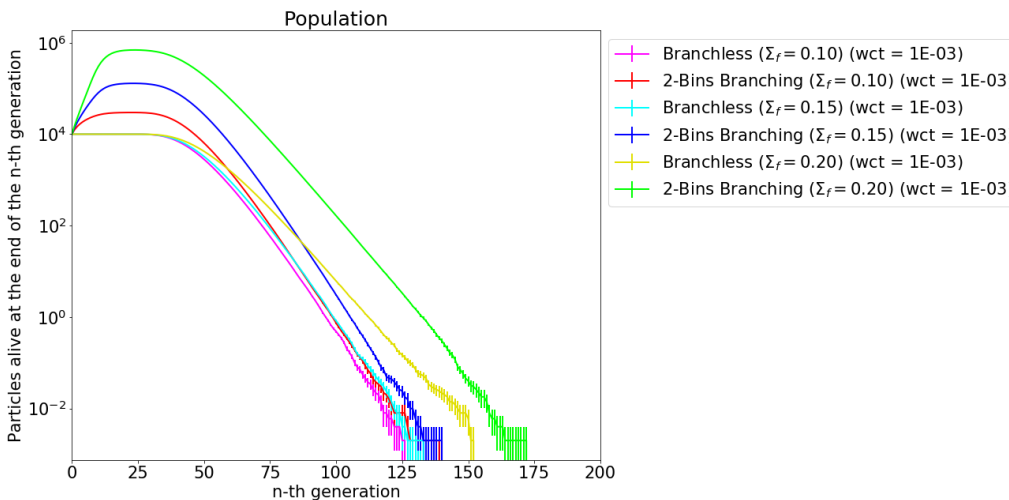


Figure 5.13: Case A2: evolution of the population for the branching zero-variance and branchless zero-variance simulations

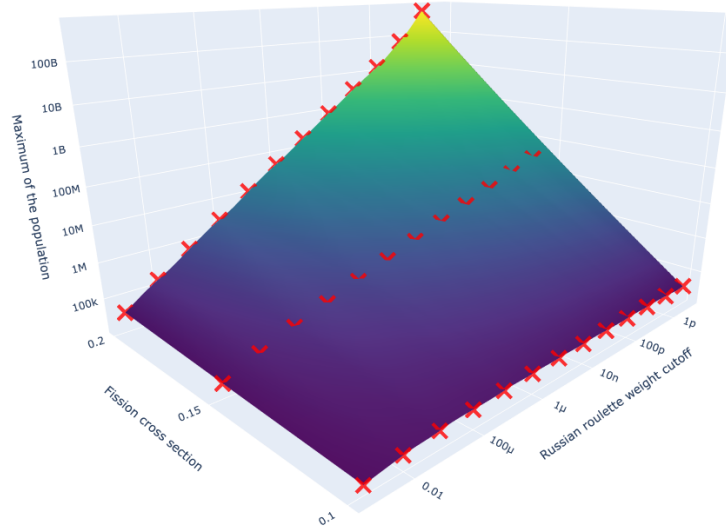


Figure 5.14: Case A2: three-dimensional plot of the maximum value of the population (on the z-axis) with respect to $\Sigma_{f,1}$ (x-axis) and the weight cutoff (y-axis). The red crosses are the numerical datas while the colored surface is obtained interpolating between these datas.

Effect of different probability density functions

Having probed the relation between the degree of criticality of the system and the simulations results, the rules of the branching process were then modified by changing the fission children probability density function. As a first step, two small variations to the original function were implemented, increasing the number of possible cases to be sampling process; in particular the two following probability density functions in Table 5.6 and 5.7 were used.

n outgoing particles	q_n
1	0.15
2	0.45
3	0.40

Table 5.6: 3-bins-low branching scheme fission children probabilities

n outgoing particles	q_n
2	0.85
3	0.05
4	0.1

Table 5.7: 3-bins-high branching scheme fission children probabilities

It is worth mentioning that the two probability density functions above were derived for the case with $\nu_f = 2.25$, so if this number changes the values of the q_n for each of the two functions will also need to change, in order to conserve the average number of fission neutrons. Together with the previous two a more complex was also implemented, namely the Poisson distribution:

$$q_n = f(n|\nu_f) = \frac{(\nu_f)^n \cdot \exp(-\nu_f)}{n!} \quad \text{for } n \in [0, +\infty[\quad (5.13)$$

The immediate drawback of using this type of function is that it is defined in an infinite interval, but for practical purposes a truncation to some upper limit is necessary. In all

of the cases under investigation the value of ν_f will always be smaller, or at most around 3, so having to truncate the function will not pose a problem: as it is possible to see in Figure 5.15 the q_n for $n > 15$ have negligible relevance compared to the ones for $n < 5$.

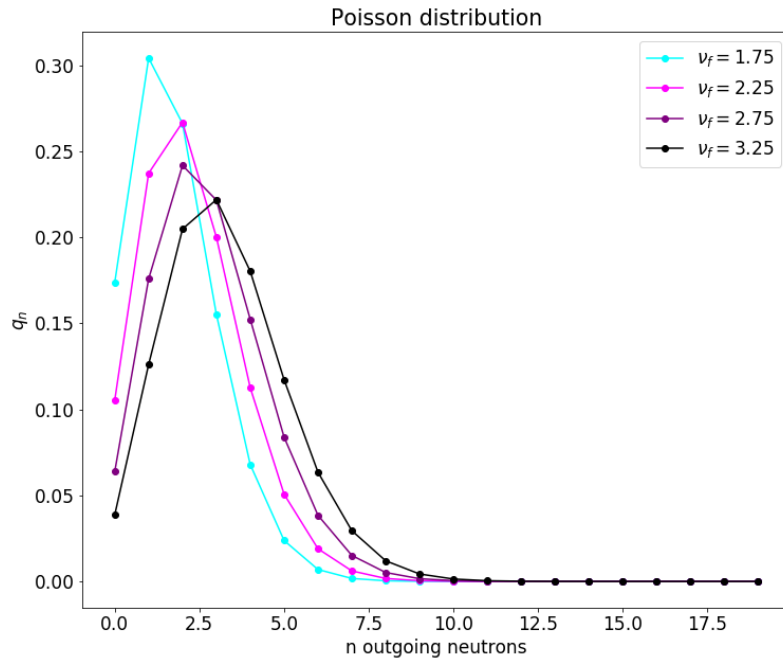


Figure 5.15: Case A3: q_n generated with a Poisson probability density function

Thanks to the formulation described in the previous chapters it is possible to compute for a given point in the phase space the modified probability \hat{c}_n to get n outgoing particles, as well as the expected number of particles coming out from the biased collisions. These information are depicted in the Figures 5.16 and 5.17.

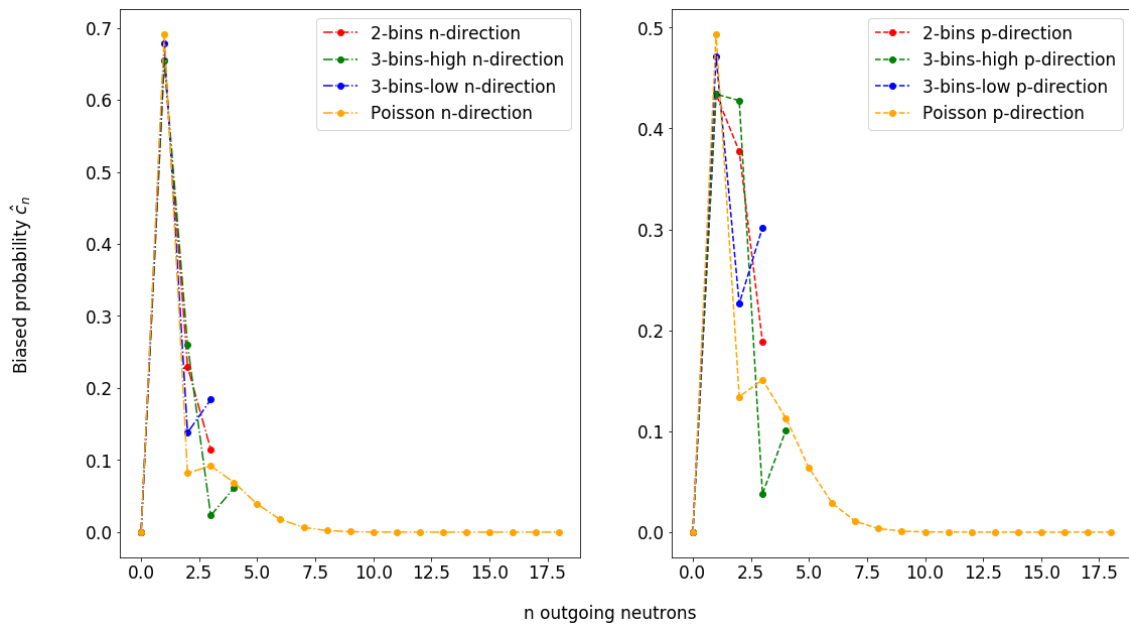


Figure 5.16: Case A3: comparison of the $\hat{c}_n(P)$ for different fission children probability density functions ($\Sigma_{f,1} = 0.15, \nu_f = 2.25$) in the two direction of flight

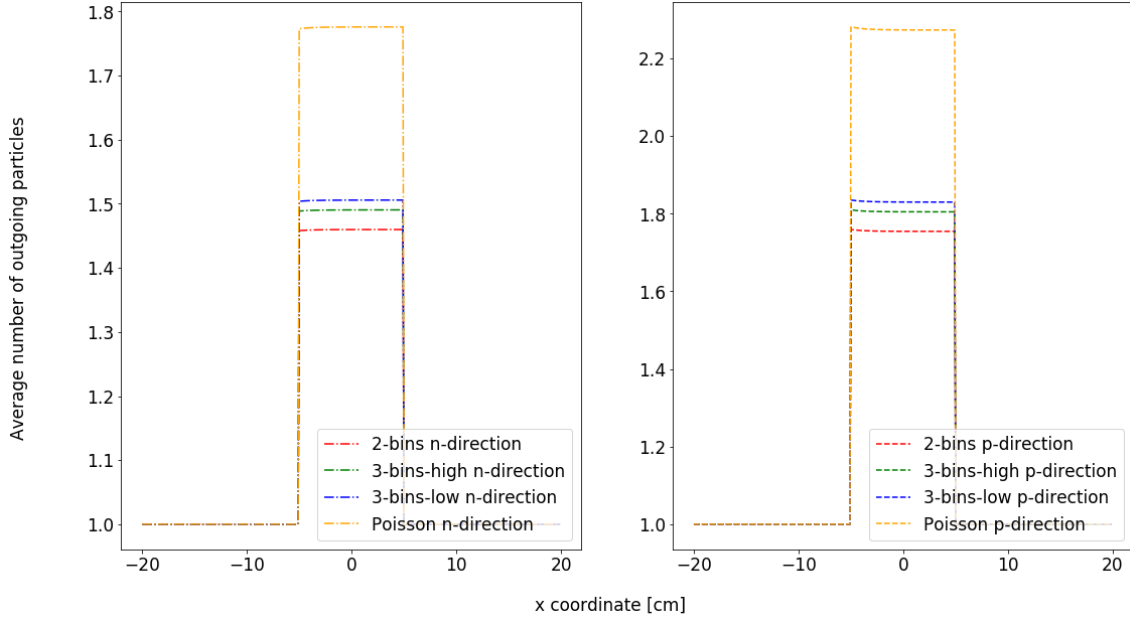


Figure 5.17: Case A3: average number of outgoing particles from the biased collision for different fission children probability density function ($\Sigma_{f,1} = 0.15, \nu_f = 2.25$) in the two direction of flight

The biasing affects differently the four functions as shown in the Figure 5.17: the average number of particle coming out from a collision with the Poisson distribution is almost 20% more than the same number but with the 2-bins distribution. This means that every 5 collisions on average 1 additional particle that needs to be simulated is generated, even though the non-biased distributions gave the exact same mean. The effect of this is not trivial and it will result in much longer and expensive computations especially for the higher values of k_{eff} . For the sake of simplicity, a smaller number of runs (all with 10000 particles and 500 batches) was simulated with respect to the previous cases: it was in fact decided to fix the fission cross section of the first media to $\Sigma_{f,1} = 0.15$ and to run only three simulations with different cutoffs per case. The simulation results are shown in Table 5.8.

Cutoff	STT			Detector error		
	3-bins-high	3-bins-low	Poisson	3-bins-high	3-bins-low	Poisson
10^{-1}	4.65×10^{-1}	3.29×10^{-1}	-9.92×10^{-1}	5.29×10^{-10}	5.40×10^{-10}	6.15×10^{-10}
10^{-3}	-1.08×10^{-1}	4.87×10^{-1}	9.87×10^{-1}	1.11×10^{-11}	1.14×10^{-11}	1.73×10^{-11}
10^{-6}	1.27	-1.94×10^{-1}	1.23	3.51×10^{-14}	3.82×10^{-14}	9.19×10^{-14}

Table 5.8: Case A3: Detector error and Student t-test of the detector response for the zero variance branching simulations with different fission children probability density functions

As expected, the total simulation times vary depending on the total number of particles in the system: comparing the theoretical results of Figure 5.17 with the simulation's results of Figure 5.18 it is possible to see that the slowest scheme is the one that uses the Poisson distribution and it is followed by the 3-bins-low distribution, then by the 3-bins-high distribution and lastly by the 2-bins distribution. This same order was found just by analyzing the expected average number of particles leaving a collision in Figure 5.17.

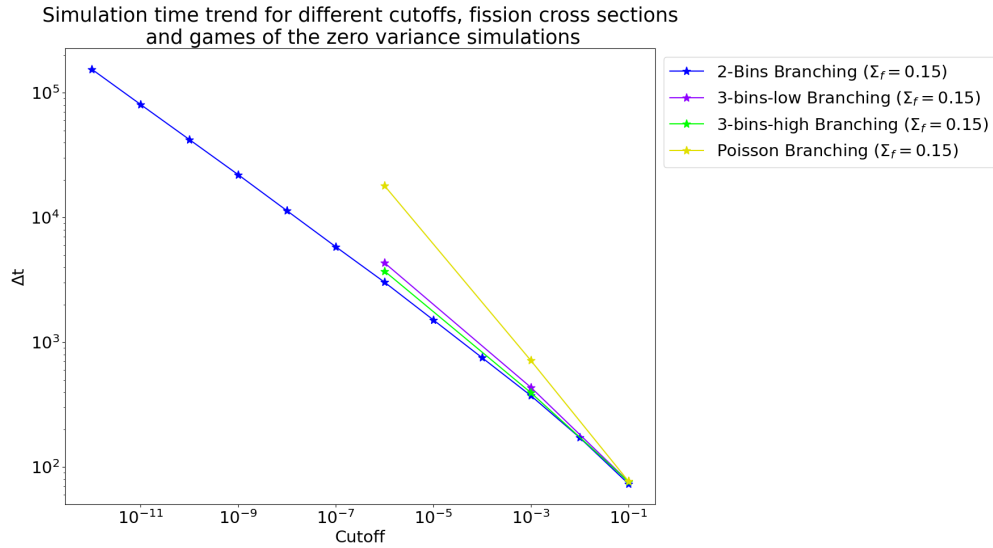


Figure 5.18: Case A3: simulation times for different fission children probability density function ($\Sigma_{f,1} = 0.15, \nu_f = 2.25$)

5.1.4 Branching zero variance: implicit capture game

The purpose of this section is to investigate the case where the starting game from which the zero-variance scheme is derived is not the analog game but an implicit capture game. As it was demonstrated easily in 3.4.4, the variance of the results does not depend on the type of the starting game, since the condition to reach zero variance is unique: the trend toward the zero-variance condition can, nevertheless, be different compared to the previous cases. As done previously, a series of results is presented in the Figures 5.19, 5.20, 5.21 and 5.22 comparing the zero-variance implicit capture game with the zero-variance analog game. In both cases, the chosen probability density function for fission children is the 2-bins model.

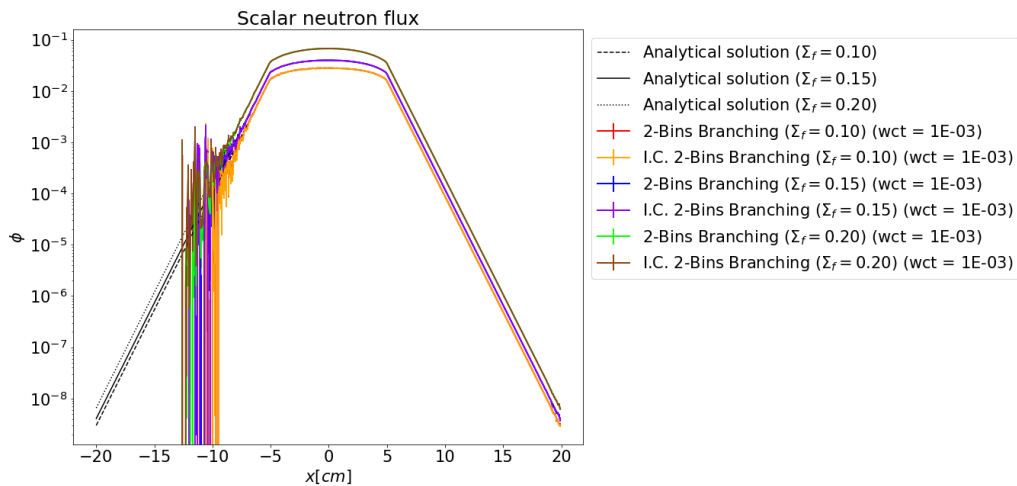


Figure 5.19: Case A4: scalar neutron flux comparison

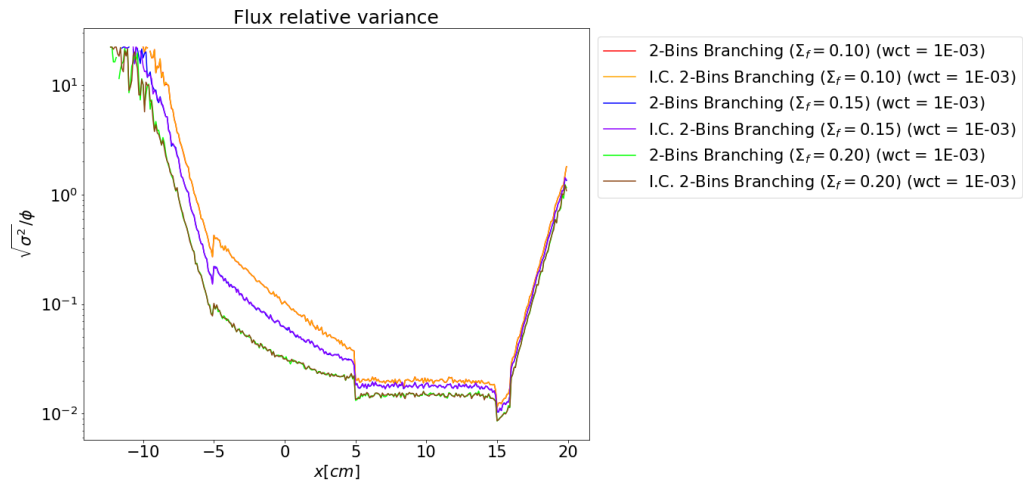


Figure 5.20: Case A4: scalar neutron flux relative variance comparison

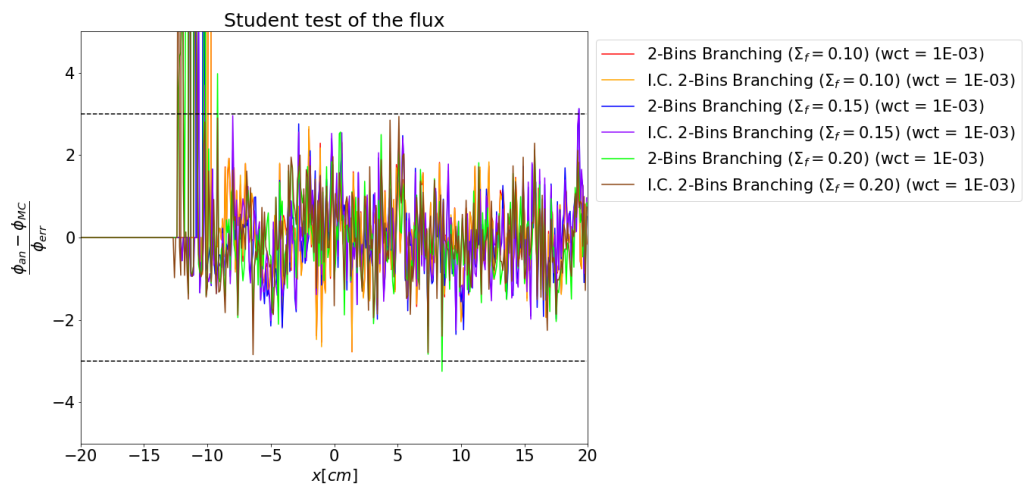


Figure 5.21: Case A4: Student t-test of the scalar neutron flux comparison

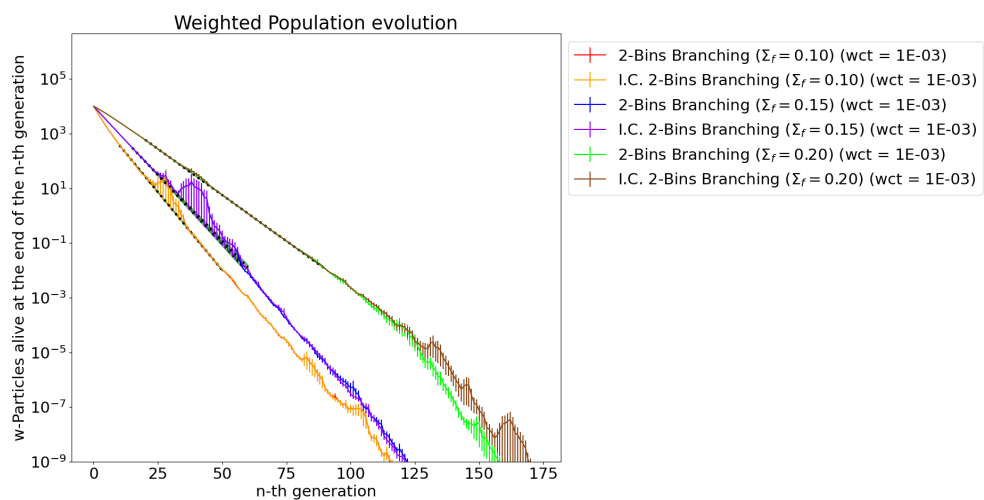


Figure 5.22: Case A4: weighted population evolution comparison

Analyzing all the previous figures it is possible to note that there are no relevant differences between the two zero variance schemes and in almost all the case the plots for every quantity of interest overlaps: this can especially be seen in Figure 5.20 and 5.22. From Figure 5.19 and 5.21 it is also possible to see that the new zero-variance game from the implicit capture scheme gives unbiased results.

The reason of this many similarity can be found in the fact that the two theoretical schemes have an almost identical formulation in the expression of the kernels, so these results was to be expected. Even the total simulations time (not depicted in the current work) shows the same trend. As usual, the simulation results for the detector error and the STT associated are depicted in Table 5.9 for three different runs and for varying cutoff values. Comparing Table 5.5 and Table 5.9 it is possible to see that the numerical values of the detector error and even the Student t-test of it are similar.

Branching implicit capture zero-variance

Cutoff	N° particles			N° batches			STT			Detector error		
	<i>RUN 1</i>	<i>RUN 2</i>	<i>RUN 3</i>	<i>RUN 1</i>	<i>RUN 2</i>	<i>RUN 3</i>	<i>RUN 1</i>	<i>RUN 2</i>	<i>RUN 3</i>	<i>RUN 1</i>	<i>RUN 2</i>	<i>RUN 3</i>
10^{-1}	10000	10000	10000	500	500	500	7.70×10^{-1}	-7.34×10^{-2}	4.06×10^{-1}	2.63×10^{-10}	4.85×10^{-10}	1.31×10^{-9}
10^{-2}	10000	10000	10000	500	500	500	-3.46×10^{-1}	-1.04	1.83	3.00×10^{-11}	7.42×10^{-11}	2.77×10^{-10}
10^{-3}	10000	10000	10000	500	500	500	-1.70	-1.70	8.29×10^{-1}	2.87×10^{-12}	1.09×10^{-11}	5.46×10^{-11}
10^{-4}	10000	10000	10000	500	500	500	-2.62×10^{-1}	-2.63×10^{-2}	-6.20×10^{-1}	3.15×10^{-13}	1.49×10^{-12}	1.11×10^{-11}
10^{-5}	10000	10000	10000	500	500	500	-6.43×10^{-1}	-7.27×10^{-1}	2.16×10^{-1}	3.21×10^{-14}	1.99×10^{-13}	2.53×10^{-12}
10^{-6}	10000	10000	10000	500	500	500	2.98×10^{-1}	1.14	-4.80×10^{-1}	3.25×10^{-15}	2.84×10^{-14}	7.11×10^{-13}
10^{-7}	10000	10000	10000	500	500	5	1.76×10^{-1}	-2.69×10^{-2}	-2.68×10^{-2}	3.26×10^{-16}	4.17×10^{-15}	$3.29 \times 10^{-13} *$
10^{-8}	10000	10000	5000	500	500	5	-2.66	9.54×10^{-1}	1.54	3.16×10^{-17}	5.65×10^{-16}	$1.03 \times 10^{-13} *$
10^{-9}	10000	10000	500	500	500	5	9.68×10^{-1}	1.26	3.89	3.31×10^{-18}	7.67×10^{-17}	$3.41 \times 10^{-15} *$
10^{-10}	10000	10000	50	500	500	2	5.17×10^{-1}	-7.75	1.59	3.30×10^{-19}	1.12×10^{-17}	$3.43 \times 10^{-16} *$
10^{-11}	10000	10000	-	500	500	-	-2.41×10^1	-2.80×10^2	-	3.42×10^{-20}	2.30×10^{-18}	-
10^{-12}	10000	10000	-	500	500	-	8.09	1.00×10^2	-	6.28×10^{-21}	1.57×10^{-17}	-
10^{-13}	10000	-	-	500	-	-	5.29×10^2	-	-	1.23×10^{-20}	-	-

Table 5.9: Case A4: Detector error and Student t-test of the detector response for the implicit capture zero variance branching simulations. In red are highlighted the first run in which the test fails and eventually some extra runs.

5.1.5 Branching zero variance: forced fission game

We compare now the zero-variance schemes from the branching analog game and from the branching forced fission game. Unlike the previous comparison, the two schemes stem from different hypothesis so some of the results are expected to be different, especially for what concerns the trend toward the zero variance. As usual, the chosen fission children probability density function is the 2-bins one.

From the Figures 5.23, 5.25 and 5.26 we note that the new zero-variance branching game from a forced fission scheme gives unbiased results for the flux estimate, confirming that our derivation was correct. It can be noted in Figure 5.24, that the flux relative variance obtained with this new zero-variance game is lower than the previous one, and consequently even lower than the branchless zero-variance one.

Figures 5.27 and 5.28 display the connection between population and total simulation time, highlighting the fact that the new forced fission scheme has a much higher computational cost than the original one.

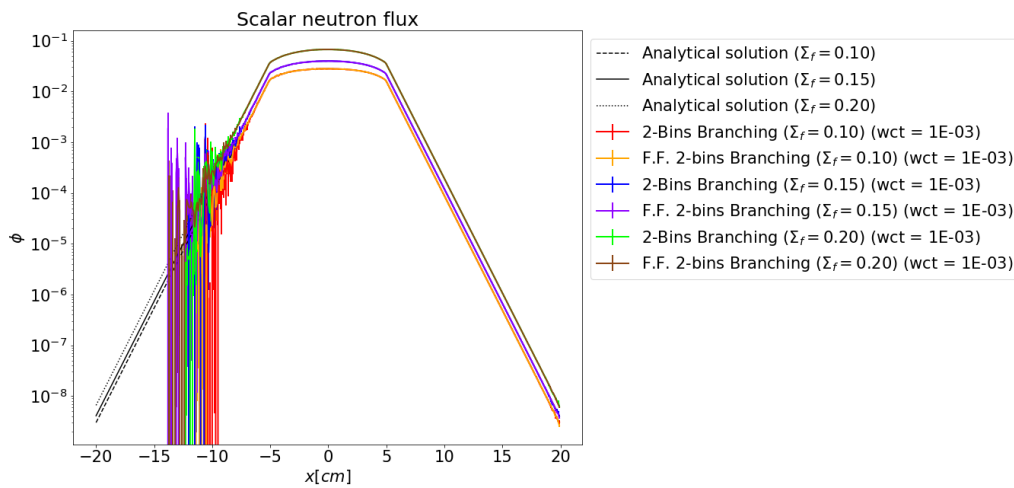


Figure 5.23: Case A5: scalar neutron flux comparison

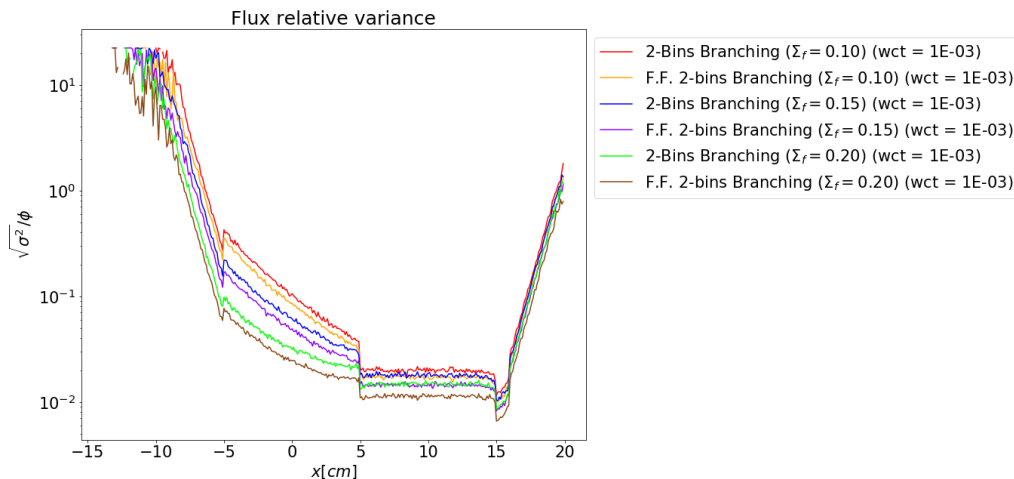


Figure 5.24: Case A5: scalar neutron flux relative variance comparison

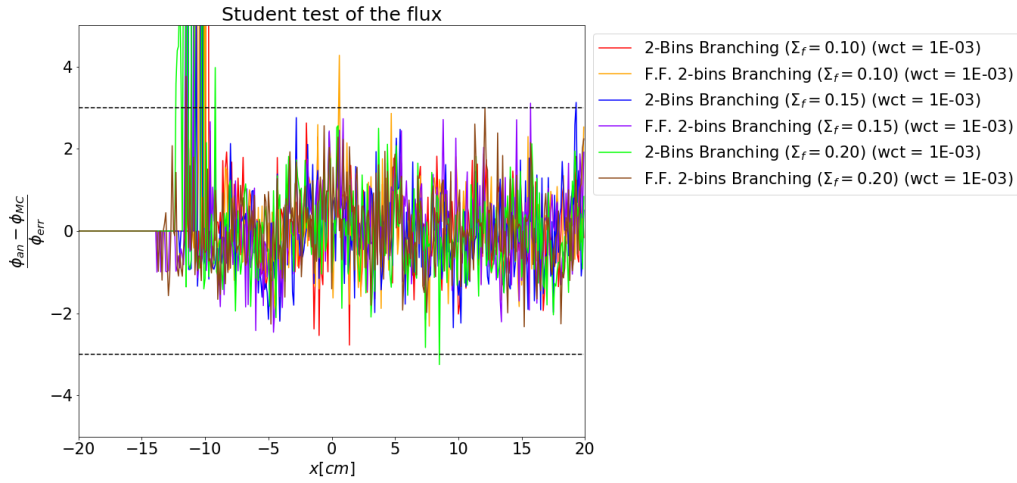


Figure 5.25: Case A5: Student t-test of the scalar neutron flux comparison

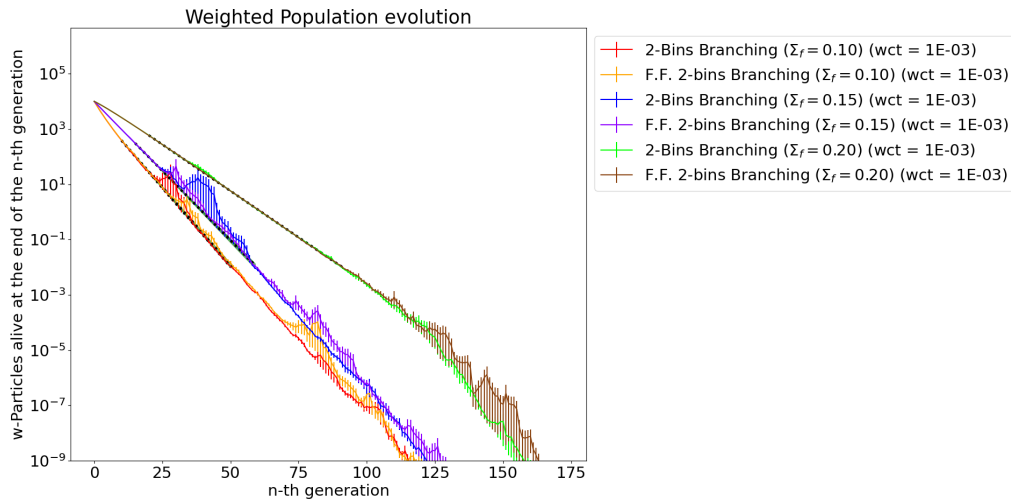


Figure 5.26: Case A5: weighted population evolution comparison

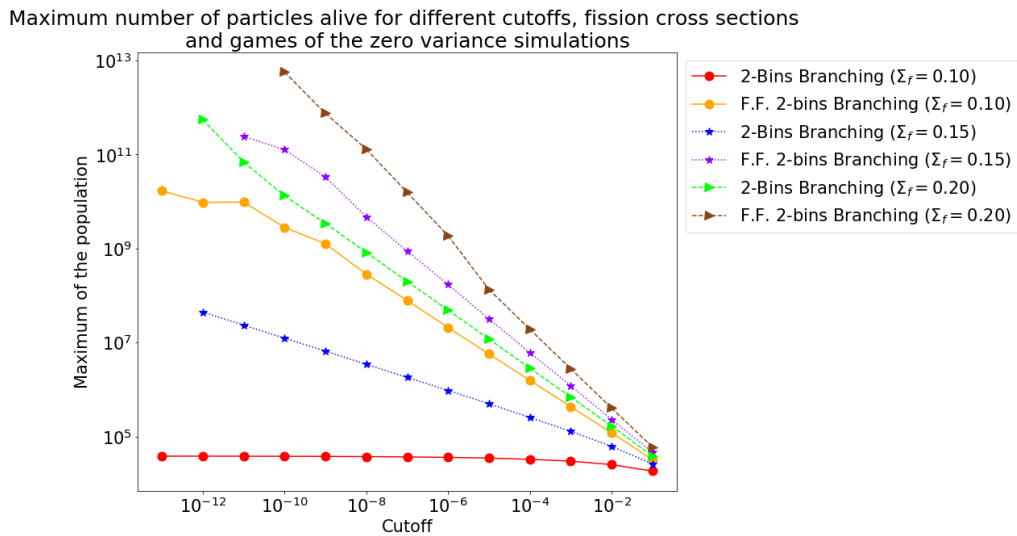


Figure 5.27: Case A5: maximum of the population comparison (some values were extrapolated)

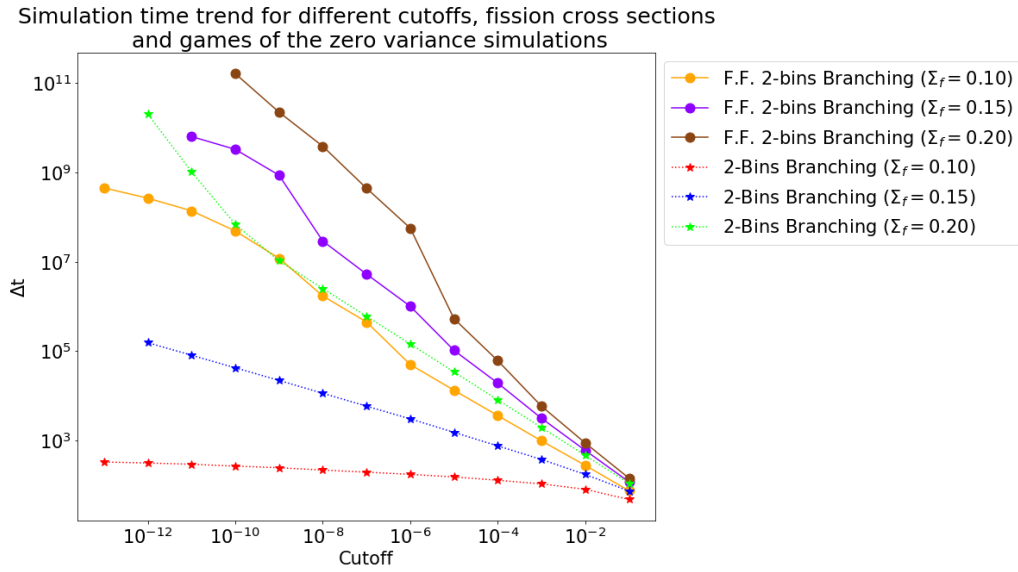


Figure 5.28: Case A5: simulation times comparison (some values were extrapolated)

It is necessary to say that the points at lower cutoffs for the two previous figures were obtained through a rescaling process, since the simulation setup for those games was made up of a lower amount of source particles and batches due to the high computational cost of the zero-variance forced fission scheme. The curves shown in Figure 5.27 and 5.28 represent the expected trend that would be observed if sufficient time and computational resources were available to perform simulations with a higher number of particles and batches.

Similarly to the previous sections, the simulation results for the detector error and the associated STT can be found within the sum-up Table 5.10.

Branching forced fission zero-variance

Cutoff	N° particles			N° batches			STT			Detector error		
	<i>RUN 1</i>	<i>RUN 2</i>	<i>RUN 3</i>	<i>RUN 1</i>	<i>RUN 2</i>	<i>RUN 3</i>	<i>RUN 1</i>	<i>RUN 2</i>	<i>RUN 3</i>	<i>RUN 1</i>	<i>RUN 2</i>	<i>RUN 3</i>
10^{-1}	10000	10000	10000	500	500	500	-4.43×10^{-1}	-9.26×10^{-1}	8.05×10^{-1}	4.48×10^{-10}	8.63×10^{-10}	2.07×10^{-9}
10^{-2}	10000	10000	10000	500	500	500	6.46×10^{-1}	2.82×10^{-1}	-8.49×10^{-1}	7.97×10^{-11}	1.99×10^{-10}	5.63×10^{-10}
10^{-3}	10000	10000	10000	500	500	500	8.77×10^{-1}	-9.72×10^{-1}	3.74×10^{-2}	1.61×10^{-11}	4.70×10^{-11}	1.51×10^{-10}
10^{-4}	10000	200	100	500	100	50	-7.46×10^{-1}	-2.85×10^{-1}	6.32×10^{-1}	$3.19 \times 10^{-12} *$	$1.07 \times 10^{-11} *$	$5.72 \times 10^{-11} *$
10^{-5}	10000	200	50	500	100	10	4.41×10^{-1}	5.48×10^{-2}	-3.55×10^{-1}	$6.29 \times 10^{-13} *$	$2.54 \times 10^{-12} *$	$9.13 \times 10^{-12} *$
10^{-6}	10000	40	1	500	50	2	-1.70×10^{-1}	-7.23×10^{-1}	1.78×10^{-1}	$1.38 \times 10^{-13} *$	$6.74 \times 10^{-13} *$	$1.41 \times 10^{-12} *$
10^{-7}	100	40	1	50	50	2	-4.32×10^{-1}	6.74×10^{-1}	-1.78×10^{-1}	$2.77 \times 10^{-14} *$	$1.26 \times 10^{-13} *$	$1.36 \times 10^{-12} *$
10^{-8}	100	40	1	50	50	2	1.77	9.59×10^{-2}	3.08	$4.79 \times 10^{-15} *$	$3.05 \times 10^{-14} *$	$1.26 \times 10^{-14} *$
10^{-9}	50	1	1	10	10	2	7.31×10^{-1}	-4.41×10^{-1}	1.68	$1.51 \times 10^{-15} *$	$3.69 \times 10^{-15} *$	$3.15 \times 10^{-14} *$
10^{-10}	10	1	1	5	5	2	-7.29×10^{-1}	-2.20	-3.29	$1.25 \times 10^{-16} *$	$9.69 \times 10^{-16} *$	$7.66 \times 10^{-15} *$
10^{-11}	10	1	-	5	2	-	1.23×10^{-1}	-1.41	-	$4.20 \times 10^{-17} *$	$7.01 \times 10^{-17} *$	-
10^{-12}	1	-	-	2	-	-	1.41	-	-	$1.81 \times 10^{-18} *$	-	-*
10^{-13}	1	-	-	2	-	-	1.42	-	-	$4.60 \times 10^{-20} *$	-	-

Table 5.10: Case A5: Detector error and Student t-test of the detector response for the forced fission zero variance branching simulations. In red are highlighted the first run in which the test fails and eventually some extra runs.

5.2 Case B

In the second configuration the source was moved outside the fissile medium and the position of the detector was also changed compared to *Case A*, all in order to create a so called *bi-modal configuration* for the importance. By slightly changing the physical parameters and the detector position it was possible, in fact, to change the shape of the adjoint flux so that it had two peaks of approximately the same height, and then by putting the source in the depression between those two peaks the bi-modal configuration was created. The geometry used for this case is depicted in Figure 5.29.

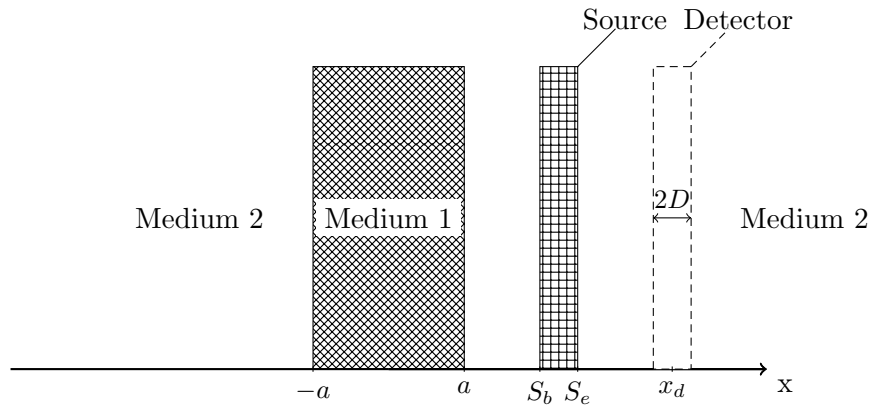


Figure 5.29: Case B geometry: the fissile Medium 1, the absorbing Medium 2, as well as the source and the detector are highlighted

The coordinates of the different planes in the figure are:

- $a = 5 \text{ cm}$;
- $x_d = 8 \text{ cm}$;
- $2D = 1 \text{ cm}$;
- $S_b = 6.25 \text{ cm}$;
- $S_e = 6.5 \text{ cm}$;

5.2.1 Analytical results

Since the scalar importance does not depend on the position of the source, see Equation 5.10, the structure of the equation remains the same and only the numerical values of certain parameters have been changed. In the plot in Figure 5.31 it is possible to see the aforementioned *bi-modal shape* for the importance with two peaks respectively in the fissile media and in the detector region.

Since the scalar flux instead depends on the source position 5 different regions can be identified, similarly for the previous case. The final expression for the scalar flux is then the one described by Equation 5.14.

Like the previous case, an increase in the value of the k_{eff} has the effect of increasing the scalar neutron flux in the region of the fissile material, as it is possible to see from Figure 5.30. Differently from *Case A*, the parameter which is used to vary the criticality level of the system in this case is the $\nu_{f,1}$, ie the fission multiplicity: it was decided to do so in order to see the effect of a different physical parameter on the final results.

$$\phi(x) = \begin{cases} B_1 \exp(\sqrt{\Sigma_{tr,2}\Sigma_{e,2}}x) & \text{if } x < -a \\ A_2 \cos(\beta x) + B_2 \sin(\beta x) & \text{if } |x| < a \\ A_3 \exp(-\sqrt{\Sigma_{tr,2}\Sigma_{e,2}}x) + B_3 \exp(\sqrt{\Sigma_{tr,2}\Sigma_{e,2}}x) & \text{if } x \in (a, S_{beginning}) \\ \frac{1}{\Sigma_{e,2}(S_{end}-S_{beginning})} + A_4 \exp(-\sqrt{\Sigma_{tr,2}\Sigma_{e,2}}x) \\ \quad + B_4 \exp(\sqrt{\Sigma_{tr,2}\Sigma_{e,2}}x) & \text{if } x \in (S_{beginning}, S_{end}) \\ A_5 \exp(-\sqrt{\Sigma_{tr,2}\Sigma_{e,2}}x) & \text{if } x > S_{end} \end{cases} \quad (5.14)$$

The values of the constants in Equation 5.14 can be found imposing the condition of continuity of the neutron flux and neutron current at the interfaces.

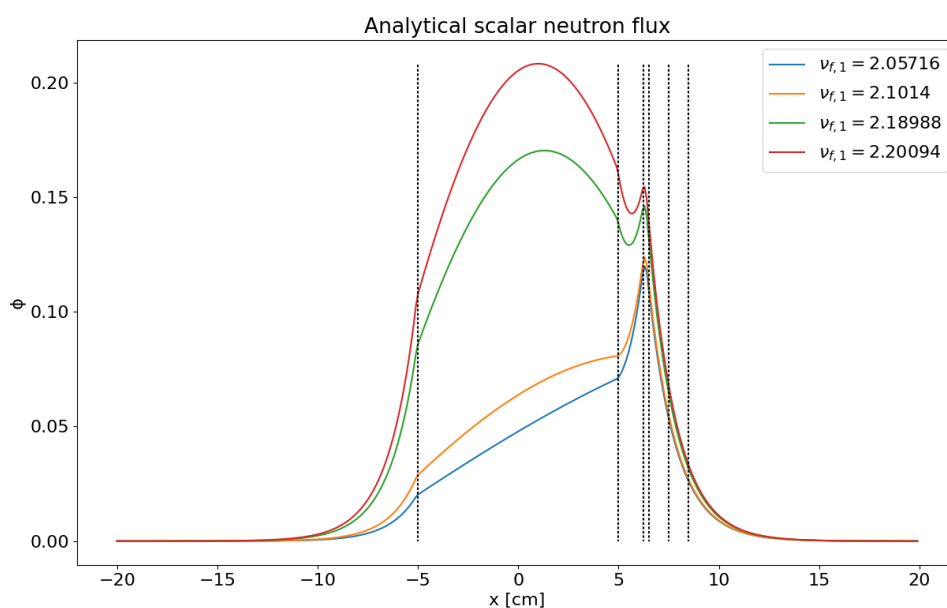


Figure 5.30: Case B: Analytical scalar flux

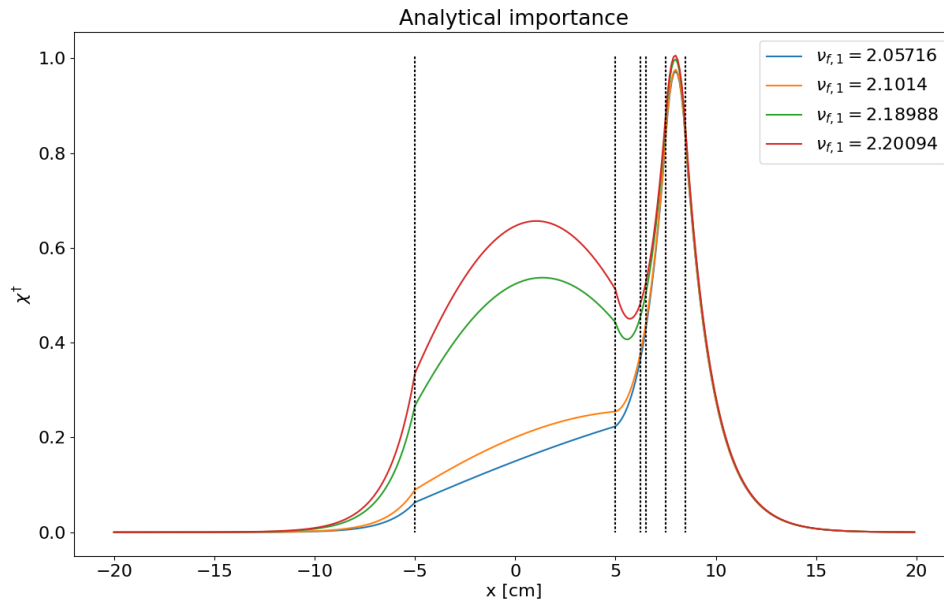


Figure 5.31: Case B: Analytical scalar importance

5.2.2 Analog and branchless zero variance

As it was done for the *Case A*, first the simulations setups for the different runs will be summed up (see Table 5.11) and then k_{eff} of the system will be estimated with a branchless k-eigenvalue simulation (see Table 5.12).

	$\Sigma_t[cm^{-1}]$	$\Sigma_s[cm^{-1}]$	$\Sigma_a[cm^{-1}]$	$\Sigma_f[cm^{-1}]$	$\nu_f[-]$	$\nu_s[-]$	$\bar{\mu}_s[-]$	$\bar{\mu}_f[-]$
Medium 1	1.0	0.45	0.55	0.27	2.05716/2.18988/2.20094	1.0	0.75	0.0
Medium 2	3.0	2.685	0.315	0.0	0.0	1.0	0.5	0.0

Table 5.11: Case B physical parameters

Simulation	$\nu_{f,1}[-]$	k_{eff}
Tes 1	2.05716	0.914415 ± 0.000347
Tes 2	2.18988	0.973139 ± 0.000360
Tes 3	2.20094	0.977888 ± 0.000356

Table 5.12: Case B k_{eff} of the system in the different simulations

An immediate consequence of the fact that some physical parameter have been changed is that the system has become much more critical: from the knowledge derived from the previous case it is already possible to predict that this will negatively effect the branching simulations.

The reference solutions for the flux and flux relative variance obtained with the purely analog scheme and the zero-variance branchless scheme for the 3 new configurations of the *Case B* are depicted in Figure 5.32 and 5.33.

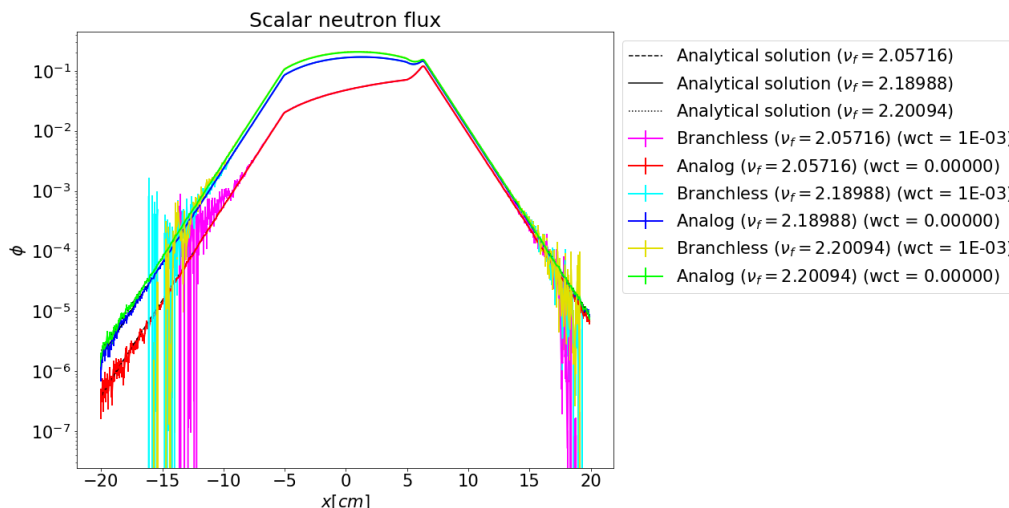


Figure 5.32: Case B1: scalar neutron flux comparison

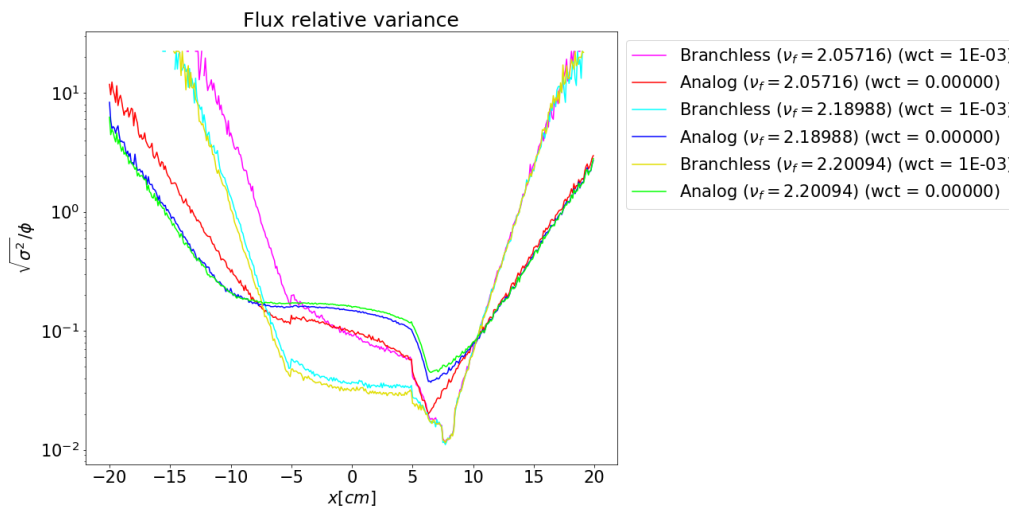


Figure 5.33: Case B1: scalar neutron flux relative variance comparison

From the Student t-test on the flux in Figure 5.34 it is clear that the solution is unbiased in the regions of higher importance and similar to the previous case it is affected by the limited statistical information in the regions of lower importance. Looking also at the Figure 5.35 and comparing it with the other weighted population evolutions it can be seen how the total population is able to survive much longer through the generations, arriving even at more than one thousand generations.

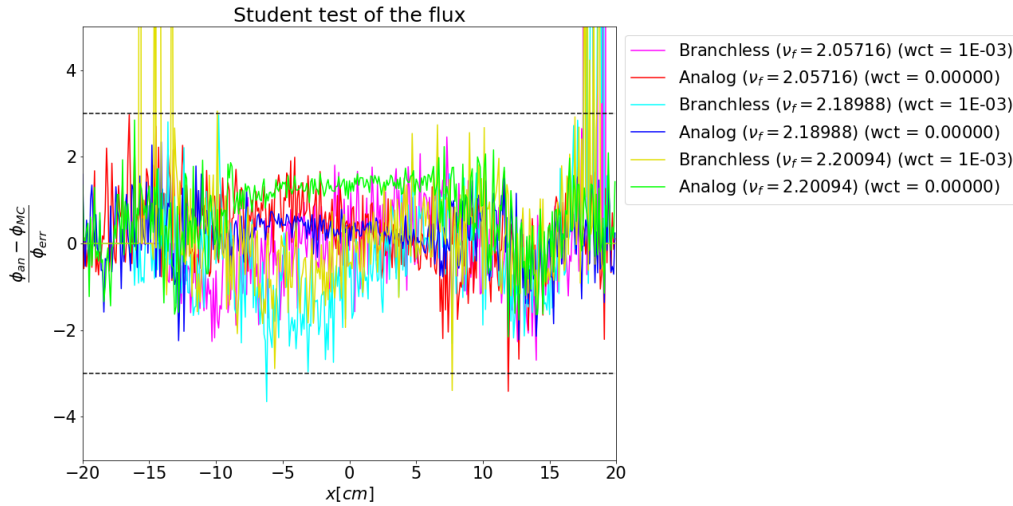


Figure 5.34: Case B1: Student t-test of the scalar neutron flux comparison

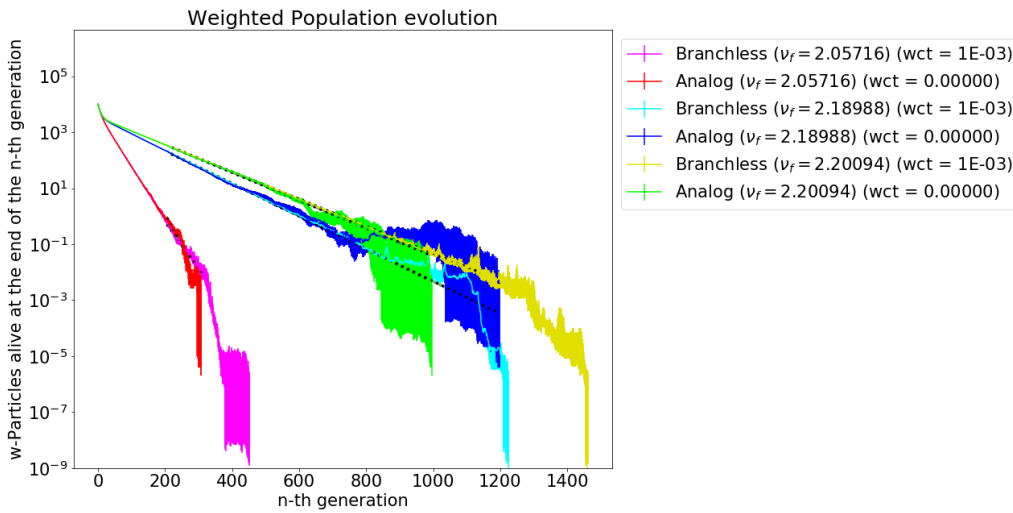


Figure 5.35: Case B1: weighted population evolution comparison

Following the same procedure of the previous case, the results of the different simulations in terms of detector error and related STT are summed up in the Table 5.13. From this table it is possible to see that, with the limit of the population control even in this new configuration the branchless scheme is able to attain the zero-variance condition, but it does so with a slower speed compared to *Case A*. The reason of this slower "convergence" is not the higher degree criticality, since it was seen that the branchless schemes are not influenced in a sensible manner by it, but the new shape the importance. At the beginning of the simulation, a source particle can go towards either one of the two importance peaks; if the particle randomly goes toward the Medium 1 region it will be trapped into a high importance region far away from the detector, leaving less particles that can contribute to the estimate of the detector response.

Branchless zero-variance

Cutoff	N° particles			N° batches			STT			Detector error		
	<i>TES 1</i>	<i>TES 2</i>	<i>TES 3</i>	<i>TES 1</i>	<i>TES 2</i>	<i>TES 3</i>	<i>TES 1</i>	<i>TES 2</i>	<i>TES 3</i>	<i>TES 1</i>	<i>TES 2</i>	<i>TES 3</i>
10^{-1}	10000	10000	10000	500	500	500	1.47	-9.05×10^{-1}	-7.13×10^{-1}	2.28×10^{-5}	2.83×10^{-5}	2.86×10^{-5}
10^{-2}	10000	10000	10000	500	500	500	-1.66×10^{-1}	-9.45×10^{-1}	-4.82×10^{-1}	2.46×10^{-6}	2.81×10^{-6}	2.95×10^{-6}
10^{-3}	10000	10000	10000	500	500	500	5.52×10^{-1}	-8.43×10^{-2}	-1.61	2.33×10^{-7}	2.80×10^{-7}	2.84×10^{-7}
10^{-4}	10000	10000	10000	500	500	500	1.64	1.91×10^{-1}	1.05	2.24×10^{-8}	2.91×10^{-8}	2.90×10^{-8}
10^{-5}	10000	10000	10000	500	500	500	-1.80	1.08×10^{-1}	-8.92×10^{-1}	2.20×10^{-9}	2.75×10^{-9}	2.95×10^{-9}
10^{-6}	10000	10000	10000	500	500	500	-1.21	1.87	-4.36×10^{-2}	2.25×10^{-10}	2.70×10^{-10}	2.92×10^{-10}
10^{-7}	10000	10000	10000	500	500	500	-1.29	-6.20×10^{-1}	-1.99×10^{-1}	2.29×10^{-11}	2.78×10^{-11}	2.92×10^{-11}
10^{-8}	10000	10000	10000	500	500	500	-4.56×10^{-2}	-3.28×10^{-1}	-7.20×10^{-1}	2.25×10^{-12}	2.85×10^{-12}	2.93×10^{-12}
10^{-9}	10000	10000	10000	500	500	500	1.08	3.82×10^{-1}	-1.10	2.20×10^{-13}	2.88×10^{-13}	2.79×10^{-13}
10^{-10}	10000	10000	10000	500	500	500	-1.46×10^{-1}	9.27×10^{-1}	-9.33×10^{-1}	2.36×10^{-14}	2.74×10^{-14}	2.86×10^{-14}
10^{-11}	10000	10000	10000	500	500	500	-2.87	-1.10×10^1	-1.24×10^1	2.40×10^{-15}	2.65×10^{-15}	2.96×10^{-15}
10^{-12}	10000	10000	10000	500	500	500	3.26×10^2	3.14×10^2	2.79×10^2	4.87×10^{-16}	5.31×10^{-16}	5.66×10^{-16}
10^{-13}	10000	10000	10000	500	500	500	7.45×10^2	7.72×10^2	7.80×10^2	4.32×10^{-16}	4.78×10^{-16}	4.95×10^{-16}

Table 5.13: Case B1: Detector error and Student t-test of the detector response for the zero variance branchless simulations. In red are highlighted the first run in which the test fails and eventually some extra runs.

5.2.3 Branching zero variance: analog game

As shown in Figure 5.36 and 5.38, using the zero-variance branching game derived from the analog one gives once again unbiased results for the flux. The plot in Figure 5.39 confirms that also in this case the zero-variance branching scheme do not change the total weighted population evolution. For the same reasons of *Case A*, the relative variance of the flux of the branching games is lower than the corresponding one in the branchless games, see Figure 5.37.

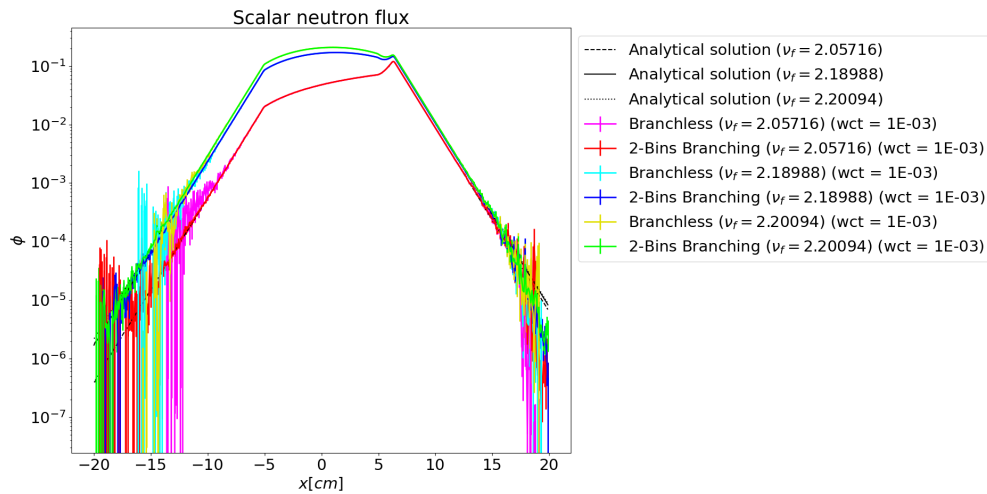


Figure 5.36: Case B2: scalar neutron flux comparison

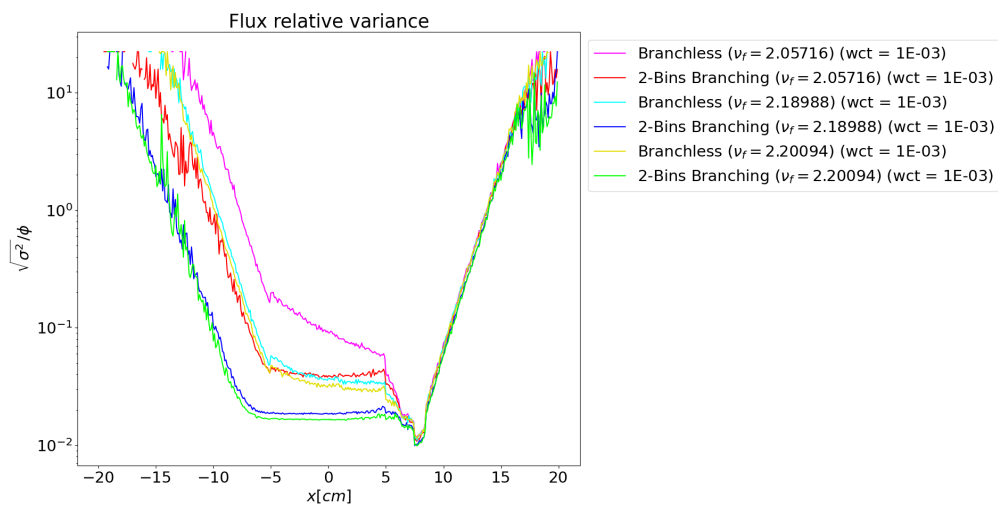


Figure 5.37: Case B2: scalar neutron flux relative variance comparison

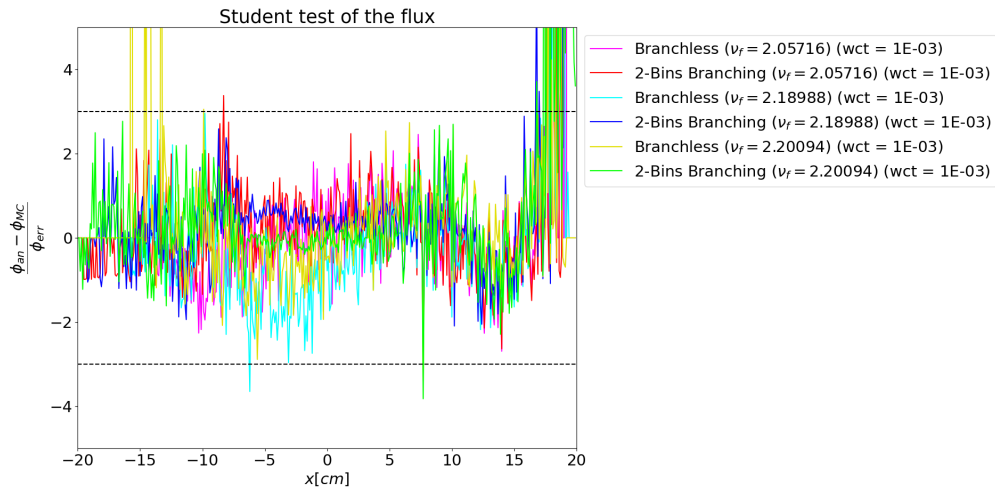


Figure 5.38: Case B2: Student t-test of the scalar neutron flux comparison

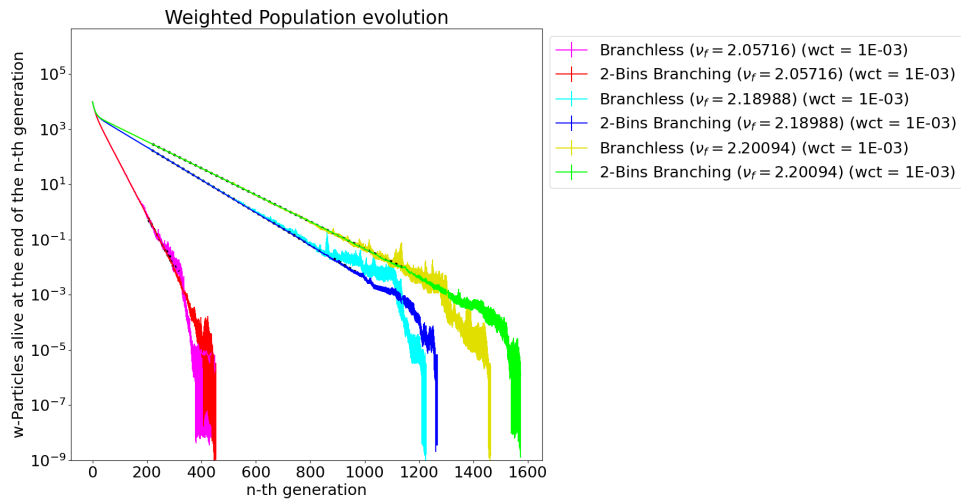


Figure 5.39: Case B2: weighted population evolution comparison

For what concerns the trend to the zero-variance regime, it is evident from the sum-up Table 5.14 how the branching game has a slower "convergence" speed and even with a relatively low cutoff of 10^{-10} the error can only be around the order of $10^{-9} - 10^{-10}$. The computational cost of the branching scheme will be detailed in the next paragraph.

Branching analog zero-variance

Cutoff	N° particles			N° batches			STT			Detector error		
	<i>TES 1</i>	<i>TES 2</i>	<i>TES 3</i>	<i>TES 1</i>	<i>TES 2</i>	<i>TES 3</i>	<i>TES 1</i>	<i>TES 2</i>	<i>TES 3</i>	<i>TES 1</i>	<i>TES 2</i>	<i>TES 3</i>
10^{-1}	10000	10000	10000	500	500	500	1.95	-1.20	-1.12	5.64×10^{-5}	1.81×10^{-4}	2.31×10^{-4}
10^{-2}	10000	10000	10000	500	500	500	2.44×10^{-1}	-1.21	-2.22	1.46×10^{-5}	5.77×10^{-5}	7.29×10^{-5}
10^{-3}	10000	10000	10000	500	500	500	-8.76×10^{-1}	-5.04×10^{-1}	-1.53	3.94×10^{-6}	2.06×10^{-5}	2.92×10^{-5}
10^{-4}	10000	10	1000	500	20	100	-1.54	1.76	-1.01	1.14×10^{-6}	3.97×10^{-6} *	2.08×10^{-5} *
10^{-5}	10000	10	50	500	50	50	-1.06	5.39	1.46	4.24×10^{-7}	1.76×10^{-6} *	4.17×10^{-6} *
10^{-6}	10000	1	10	500	10	5	-2.51×10^{-1}	7.58×10^{-1}	2.08	2.52×10^{-7}	5.13×10^{-7} *	7.67×10^{-7} *
10^{-7}	100	1	1	50	10	2	7.33	4.02×10^{-1}	-3.04	2.06×10^{-8} *	1.50×10^{-7} *	1.91×10^{-7} *
10^{-8}	50	1	1	50	2	2	5.52	-3.39	3.56×10^{-2}	6.93×10^{-9} *	4.79×10^{-8} *	9.37×10^{-8} *
10^{-9}	10	1	-	25	2	-	6.81×10^{-2}	-7.07×10^{-1}	-	9.18×10^{-10} *	2.58×10^{-8} *	-
10^{-10}	1	-	-	5	-	-	-6.61×10^{-1}	-	-	6.84×10^{-10} *	-	-
10^{-11}	-	-	-	-	-	-	-	-	-	-	-	-
10^{-12}	-	-	-	-	-	-	-	-	-	-	-	-
10^{-13}	-	-	-	-	-	-	-	-	-	-	-	-

Table 5.14: Case B2: Detector error and Student t-test of the detector response for the zero variance branching analog simulations. In red are highlighted the first run in which the test fails and eventually some extra runs.

5.2.4 Branching zero variance: forced fission game

From *Case A* it was seen how the implicit capture zero-variance game presents no differences with respect to the analog zero-variance game: for this reason it was decided to not present a new comparison of the two for *Case B*. It was also decided not to show the flux and weighted population plots, since they are similar to the already shown ones.

In Figure 5.41 it is apparent that how even the zero-variance forced fission scheme is unbiased and the flux estimate is within the acceptable range, at least for the regions of higher importance. As usual, the scheme that produces more particles is able to reach a lower relative variance for the flux in the fissile medium, as shown in Figure 5.40.

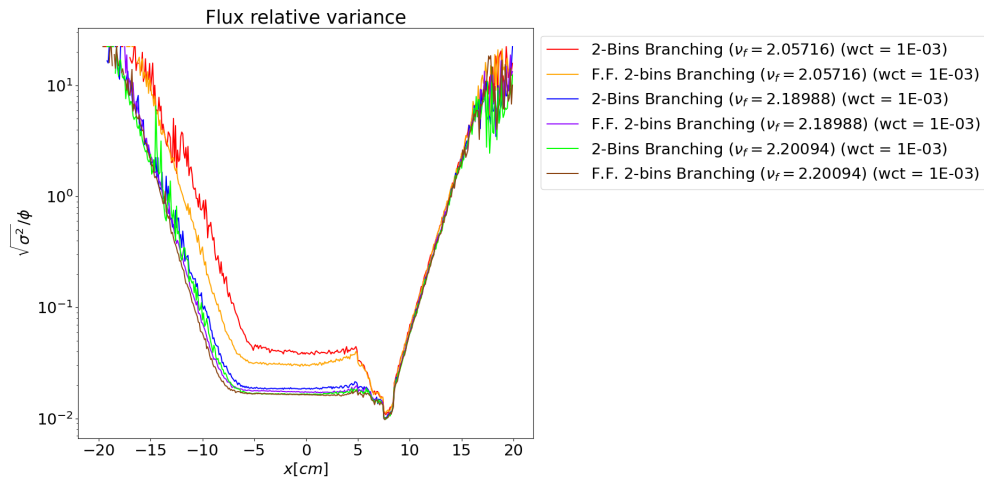


Figure 5.40: Case B3: scalar neutron flux relative variance comparison

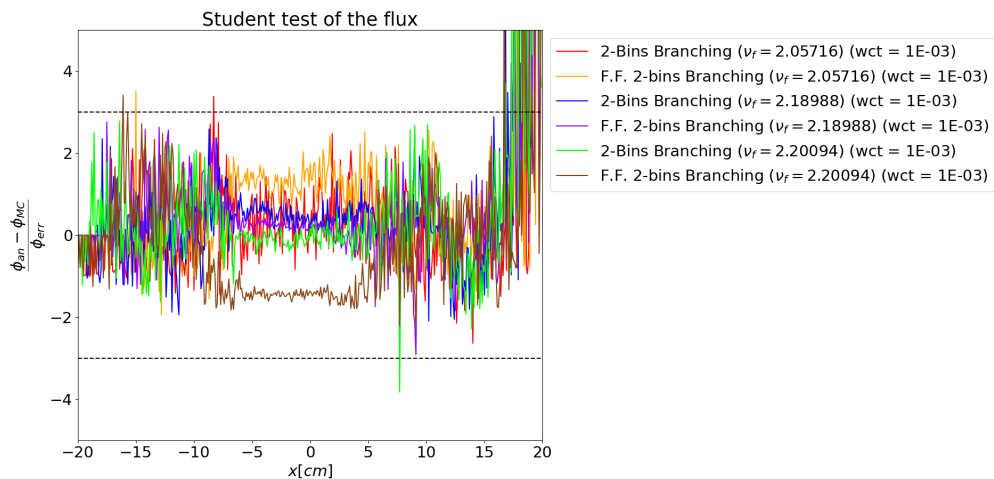


Figure 5.41: Case B3: Student t-test of the scalar neutron flux comparison

Using zero-variance branching schemes in a system with a $k_{eff} > 0.9$ has proven to be extremely challenging from the computation time point of view, see Figure 5.43 (like for *Case A*, the data at lower cutoffs value of Figures 5.42 and 5.43 were obtained through a rescaling process). Comparing Figure 5.42 and 5.43 it is again possible to appreciate the strong link of the total simulation time and the population size.

Maximum number of particles alive for different cutoffs, fission multiplicities and games of the zero variance simulations

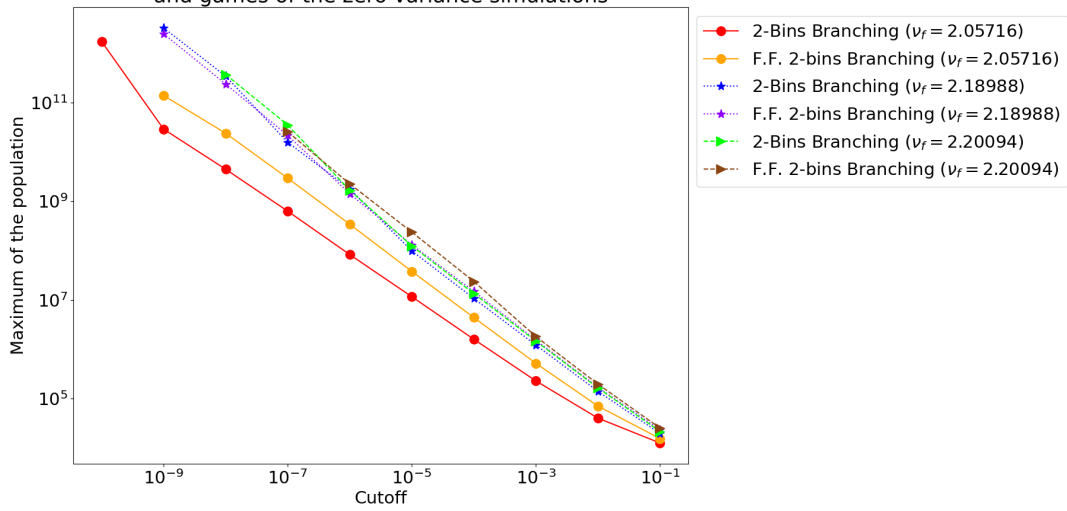


Figure 5.42: Case B3: maximum of the population comparison

Simulation time trend for different cutoffs, fission multiplicities and games of the zero variance simulations

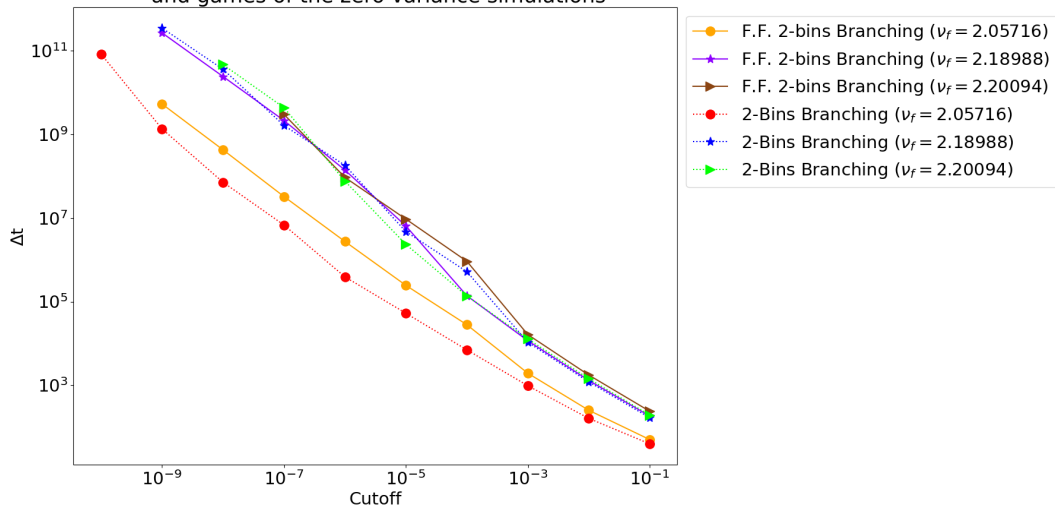


Figure 5.43: Case B3: simulation time comparison

Table 5.15 contains the simulation results for the zero-variance branching game derived from a forced fission scheme for what concerns the detector error and the STT to it associated. In this Table it is possible to appreciate how this new scheme tends towards the zero variance regime with a much slower speed compared to any other tested before.

Branching forced fission zero-variance

Cutoff	N° particles			N° batches			STT			Detector error		
	<i>TES 1</i>	<i>TES 2</i>	<i>TES 3</i>	<i>TES 1</i>	<i>TES 2</i>	<i>TES 3</i>	<i>TES 1</i>	<i>TES 2</i>	<i>TES 3</i>	<i>TES 1</i>	<i>TES 2</i>	<i>TES 3</i>
10^{-1}	10000	10000	10000	500	500	500	-4.34×10^{-1}	5.19×10^{-1}	1.94×10^{-1}	7.86×10^{-5}	2.87×10^{-4}	3.47×10^{-4}
10^{-2}	10000	10000	10000	500	500	500	2.87×10^{-1}	8.90×10^{-1}	2.04	2.19×10^{-5}	8.15×10^{-5}	1.07×10^{-4}
10^{-3}	10000	10000	10000	500	500	500	-7.12×10^{-2}	1.73	1.10	7.08×10^{-6}	3.62×10^{-5}	4.87×10^{-5}
10^{-4}	200	500	10	100	10	5	-6.39×10^{-2}	2.17	5.64×10^{-1}	$2.65 \times 10^{-6} *$	$1.10 \times 10^{-5} *$	$1.12 \times 10^{-5} *$
10^{-5}	200	10	10	100	50	5	5.50×10^{-1}	3.51	3.03	$9.88 \times 10^{-7} *$	$2.25 \times 10^{-6} *$	$3.16 \times 10^{-6} *$
10^{-6}	100	1	10	100	10	5	2.56	7.69×10^{-1}	7.00×10^{-1}	$2.86 \times 10^{-7} *$	$8.48 \times 10^{-7} *$	$1.19 \times 10^{-6} *$
10^{-7}	50	1	1	50	5	2	-8.01×10^{-1}	-1.82	1.41	$4.27 \times 10^{-8} *$	$3.15 \times 10^{-7} *$	$5.99 \times 10^{-7} *$
10^{-8}	25	1	-	25	2	-	-6.27	1.41	-	$1.91 \times 10^{-8} *$	$1.01 \times 10^{-8} *$	-
10^{-9}	5	1	-	5	2	-	-1.05	1.41	-	$3.84 \times 10^{-9} *$	$9.18 \times 10^{-9} *$	-
10^{-10}	-	-	-	-	-	-	-	-	-	-	-	-
10^{-11}	-	-	-	-	-	-	-	-	-	-	-	-
10^{-12}	-	-	-	-	-	-	-	-	-	-	-	-
10^{-13}	-	-	-	-	-	-	-	-	-	-	-	-

Table 5.15: Case B3: Detector error and Student t-test of the detector response for the zero variance branching forced fission simulations. In red are highlighted the first run in which the test fails and eventually some extra runs.

5.3 FOM comparison

As last, a comparison between all the schemes for the two cases is presented in this section. To have a single and reliable parameter that can express the performance of the scheme with respect to the others, it was defined the following Figure Of Merit (FOM):

$$FOM = \frac{1}{\left(\frac{R_{err}}{R_{an}}\right)^2 \Delta t} \quad (5.15)$$

the higher the FOM, the better the result achieved with the simulation considered the time taken to complete it. In the two following Figures 5.44 and 5.45 the FOM trend for all the simulations of *RUN 2* and *TES 2* are depicted: the branchless simulations have an overall better FOM compared to all the others.

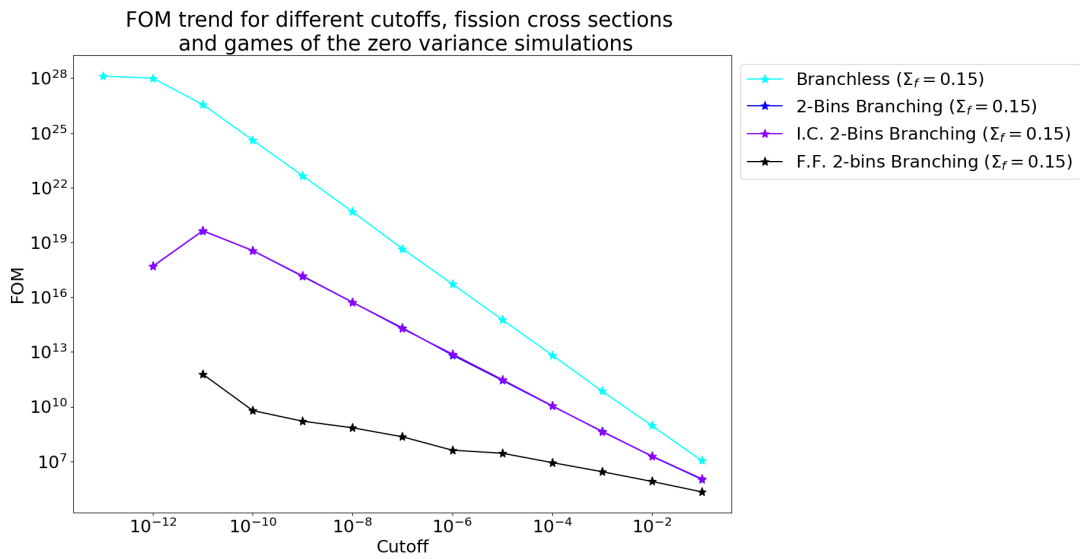


Figure 5.44: FOM comparison for Case A

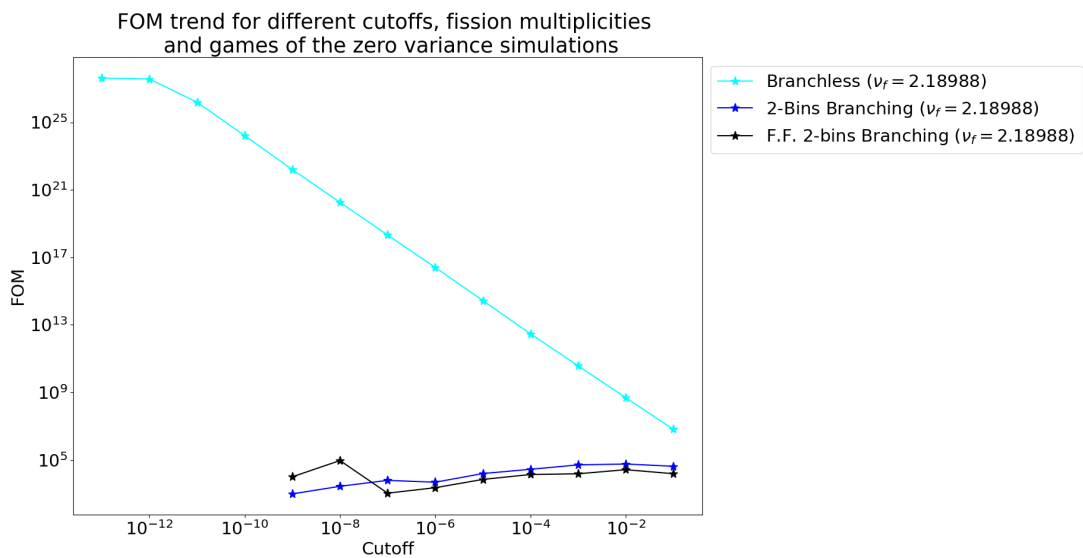


Figure 5.45: FOM comparison for Case B

Chapter 6

Conclusions

Monte Carlo methods are extensively applied to radiation shielding problems, but variance reduction techniques, such as importance sampling, are essential to enhance efficiency. Zero-variance games, in particular, are of great interest due to their potential to provide exact solutions with no statistical error, though they require knowledge of the solution to the adjoint equation to be effective. In view of the prominent role that zero-variance games play in inspiring practical importance sampling schemes such as the well-known CADIS method, it is of utmost importance to fully characterize how zero-variance games would behave in neutron transport problems involving neutron multiplication, which might occur for instance for ex-core flux monitoring during reactor start-up, and how their performance would be affected in these scenarios.

In this thesis, the theoretical foundation of branching zero-variance games was applied to derive new zero-variance games, starting from implicit capture or forced fission games, and the results were compared to the branchless zero-variance games. The new types of games were implemented within the MGMC Monte Carlo transport code and compared also with the purely analog simulation to test the efficacy of this particular importance sampling schemes.

All the simulations gave unbiased results and, reducing gradually the population control methods implemented, each scheme approached the zero variance regime. To probe the behavior of the different schemes, various test were conducted with different levels of criticality. For this purpose, we introduced also two distinct benchmark configurations to test the performance of these games with different importance functions.

From the simulation results, it can be inferred that branching zero-variance Monte Carlo games are suitable for multiplicative media, yielding unbiased solutions. However, the practicality of using these games decreases as the number of branching histories increases. We showed that the more particles are simulated by the code, the higher the computational cost becomes and a longer time is needed for the completion of the run. Branchless zero-variance games exhibit superior overall performance in terms of figure of merit (FOM). Still, understanding the performance of branching games remains important, as they are widely used in most production Monte Carlo codes.

Appendix A

Analog games derivation of the moments

According to the definition of the transport kernel for a particle leaving a collision in P' and entering a collision in P ("average number of particles having coordinates P given a particle starting a flight with coordinates P' "):

$$T(P', P) = \Sigma(r, E) \exp \left[- \int_0^{|r-r'|} \Sigma(r' + l\Omega', E') dl \right] \cdot \frac{\Omega' - \frac{r-r'}{|r-r'|}}{(r-r')^2} \cdot \delta(\Omega - \Omega') \delta(E - E') \quad (\text{A.1})$$

And according to the definition of the collision kernel for the particles coming out from a collision in P with coordinates before the collision equal to P' ("average number of particles having coordinates P given a particle having had a collision with coordinates P' "):

$$C(P', P) = \sum_{i=1}^n \sum_{j=1}^m \frac{\Sigma_{t,i}(r', E)}{\Sigma_t(r', E)} \cdot \frac{\sigma_{i,j}(E')}{\sigma_{t,i}(E')} \nu_{i,j}(E') f_{i,j}(\Omega', E' \rightarrow \Omega, E) \delta(r - r') \quad (\text{A.2})$$

In a simple game with capture, fission and scattering and only 1 type of nuclide :

$$C(P', P) = C_{capture} + C_{scattering} + C_{fission} \quad (\text{A.3})$$

$$= \frac{\sigma_c(E')}{\sigma_t(E')} \cdot 0 \cdot \delta(P') + \frac{\sigma_s(E')}{\sigma_t(E')} \cdot \nu_s(E') \cdot f_s(\Omega', E' \rightarrow \Omega, E) \delta(r - r') \quad (\text{A.4})$$

$$+ \sum_{n=1}^{\infty} \frac{\sigma_f}{\sigma_t} \cdot q_n \cdot \nu_{f,n}(E') \cdot f_f(\Omega', E' \rightarrow \Omega, E) \delta(r - r') \quad (\text{A.5})$$

First order moment:

$$\begin{aligned} M_1(P) &= \int dP' T(P, P') [f(P, P') + c_c(P',) f_c(P')] \quad (\text{A.6}) \\ &+ c_s(P') \int dP'' C_s(P', P'') f_s(P', P'') \\ &+ c_f(P') \sum_{n=1}^{\infty} n q_n(P') \int dP''' C_n(P', P''') f_n(P', P''') \\ &+ \int dP' T(P, P') \int dP'' C(P', P'') M_1(P'') \end{aligned}$$

To score the flux, it is necessary to consider a flight-based estimator, so $f_c(P') = f_s(P', P'') = f_n(P', P'') = 0$, and:

$$M_1(P) = \int dP' T(P, P') f(P, P') + \int dP' T(P, P') \int dP'' C(P', P'') M_1(P'') \quad (\text{A.7})$$

Regardless of the type of game being simulated, the first order moment needs to be preserved.

Second order moment is instead:

$$\begin{aligned} M_2(P) = & \int dP' T(P, P') c_c(P') [f(P, P') + f_c(P')]^2 \quad (\text{A.8}) \\ & + \left[1 \int dP' T(P, P') c_s(P') \int dP'' C_s(P', P'') [f(P, P') + f_s(P', P'')]^2 \right] \\ & + \left[2 \int dP' T(P, P') c_s(P') \int dP'' C_s(P', P'') [f(P, P') + f_s(P', P'')] M_1(P'') \right] \\ & + \left[1 \int dP' T(P, P') c_s(P') \int dP'' C_s(P', P'') M_2(P'') \right] \\ & + \left[1 \int dP' T(P, P') c_f(P') \sum_{n=1}^{\infty} n q_n \cdot \left(\int dP'' C_n(P', P'') (f(P, P') + f_n(P', P''))^2 \right) \right] \\ & + \left[2 \int dP' T(P, P') c_f(P') \sum_{n=1}^{\infty} n q_n \cdot \left(\int dP'' C_n(P', P'') (f(P, P') + f_n(P', P'')) M_1(P'') \right) \right] \\ & + \left[1 \int dP' T(P, P') c_f(P') \sum_{n=1}^{\infty} n q_n \cdot \left(\int dP'' C_n(P', P'') M_2(P'') \right) \right] \\ & + \int dP' T(P, P') c_f(P') \sum_{n=1}^{\infty} n(n-1) q_n \cdot \left[\int dP'' C_n(P', P'') (f_n(P', P'') + M_1(P'')) \right]^2 \\ & - \int dP' T(P, P') c_f(P') \sum_{n=1}^{\infty} (n-1) q_n f^2(P, P') \end{aligned}$$

Similarly, to score the flux, the second order moment becomes:

$$\begin{aligned}
M_2(P) = & \int dP' T(P, P') c_c(P') [f(P, P')]^2 \\
& + \left[1 \int dP' T(P, P') c_s(P') \int dP'' C_s(P', P'') [f(P, P')]^2 \right] \\
& + \left[2 \int dP' T(P, P') c_s(P') \int dP'' C_s(P', P'') [f(P, P')] M_1(P'') \right] \\
& + \left[1 \int dP' T(P, P') c_s(P') \int dP'' C_s(P', P'') M_2(P'') \right] \\
& + \left[1 \int dP' T(P, P') c_f(P') \sum_{n=1}^{\infty} n q_n \cdot \left(\int dP'' C_n(P', P'') (f(P, P'))^2 \right) \right] \\
& + \left[2 \int dP' T(P, P') c_f(P') \sum_{n=1}^{\infty} n q_n \cdot \left(\int dP'' C_n(P', P'') (f(P, P')) M_1(P'') \right) \right] \\
& + \left[1 \int dP' T(P, P') c_f(P') \sum_{n=1}^{\infty} n q_n \cdot \left(\int dP'' C_n(P', P'') M_2(P'') \right) \right] \\
& + \int dP' T(P, P') c_f(P') \sum_{n=1}^{\infty} n(n-1) q_n \cdot \left[\int dP'' C_n(P', P'') (M_1(P'')) \right]^2 \\
& - \int dP' T(P, P') c_f(P') \sum_{n=1}^{\infty} (n-1) q_n f^2(P, P')
\end{aligned} \tag{A.9}$$

The expressions of the first and second order moment were derived by Lux [1] in the case of a particle with general weight W ; if the game is a purely analog game it is possible to derive these expressions by putting the particle weight equal to unity. An example of the full derivation of the moments equation will be given in Appendix C of this current work.

Appendix B

Implicit capture games derivation of the moments

The transport kernel is the same as the one in Appendix A, since this game does not affect it.

$$T(P', P) = T^*(P', P) \quad (\text{B.1})$$

The collision kernel is obtained with modified probabilities that are going to be indicated with the symbol *:

$$C^*(P', P) = \sum_{i=1}^n \sum_{j=1}^m \frac{\Sigma_{t,i}^*(r', E)}{\Sigma_t^*(r', E)} \cdot \frac{\sigma_{i,j}^*(E')}{\sigma_{t,i}^*(E')} \nu_{i,j}(E') f_{i,j}(\Omega', E' \rightarrow \Omega, E) \delta(r - r') \quad (\text{B.2})$$

And in the same simple case as Appendix A:

$$C^*(P', P) = \frac{\sigma_s^*(E')}{\sigma_t^*(E')} \cdot \nu_s(E') \cdot f_s(\Omega', E' \rightarrow \Omega, E) \delta(r - r') \quad (\text{B.3})$$

$$+ \sum_{n=1}^{\infty} \frac{\sigma_f^*}{\sigma_t^*} \cdot q_n \cdot \nu_{f,n}(E') \cdot f_f(\Omega', E' \rightarrow \Omega, E) \delta(r - r')$$

$$= c_s^*(P') \cdot \nu_s(E') \cdot f_s(\Omega', E' \rightarrow \Omega, E) \delta(r - r') \quad (\text{B.4})$$

$$+ \sum_{n=1}^{\infty} c_f^*(P') \cdot q_n \cdot \nu_{f,n}(E') \cdot f_f(\Omega', E' \rightarrow \Omega, E) \delta(r - r')$$

Where:

$$c_s^*(P') = \frac{\sigma_s(P')}{\sigma_t(P')} / \left(1 - \frac{\sigma_c}{\sigma_t}\right) = \frac{c_s(P')}{1 - c_c(P')} \quad (\text{B.5})$$

$$c_f^*(P') = \frac{\sigma_f(P')}{\sigma_t(P')} / \left(1 - \frac{\sigma_c}{\sigma_t}\right) = \frac{c_f(P')}{1 - c_c(P')} \quad (\text{B.6})$$

Introducing a biasing in the collision kernel it is necessary to introduce a weight correction in the particles.

The first order moment is then:

$$\begin{aligned}
M_1^*(P) &= \int dP' T^*(P, P) \left[\frac{W'}{W} f^*(P, P') + c_c^*(P') \frac{W^c}{W} f_c^*(P') \right. \\
&\quad + c_s^*(P') \int dP'' C_s^*(P', P'') \frac{W''}{W} f_s^*(P', P'') \\
&\quad \left. + c_f^*(P') \sum_{n=1}^{\infty} n q_n \int dP'' C_n^*(P', P'') \frac{W_n''}{W} f_n^*(P', P'') \right] \\
&\quad + \int dP' T^*(P, P') \left[c_s^*(P') \int dP'' C_s^*(P', P'') \frac{W''}{W} M_1^*(P'') \right] \\
&\quad + \int dP' T^*(P, P') \left[c_f^*(P') \sum_{n=1}^{\infty} n q_n \int dP'' C_n^*(P', P'') \frac{W_n''}{W} M_1^*(P'') \right]
\end{aligned} \tag{B.7}$$

Then substituting:

$$W' = W \tag{B.8}$$

$$W'' = W(1 - c_c(P')) \tag{B.9}$$

$$W_n'' = W(1 - c_c(P')) \tag{B.10}$$

$$c_c^*(P') = 0 \tag{B.11}$$

$$c_s^*(P') = \frac{c_s(P')}{1 - c_c(P')} \tag{B.12}$$

$$c_f^*(P') = \frac{c_f(P')}{1 - c_c(P')} \tag{B.13}$$

$$f^*(P, P') = f(P, P') \tag{B.14}$$

It is possible to obtain:

$$\begin{aligned}
M_1^*(P) &= \int dP' T(P, P) [f(P, P') \\
&\quad + \frac{c_s(P')}{1 - c_c(P')} \int dP'' C_s(P', P'') \frac{W(1 - c_c(P'))}{W} f_s^*(P', P'') \\
&\quad + \frac{c_f(P')}{1 - c_c(P')} \sum_{n=1}^{\infty} n q_n \int dP'' C_n(P', P'') \frac{W(1 - c_c(P'))}{W} f_n^*(P', P'')] \\
&\quad + \int dP' T(P, P') \left[\frac{c_s(P')}{1 - c_c(P')} \int dP'' C_s(P', P'') \frac{W(1 - c_c(P'))}{W} M_1^*(P'') \right] \\
&\quad + \int dP' T(P, P') \left[\frac{c_f(P')}{1 - c_c(P')} \sum_{n=1}^{\infty} n q_n(P') \int dP'' C_n(P', P'') \frac{W(1 - c_c(P'))}{W} M_1^*(P'') \right]
\end{aligned} \tag{B.15}$$

Then by simplifying the common terms and looking to a flight based estimator:

$$M_1^*(P) = \int dP' T(P, P) f(P, P') \tag{B.16}$$

$$+ \int dP' T(P, P') \int dP'' \left[c_s(P') C_s(P', P'') + c_f(P') \sum_{n=1}^{\infty} n q_n(P') C_n(P', P'') \right] M_1^*(P'')$$

$$= \int dP' T(P, P') f(P, P') + \int dP' T(P, P') \int dP'' C(P', P'') M_1^*(P'')$$

$$= M_1(P) \tag{B.17}$$

And the second order moment is:

$$\begin{aligned}
M_2^*(P) &= \frac{1}{W^2} \cdot \left[\int dP' T^*(P, P') c_c^*(P') [W' f^*(P, P') + W^c f_c^*(P')]^2 \right] \\
&+ \frac{1}{W^2} \cdot \left[1 \int dP' T^*(P, P') c_s^*(P') \int dP'' C_s^*(P', P'') [W' f^*(P, P') + W'' f_s^*(P', P'')]^2 \right] \\
&+ \frac{1}{W^2} \cdot \left[2 \int dP' T^*(P, P') c_s^*(P') \int dP'' C_s^*(P', P'') [W' f^*(P, P') + W'' f_s^*(P', P'')] (W'') M_1^*(P'') \right] \\
&+ \frac{1}{W^2} \cdot \left[1 \int dP' T^*(P, P') c_s^*(P') \int dP'' C_s^*(P', P'') (W'')^2 M_2^*(P'') \right] \\
&+ \frac{1}{W^2} \cdot \left[1 \int dP' T^*(P, P') c_f^*(P') \sum_{n=1}^{\infty} n q_n \right. \\
&\quad \cdot \left. \int dP'' C_n^*(P', P'') (W' f^*(P, P') + W_n^* f_n^*(P', P''))^2 \right] \\
&+ \frac{1}{W^2} \cdot \left[2 \int dP' T^*(P, P') c_f^*(P') \sum_{n=1}^{\infty} n q_n \right. \\
&\quad \cdot \left. \int dP'' C_n^*(P', P'') (W' f^*(P, P') + W_n^* f_n^*(P', P'')) W_n'' M_1^*(P'') \right] \\
&+ \frac{1}{W^2} \cdot \left[1 \int dP' T^*(P, P') c_f^*(P') \sum_{n=1}^{\infty} n q_n \right. \\
&\quad \cdot \left. \int dP'' C_n^*(P', P'') (W_n'')^2 M_2^*(P'') \right] \\
&+ \frac{1}{W^2} \int dP' T^*(P, P') c_f^*(P') \sum_{n=1}^{\infty} n(n-1) q_n \\
&\quad \cdot \left[\int dP'' C_n^*(P', P'') W_n'' [f_n^*(P', P'') + M_1^*(P'')] \right]^2 \\
&- \frac{1}{W^2} \int dP' T^*(P, P') c_f^*(P') \sum_{n=1}^{\infty} (n-1) q_n W^2 (f^*(P, P'))^2 \\
&= \mathbb{Z} + \mathbb{A} + \mathbb{B} + \mathbb{C} + \mathbb{D} \cdot \mathbb{E} + \mathbb{F} \cdot \mathbb{G} + \mathbb{H} \cdot \mathbb{I} + \mathbb{J} \cdot \mathbb{K} - \mathbb{L}
\end{aligned} \tag{B.18}$$

$$\begin{aligned}
\mathbb{Z} &= \frac{1}{W^2} \cdot \left[\int dP' T^*(P, P') c_c^*(P') [W' f^*(P, P') + W^c f_c^*(P')]^2 \right] \\
&= \frac{1}{W^2} \cdot \left[\int dP' T(P, P') \cdot 0 \cdot [W f(P, P') + W^c f_c^*(P')]^2 \right] \\
&= 0
\end{aligned} \tag{B.19}$$

$$\begin{aligned}
\mathbb{A} &= \frac{1}{W^2} \cdot \left[1 \int dP' T^*(P, P') c_s^*(P') \int dP'' C_s^*(P', P'') [W' f^*(P, P') + W'' f_s^*(P', P'')]^2 \right] \\
&= \frac{1}{W^2} \cdot \left[1 \int dP' T(P, P') \frac{c_s(P')}{1 - c_c(P')} \int dP'' C_s(P', P'') [W f(P, P') + W(1 - c_c(P')) f_s(P', P'')]^2 \right] \\
&= \frac{1}{W^2} \cdot \left[1 \int dP' T(P, P') \frac{c_s(P')}{1 - c_c(P')} \int dP'' C_s(P', P'') W^2 f^2(P, P') \right] \\
&= \left[1 \int dP' T(P, P') c_s(P') \int dP'' C_s(P', P'') \frac{f^2(P, P')}{1 - c_c(P')} \right]
\end{aligned} \tag{B.20}$$

$$\begin{aligned}
\mathbb{B} &= \frac{1}{W^2} \cdot \left[2 \int dP' T^*(P, P') c_s^*(P') \int dP'' C_s^*(P', P'') [W' f^*(P, P') + W'' f_s^*(P', P'')] (W'') M_1^*(P'') \right] \\
&= \frac{1}{W^2} \cdot \left[2 \int dP' T(P, P') \frac{c_s(P')}{1 - c_c(P')} \int dP'' C_s(P', P'') [W f(P, P') + W(1 - c_c(P')) f_s(P', P'')] W(1 - c_c(P')) \right] \\
&= \frac{1}{W^2} \cdot \left[2 \int dP' T(P, P') \frac{c_s(P')}{1 - c_c(P')} \int dP'' C_s(P', P'') W^2 f(P, P') (1 - c_c(P')) M_1(P'') \right] \\
&= \left[2 \int dP' T(P, P') c_s(P') \int dP'' C_s(P', P'') f(P, P') M_1(P'') \right] \tag{B.21}
\end{aligned}$$

$$\begin{aligned}
\mathbb{C} &= \frac{1}{W^2} \cdot \left[1 \int dP' T^*(P, P') c_s^*(P') \int dP'' C_s^*(P', P'') (W'')^2 M_2^*(P'') \right] \\
&= \frac{1}{W^2} \cdot \left[1 \int dP' T(P, P') \frac{c_s(P')}{1 - c_c(P')} \int dP'' C_s(P', P'') (W(1 - c_c(P')))^2 M_2^*(P'') \right] \\
&= \left[1 \int dP' T(P, P') c_s(P') \int dP'' C_s(P', P'') (1 - c_c(P')) M_2^*(P'') \right] \tag{B.22}
\end{aligned}$$

$$\begin{aligned}
\mathbb{D} &= \frac{1}{W^2} \cdot \int dP' T^*(P, P') c_f^*(P') \\
&= \frac{1}{W^2} \cdot \int dP' T(P, P') \frac{c_f(P')}{1 - c_c(P')} \tag{B.23}
\end{aligned}$$

$$\begin{aligned}
\mathbb{E} &= \sum_{n=1}^{\infty} n q_n \int dP'' C_n^*(P', P'') (W' f^*(P, P') + W_n^* f_n^*(P', P''))^2 \\
&= \sum_{n=1}^{\infty} n q_n \int dP'' C_n(P', P'') (W f(P, P') + W_n(1 - c_c(P')) f_n(P', P''))^2 \\
&= \sum_{n=1}^{\infty} n q_n \int dP'' C_n(P', P'') W^2 f^2(P, P') \tag{B.24}
\end{aligned}$$

$$\begin{aligned}
\mathbb{D} \cdot \mathbb{E} &= \frac{1}{W^2} \cdot \left[\int dP' T(P, P') \frac{c_f(P')}{1 - c_c(P')} \sum_{n=1}^{\infty} n q_n \int dP'' C_n(P', P'') W^2 f^2(P, P') \right] \\
&= \left[\int dP' T(P, P') c_f(P') \sum_{n=1}^{\infty} n q_n \int dP'' C_n(P', P'') \frac{f^2(P, P')}{1 - c_c(P')} \right] \tag{B.25}
\end{aligned}$$

$$\begin{aligned}
\mathbb{F} &= \frac{1}{W^2} \cdot 2 \cdot \int dP' T^*(P, P') c_f^*(P') \\
&= \frac{1}{W^2} \cdot 2 \cdot \int dP' T(P, P') \frac{c_f(P')}{1 - c_c(P')} \tag{B.26}
\end{aligned}$$

$$\begin{aligned}
\mathbb{G} &= \sum_{n=1}^{\infty} n q_n \int dP'' C_n^*(P', P'') (W' f^*(P, P') + W_n^* f_n^*(P', P'')) W_n'' M_1^*(P'') \\
&= \sum_{n=1}^{\infty} n q_n \int dP'' C_n(P', P'') (W f(P, P') + W_n(1 - c_c(P')) f_n(P', P'')) W(1 - c_c(P')) M_1(P'') \\
&= \sum_{n=1}^{\infty} n q_n \int dP'' C_n(P', P'') W^2 f(P, P') (1 - c_c(P')) M_1(P'') \tag{B.27}
\end{aligned}$$

$$\begin{aligned}
\mathbb{F} \cdot \mathbb{G} &= \frac{1}{W^2} \cdot \left[2 \int dP' T(P, P') \frac{c_f(P')}{1 - c_c(P')} \sum_{n=1}^{\infty} n q_n \int dP'' C_n(P', P'') W^2 f(P, P') (1 - c_c(P')) M_1(P'') \right] \\
&= \left[2 \int dP' T(P, P') c_f(P') \sum_{n=1}^{\infty} n q_n \int dP'' C_n(P', P'') f(P, P') M_1(P'') \right] \quad (\text{B.28})
\end{aligned}$$

$$\begin{aligned}
\mathbb{H} &= \frac{1}{W^2} \cdot \int dP' T^*(P, P') c_f^*(P') \\
&= \frac{1}{W^2} \cdot \int dP' T(P, P') \frac{c_f(P')}{1 - c_c(P')} \quad (\text{B.29})
\end{aligned}$$

$$\begin{aligned}
\mathbb{I} &= \sum_{n=1}^{\infty} n q_n \int dP'' C_n^*(P', P'') (W_n'')^2 M_2^*(P'') \\
&= \sum_{n=1}^{\infty} n q_n \int dP'' C_n(P', P'') (W(1 - c_c(P')))^2 M_2^*(P'') \\
&= \sum_{n=1}^{\infty} n q_n \int dP'' C_n(P', P'') W^2 (1 - c_c(P'))^2 M_2^*(P'') \quad (\text{B.30})
\end{aligned}$$

$$\begin{aligned}
\mathbb{H} \cdot \mathbb{I} &= \frac{1}{W^2} \cdot \left[\int dP' T(P, P') \frac{c_f(P')}{1 - c_c(P')} \sum_{n=1}^{\infty} n q_n \int dP'' C_n(P', P'') W^2 (1 - c_c(P'))^2 M_2^*(P'') \right] \\
&= \left[\int dP' T(P, P') c_f(P') \sum_{n=1}^{\infty} n q_n \int dP'' C_n(P', P'') (1 - c_c(P')) M_2^*(P'') \right] \quad (\text{B.31})
\end{aligned}$$

$$\begin{aligned}
\mathbb{J} &= \frac{1}{W^2} \int dP' T^*(P, P') c_f^*(P') \\
&= \frac{1}{W^2} \int dP' T(P, P') \frac{c_f(P')}{1 - c_c(P')} \quad (\text{B.32})
\end{aligned}$$

$$\begin{aligned}
\mathbb{K} &= \sum_{n=1}^{\infty} n(n-1) q_n \left[\int dP'' C_n^*(P', P'') W_n'' [f_n^*(P', P'') + M_1^*(P'')] \right]^2 \\
&= \sum_{n=1}^{\infty} n(n-1) q_n \left[\int dP'' C_n(P', P'') W(1 - c_c(P')) [f_n(P', P'') + M_1(P'')] \right]^2 \\
&= \sum_{n=1}^{\infty} n(n-1) q_n \left[\int dP'' C_n(P', P'') W(1 - c_c(P')) M_1(P'') \right]^2 \quad (\text{B.33})
\end{aligned}$$

$$\begin{aligned}
\mathbb{J} \cdot \mathbb{K} &= \frac{1}{W^2} \int dP' T(P, P') \frac{c_f(P')}{1 - c_c(P')} \sum_{n=1}^{\infty} n(n-1) q_n \left[\int dP'' C_n(P', P'') W(1 - c_c(P')) M_1(P'') \right]^2 \\
&= \frac{1}{W^2} \int dP' T(P, P') \frac{c_f(P')}{1 - c_c(P')} \sum_{n=1}^{\infty} n(n-1) q_n W^2 (1 - c_c(P'))^2 \left[\int dP'' C_n(P', P'') M_1(P'') \right]^2 \\
&= \int dP' T(P, P') c_f(P') \sum_{n=1}^{\infty} n(n-1) q_n (1 - c_c(P')) \left[\int dP'' C_n(P', P'') M_1(P'') \right]^2 \quad (\text{B.34})
\end{aligned}$$

$$\begin{aligned}
\mathbb{L} &= \frac{1}{W^2} \int dP' T^*(P, P') c_f^*(P') \sum_{n=1}^{\infty} (n-1) q_n W^2 (f^*(P, P'))^2 \\
&= \frac{1}{W^2} \int dP' T(P, P') \frac{c_f(P')}{1 - c_c(P')} \sum_{n=1}^{\infty} (n-1) q_n W^2 f^2(P, P') \\
&= \int dP' T(P, P') c_f(P') \sum_{n=1}^{\infty} (n-1) q_n \frac{f^2(P, P')}{1 - c_c(P')} \tag{B.35}
\end{aligned}$$

So, in the case of a flight-based estimator:

$$\begin{aligned}
M_2^*(P) &= 0 \tag{B.36} \\
&+ \left[1 \int dP' T(P, P') c_s(P') \int dP'' C_s(P', P'') \frac{f^2(P, P')}{1 - c_c(P')} \right] \\
&+ \left[2 \int dP' T(P, P') c_s(P') \int dP'' C_s(P', P'') f(P, P') M_1(P'') \right] \\
&+ \left[1 \int dP' T(P, P') c_s(P') \int dP'' C_s(P', P'') (1 - c_c(P')) M_2^*(P'') \right] \\
&+ \left[1 \int dP' T(P, P') c_f(P') \sum_{n=1}^{\infty} n q_n \int dP'' C_n(P', P'') \frac{f^2(P, P')}{1 - c_c(P')} \right] \\
&+ \left[2 \int dP' T(P, P') c_f(P') \sum_{n=1}^{\infty} n q_n \int dP'' C_n(P', P'') f(P, P') M_1(P'') \right] \\
&+ \left[1 \int dP' T(P, P') c_f(P') \sum_{n=1}^{\infty} n q_n \int dP'' C_n(P', P'') (1 - c_c(P')) M_2^*(P'') \right] \\
&+ \int dP' T(P, P') c_f(P') \sum_{n=1}^{\infty} n(n-1) q_n (1 - c_c(P')) \left[\int dP'' C_n(P', P'') M_1(P'') \right]^2 \\
&- \int dP' T(P, P') c_f(P') \sum_{n=1}^{\infty} (n-1) q_n \frac{f^2(P, P')}{1 - c_c(P')}
\end{aligned}$$

For which the dependency on the particle weight was removed.

Appendix C

Forced fission games derivation of the moments

Due to the different hypothesis at the foundation of the game, a new formulation of the moments equation is necessary. In the following pages the expressions for the first and second order moment of the estimator f will be derived and from them the new zero-variance scheme will follow.

Using the symbol " \wedge " to indicate a general non-analog game (particle weight $W \neq 1$), it is possible to write the expression for the quantity $\theta(P', W', s)ds$, i.e. the probability that a particle *entering* a collision P' with weight W' will yield, along with its progenies, a total score in ds about s .

$$\begin{aligned} \theta(P', W', s) &= \hat{c}_c(P') \\ &+ \int dP'' \hat{C}_s(P', P'') \pi(P'', W'', s) \\ &* \sum_{n=1}^{\infty} \hat{q}_n(P') \prod_{i=1}^n * \int dP''_{(i)} \hat{C}_n(P', P''_{(i)}) \times \pi(P''_{(i)}, W''_{n(i)}, s) \end{aligned} \quad (C.1)$$

From this quantity, a new probability is defined: $\pi(P, W, s)ds$ is the probability that a particle *leaving* a collision (or entering a flight), in P with weight W will yield, along with its progenies, a total score in ds about s . The symbol $*$ indicates a convolution product.

$$\pi(P, W, s) = \int dP' \hat{T}(P, P') \delta[s - \hat{f}(P, P', W')] * \theta(P', W', s) \quad (C.2)$$

The aim is now elaborating the previous equation by splitting it into the different contribution of the reaction channels. For the absorption part:

$$\begin{aligned} &\rightarrow \int dP' \hat{T}(P, P') \hat{c}_c(P') * \delta(s - \hat{f}(P, P', W')) \\ &\int dP' \hat{T}(P, P') \hat{c}_c(P') \delta(s - \hat{f}(P, P', W')) \end{aligned} \quad (C.3)$$

For the scattering and fission part:

$$\begin{aligned} &\rightarrow \int dP' \hat{T}(P, P') \delta(s - \hat{f}(P, P', W')) * \left\{ \int dP'' \hat{C}_s(P', P'') \delta(s) \pi(P'', W'', s) \right\} * \\ &\sum_{n=1}^{\infty} \hat{q}_n(P') \left\{ \int dP''_{(1)} \int ds_{(1)} \dots \int dP''_{(n)} \int ds_{(n)} \prod_{i=1}^n \hat{C}_n(P', P''_{(i)}) \delta(s) \pi(P''_{(i)}, W''_{n(i)}, s) \right\} \end{aligned} \quad (C.4)$$

So:

$$\begin{aligned}
\pi(P, W, s) &= \int dP' \hat{T}(P, P') \hat{c}_c(P') \delta(s - \hat{f}(P, P', W')) \\
&+ \int dP' \hat{T}(P, P') \sum_{n=1}^{\infty} \hat{q}_n(P') \left\{ \left[\int dP'' \hat{C}_s(P', P'') \int ds_s \pi(P'', W'', s_s) \cdot \right. \right. \\
&\left. \left. \left(\int dP''_{(1)} \int ds_{(1)} \dots \int dP''_{(n)} \int ds_{(n)} \prod_{i=1}^n \hat{C}_n(P', P''_{(i)}) \pi(P''_{(i)}, W''_{n(i)}, s_i) \right) \right] \right. \\
&\left. \times \delta\left(s - s_s - \sum_{k=1}^n s_k - \hat{f}(P, P', W')\right) \right\} \quad (C.5)
\end{aligned}$$

Using the notation where the scattering is the $n + 1$ of the product and using the fact that $\hat{c}_c(P') = 0$:

$$\begin{aligned}
\pi(P, W, s) &= \int dP' \hat{T}(P, P') \sum_{n=1}^{\infty} \hat{q}_n(P') \left\{ \left[\left(\int dP''_{(1)} \int ds_{(1)} \dots \int dP''_{(n+1)} \int ds_{(n+1)} \prod_{i=1}^{n+1} \hat{C}_n(P', P''_{(i)}) \right. \right. \right. \\
&\left. \left. \left. \pi(P''_{(i)}, W''_{n(i)}, s_i) \right) \right] \times \delta\left(s - \sum_{k=1}^{n+1} s_k - \hat{f}(P, P', W')\right) \right\} \quad (C.6)
\end{aligned}$$

Now the j -th moment of the score s can be found by:

$$\hat{M}_j(P) = \int_{-\infty}^{+\infty} ds s^j \pi(P, W, s) \quad (C.7)$$

The first order moment is:

$$\begin{aligned}
\hat{M}_1(P, W) &= \int_{-\infty}^{+\infty} ds s \pi(P, W, s) \\
&= \int_{-\infty}^{+\infty} ds s \int dP' \hat{T}(P, P') \sum_{n=1}^{\infty} \hat{q}_n(P') \\
&\left\{ \left[\left(\int dP''_{(1)} \int ds_{(1)} \dots \int dP''_{(n+1)} \int ds_{(n+1)} \prod_{i=1}^{n+1} \hat{C}_n(P', P''_{(i)}) \right. \right. \right. \\
&\left. \left. \left. \pi(P''_{(i)}, W''_{n(i)}, s_i) \right) \right] \times \delta\left(s - \sum_{k=1}^{n+1} s_k - \hat{f}(P, P', W')\right) \right\} \\
&= \int dP' \hat{T}(P, P') \sum_{n=1}^{\infty} \hat{q}_n(P') \left\{ \left[\left(\prod_{i=1}^{n+1} \int dP''_{(i)} \hat{C}_n(P', P''_{(i)}) \int ds_{(i)} \pi(P''_{(i)}, W''_{n(i)}, s_i) \right) \right] \right. \\
&\times \int_{-\infty}^{+\infty} ds s \delta\left(s - \sum_{k=1}^{n+1} s_k - \hat{f}(P, P', W')\right) \left. \right\} \\
&= \int dP' \hat{T}(P, P') \sum_{n=1}^{\infty} \hat{q}_n(P') \left\{ \left[\left(\prod_{i=1}^{n+1} \int dP''_{(i)} \hat{C}_n(P', P''_{(i)}) \int ds_{(i)} \pi(P''_{(i)}, W''_{n(i)}, s_i) \right) \right] \right. \\
&\times \left. \left(\sum_{k=1}^{n+1} s_k + \hat{f}(P, P', W') \right) \right\} \quad (C.8)
\end{aligned}$$

Splitting it into the terms:

$$\begin{aligned}
\hat{M}_1(P, W) &= \int dP' \hat{T}(P, P') \sum_{n=1}^{\infty} \hat{q}_n(P') \left\{ \left[\left(\sum_{k=1}^{n+1} s_k \prod_{i=1}^{n+1} \int dP''_{(i)} \hat{C}_n(P', P''_{(i)}) \int ds_{(i)} \pi(P''_{(i)}, W''_{n(i)}, s_i) \right) \right] \right\} \\
&+ \int dP' \hat{T}(P, P') \sum_{n=1}^{\infty} \hat{q}_n(P') \left\{ \left[\left(\hat{f}(P, P', W') \prod_{i=1}^{n+1} \int dP''_{(i)} \hat{C}_n(P', P''_{(i)}) \int ds_{(i)} \pi(P''_{(i)}, W''_{n(i)}, s_i) \right) \right] \right\} \\
&= I_1(P, W) + I_2(P, W)
\end{aligned} \tag{C.9}$$

$$\begin{aligned}
I_1(P, W) &= \int dP' \hat{T}(P, P') \sum_{n=1}^{\infty} \hat{q}_n(P') \left\{ \sum_{k=1}^{n+1} s_k \prod_{i=1}^{n+1} \int dP''_{(i)} \hat{C}_n(P', P''_{(i)}) \int ds_{(i)} \pi(P''_{(i)}, W''_{n(i)}, s_i) \right\} \\
&= \int dP' \hat{T}(P, P') \sum_{n=1}^{\infty} \hat{q}_n(P') \left\{ G_1 \right\}
\end{aligned} \tag{C.10}$$

$$\begin{aligned}
G_1 &= \left(s_1 + s_2 + \dots + s_{n+1} \right) \\
&\cdot \left(\int dP''_{(1)} \hat{C}_n(P', P''_{(1)}) \int dP''_{(2)} \hat{C}_n(P', P''_{(2)}) \dots \int dP''_{(n+1)} \hat{C}_n(P', P''_{(n+1)}) \right) \\
&\cdot \left(\int ds_{(1)} \pi(P''_{(1)}, W''_{n(1)}, s_1) \int ds_{(2)} \pi(P''_{(2)}, W''_{n(2)}, s_2) \dots \int ds_{(n+1)} \pi(P''_{(n+1)}, W''_{n(n+1)}, s_{n+1}) \right)
\end{aligned} \tag{C.11}$$

Which is:

$$\begin{aligned}
G_1 &= \sum_{i=1}^{n+1} \int dP''_{(i)} \hat{C}_n(P', P''_{(i)}) \hat{M}_1(P''_{(i)}, W''_{n(i)}) \\
&= \int dP'' \hat{C}_s(P', P'') \hat{M}_1(P'') W'' + \sum_{i=1}^n \int dP''_{(i)} \hat{C}_n(P', P''_{(i)}) \hat{M}_1(P''_{(i)}) W''_{n(i)}
\end{aligned} \tag{C.12}$$

And:

$$\begin{aligned}
 I_1(P, W) &= \int dP' \hat{T}(P, P') \sum_{n=1}^{\infty} \hat{q}_n(P') \\
 &\quad \left\{ \int dP'' \hat{C}_s(P', P'') \hat{M}_1(P'') W'' + \sum_{i=1}^n \int dP''_{(i)} \hat{C}_n(P', P''_{(i)}) \hat{M}_1(P''_{(i)}) W''_{n(i)} \right\} \\
 &= \int dP' \hat{T}(P, P') \left\{ \left[\int dP'' \hat{C}_s(P', P'') \hat{M}_1(P'') \right] W'' \sum_{n=1}^{\infty} \hat{q}_n(P') \right\} \\
 &\quad + \int dP' \hat{T}(P, P') \left\{ \sum_{n=1}^{\infty} \hat{q}_n(P') \left[\sum_{i=1}^n \int dP''_{(i)} \hat{C}_n(P', P''_{(i)}) \hat{M}_1(P''_{(i)}) W''_{n(i)} \right] \right\} \\
 &= \int dP' \hat{T}(P, P') \left\{ \left[\int dP'' \hat{C}_s(P', P'') \hat{M}_1(P'') \right] W'' \right\} \\
 &\quad + \int dP' \hat{T}(P, P') \left\{ \sum_{n=1}^{\infty} \hat{q}_n(P') \left[\sum_{i=1}^n \int dP''_{(i)} \hat{C}_n(P', P''_{(i)}) \hat{M}_1(P''_{(i)}) W''_{n(i)} \right] \right\}
 \end{aligned} \tag{C.13}$$

The other term is instead:

$$\begin{aligned}
 I_2(P, W) &= \int dP' \hat{T}(P, P') \hat{f}(P, P', W') \left\{ \sum_{n=1}^{\infty} \hat{q}_n(P') \left[\prod_{i=1}^{n+1} \int dP''_{(i)} \hat{C}_n(P', P''_{(i)}) \int ds_{(i)} \pi(P''_{(i)}, W''_{n(i)}, s_i) \right] \right\} \\
 &= \int dP' \hat{T}(P, P') \hat{f}(P, P', W') \left\{ \sum_{n=1}^{\infty} \hat{q}_n(P') \right\} \\
 &= \int dP' \hat{T}(P, P') \hat{f}(P, P') W'
 \end{aligned} \tag{C.14}$$

So the first order moment is:

$$\begin{aligned}
 W \hat{M}_1(P) &= \int dP' \hat{T}(P, P') \hat{f}(P, P') W' \\
 &\quad + \int dP' \hat{T}(P, P') \int dP'' \hat{C}_s(P', P'') \hat{M}_1(P'') W'' \\
 &\quad + \int dP' \hat{T}(P, P') \sum_{n=1}^{\infty} \hat{q}_n(P') \sum_{i=1}^n \int dP''_{(i)} \hat{C}_n(P', P''_{(i)}) \hat{M}_1(P''_{(i)}) W''_{n(i)}
 \end{aligned} \tag{C.15}$$

Or, alternately it is possible to make the equation look more like the original one derived from the analog game by slightly changing the weight definitions:

$$\begin{aligned}
 \hat{M}_1(P) &= \int dP' \hat{T}(P, P') \hat{f}(P, P') W' \\
 &\quad + \int dP' \hat{T}(P, P') \hat{c}_s(P') \int dP'' \hat{C}_s(P', P'') \hat{M}_1(P'') \widehat{W}'' \\
 &\quad + \int dP' \hat{T}(P, P') \hat{c}_f(P') \sum_{n=1}^{\infty} \hat{q}_n(P') \sum_{i=1}^n \int dP''_{(i)} \hat{C}_n(P', P''_{(i)}) \hat{M}_1(P''_{(i)}) \widehat{W}''_{n(i)}
 \end{aligned} \tag{C.16}$$

Assuming a starting weight $W = 1$, the weight generation rules that conserves the first order moment are:

$$\begin{aligned}
W' &= \frac{T(P, P')}{\hat{T}(P, P')} \\
\widehat{W}'' &= W' \frac{c_s(P') C_s(P', P'')}{\hat{c}_s(P') \hat{C}_s(P', P'')} \rightarrow W'' = W' \frac{c_s(P') C_s(P', P'')}{\hat{C}_s(P', P'')} \\
\widehat{W}''_{(i)} &= W' \frac{c_{f,n}(P') C_n(P', P'')}{\hat{c}_{f,n}(P') \hat{C}_n(P', P'')} \rightarrow W''_{(i)} = W' \frac{c_f(P') q_n(P') C_n(P', P'')}{\hat{q}_n(P') \hat{C}_n(P', P'')}
\end{aligned} \tag{C.17}$$

The second order moment is instead:

$$\begin{aligned}
\hat{M}_2(P, W) &= \int_{-\infty}^{+\infty} ds s^2 \pi(P, W, s) \\
&= \int_{-\infty}^{+\infty} ds s^2 \int dP' \hat{T}(P, P') \sum_{n=1}^{\infty} \hat{q}_n(P') \\
&\quad \left\{ \left[\left(\int dP''_{(1)} \int ds_{(1)} \dots \int dP''_{(n+1)} \int ds_{(n+1)} \prod_{i=1}^{n+1} \hat{C}_n(P', P''_{(i)}) \right. \right. \right. \\
&\quad \left. \left. \left. \pi(P''_{(i)}, W''_{n(i)}, s_i) \right) \right] \times \delta \left(s - \sum_{k=1}^{n+1} s_k - \hat{f}(P, P', W') \right) \right\} \\
&= \int dP' \hat{T}(P, P') \sum_{n=1}^{\infty} \hat{q}_n(P') \left\{ \left[\left(\int dP''_{(1)} \int ds_{(1)} \dots \int dP''_{(n+1)} \int ds_{(n+1)} \prod_{i=1}^{n+1} \hat{C}_n(P', P''_{(i)}) \right. \right. \right. \\
&\quad \left. \left. \left. \pi(P''_{(i)}, W''_{n(i)}, s_i) \right) \right] \times \left(\sum_{k=1}^{n+1} s_k + \hat{f}(P, P', W') \right)^2 \right\} \\
&= \int dP' \hat{T}(P, P') \sum_{n=1}^{\infty} \hat{q}_n(P') \left\{ \left[G_2 \right] \times \left(\sum_{k=1}^{n+1} s_k + \hat{f}(P, P', W') \right)^2 \right\}
\end{aligned} \tag{C.18}$$

Using the identity:

$$\begin{aligned}
\left(\sum_i s_i + b \right)^2 &= \left[\sum_i (s_i - a_i)^2 \right] + \left[\sum_i \sum_{k, k \neq i} (s_i - a_i)(s_k - a_k) \right] \\
&\quad + \left[2 \sum_i (s_i - a_i) \left(\sum_k a_k + b \right) \right] + \left[\sum_i a_i + b \right]^2
\end{aligned} \tag{C.19}$$

In this case all the a_i and a_k are null, so:

$$\left(\sum_i s_i + b \right)^2 = \left[\sum_i s_i^2 \right] + \left[\sum_i \sum_{k, k \neq i} s_i s_k \right] + \left[2 \sum_i s_i b \right] + \left[b \right]^2 \tag{C.20}$$

Renaming each of the terms $I_3(P, W)$, $I_4(P, W)$, $I_5(P, W)$ and $I_6(P, W)$ and multiplying each one by the G_2 factor:

$$\begin{aligned}
I_3(P, W) &= G_2 \times \left(\sum_{k=1}^{n+1} s_k^2 \right) \\
&= \left[\left(\int dP''_{(1)} \int ds_{(1)} \dots \int dP''_{(n+1)} \int ds_{(n+1)} \prod_{i=1}^{n+1} \hat{C}_n(P', P''_{(i)}) \pi(P''_{(i)}, W''_{n(i)}, s_i) \right) \right] \times \left(\sum_{k=1}^{n+1} s_k^2 \right) \\
&= \left[\prod_{i=1}^{n+1} \int dP''_{(i)} \hat{C}_n(P', P''_{(i)}) \int ds_i \pi(P''_{(i)}, W''_{n(i)}, s_i) \right] \times \left(\sum_{k=1}^{n+1} s_k^2 \right) \\
&= \sum_{i=1}^{n+1} \int dP''_{(i)} \hat{C}_n(P', P''_{(i)}) \hat{M}_2(P''_{(i)}, W''_{n(i)}) \\
&= \int dP'' \hat{C}_s(P', P'') \hat{M}_2(P'') W'' + \sum_{i=1}^n \int dP''_{(i)} \hat{C}_n(P', P''_{(i)}) \hat{M}_2(P''_{(i)}) W''_{n(i)}
\end{aligned} \tag{C.21}$$

$$\begin{aligned}
I_4(P, W) &= G_2 \times \left[\sum_{k=1}^{n+1} \sum_{j, j \neq k}^{n+1} s_k s_j \right] \\
&= \left[\prod_{i=1}^{n+1} \int dP''_{(i)} \hat{C}_n(P', P''_{(i)}) \int ds_i \pi(P''_{(i)}, W''_{n(i)}, s_i) \right] \times \left[\sum_{k=1}^{n+1} \sum_{j, j \neq k}^{n+1} s_k s_j \right] \\
&= \sum_{k=1}^{n+1} \sum_{j, j \neq k}^{n+1} \int dP''_{(k)} \hat{C}_n(P', P''_{(k)}) \hat{M}_1(P''_{(k)}, W''_{n(k)}) \int dP''_{(j)} \hat{C}_n(P', P''_{(j)}) \hat{M}_1(P''_{(j)}, W''_{n(j)}) \\
&= 2 \int dP'' \hat{C}_s(P', P'') \hat{M}_1(P'') W'' \sum_{k=1}^n \int dP''_{(i)} \hat{C}_n(P', P''_{(i)}) \hat{M}_1(P''_{(i)}) W''_{n(i)} \\
&+ \sum_{k=1}^n \sum_{j, j \neq k}^n \int dP''_{(k)} \hat{C}_n(P', P''_{(k)}) \hat{M}_1(P''_{(k)}, W''_{n(k)}) \int dP''_{(j)} \hat{C}_n(P', P''_{(j)}) \hat{M}_1(P''_{(j)}, W''_{n(j)})
\end{aligned} \tag{C.22}$$

$$\begin{aligned}
I_5(P, W) &= \left[\prod_{i=1}^{n+1} \int dP''_{(i)} \hat{C}_n(P', P''_{(i)}) \int ds_i \pi(P''_{(i)}, W''_{n(i)}, s_i) \right] \times \left[2 \sum_{k=1}^{n+1} s_k \hat{f}(P, P', W') \right] \\
&= 2 \hat{f}(P, P', W') \sum_{i=1}^{n+1} \int dP''_{(i)} \hat{C}_n(P', P''_{(i)}) \hat{M}_1(P''_{(i)}, W''_{n(i)}) \\
&= 2 \hat{f}(P, P', W') \int dP'' \hat{C}_s(P', P'') \hat{M}_1(P'') W'' \\
&+ 2 \hat{f}(P, P', W') \sum_{i=1}^n \int dP''_{(i)} \hat{C}_n(P', P''_{(i)}) \hat{M}_1(P''_{(i)}) W''_{n(i)}
\end{aligned} \tag{C.23}$$

$$\begin{aligned}
I_6(P, W) &= \left[\prod_{i=1}^{n+1} \int dP''_{(i)} \hat{C}_n(P', P''_{(i)}) \int ds_i \pi(P''_{(i)}, W''_{n(i)}, s_i) \right] \times \left[\hat{f}(P, P', W') \right]^2 \\
&= 1 \cdot \left(\hat{f}(P, P', W') \right)^2
\end{aligned} \tag{C.24}$$

So the second order moment is:

$$\begin{aligned}
W^2 \hat{M}_2(P) &= \int dP' \hat{T}(P, P') \sum_{n=1}^{\infty} \hat{q}_n(P') \left[\hat{f}(P, P', W') \right]^2 \\
&+ \int dP' \hat{T}(P, P') \sum_{n=1}^{\infty} \hat{q}_n(P') \left[2\hat{f}(P, P', W') \int dP'' \hat{C}_s(P', P'') \hat{M}_1(P'') W'' \right. \\
&+ \left. 2\hat{f}(P, P', W') \sum_{i=1}^n \int dP''_{(i)} \hat{C}_n(P', P''_{(i)}) \hat{M}_1(P''_{(i)}) W''_{n(i)} \right] \\
&+ \int dP' \hat{T}(P, P') \sum_{n=1}^{\infty} \hat{q}_n(P') \\
&\left[2 \int dP'' \hat{C}_s(P', P'') \hat{M}_1(P'') W'' \sum_{k=1}^n \int dP''_{(i)} \hat{C}_n(P', P''_{(i)}) \hat{M}_1(P''_{(i)}) W''_{n(i)} \right. \\
&+ \left. \sum_{k=1}^n \sum_{j, j \neq k}^n \int dP''_{(k)} \hat{C}_n(P', P''_{(k)}) \hat{M}_1(P''_{(k)}, W''_{n(k)}) \int dP''_{(j)} \hat{C}_n(P', P''_{(j)}) \hat{M}_1(P''_{(j)}, W''_{n(j)}) \right] \\
&+ \int dP' \hat{T}(P, P') \sum_{n=1}^{\infty} \hat{q}_n(P') \left[\int dP'' \hat{C}_s(P', P'') \hat{M}_2(P'') (W'')^2 + \right. \\
&\left. \sum_{i=1}^n \int dP''_{(i)} \hat{C}_n(P', P''_{(i)}) \hat{M}_2(P''_{(i)}) (W''_{n(i)})^2 \right]
\end{aligned} \tag{C.25}$$

$$\begin{aligned}
W^2 \hat{M}_2(P) &= \int dP' \hat{T}(P, P') (\hat{f}(P, P'))^2 (W')^2 \\
&+ 2 \int dP' \hat{T}(P, P') \hat{f}(P, P') W' \left[\int dP'' \hat{C}_s(P', P'') \hat{M}_1(P'') W'' \right. \\
&+ \left. \sum_{n=1}^{\infty} \hat{q}_n(P') \sum_{i=1}^n \int dP''_{(i)} \hat{C}_n(P', P''_{(i)}) \hat{M}_1(P''_{(i)}) W''_{n(i)} \right] \\
&+ \int dP' \hat{T}(P, P') \left[2 \int dP'' \hat{C}_s(P', P'') \hat{M}_1(P'') W'' \sum_{n=1}^{\infty} \hat{q}_n(P') \right. \\
&\sum_{k=1}^n \int dP''_{(i)} \hat{C}_n(P', P''_{(i)}) \hat{M}_1(P''_{(i)}) W''_{n(i)} \\
&+ \left. \sum_{n=1}^{\infty} \hat{q}_n(P') \sum_{k=1}^n \sum_{j, j \neq k}^n \int dP''_{(k)} \hat{C}_n(P', P''_{(k)}) \hat{M}_1(P''_{(k)}) W''_{n(k)} \int dP''_{(j)} \hat{C}_n(P', P''_{(j)}) \hat{M}_1(P''_{(j)}) W''_{n(j)} \right] \\
&+ \int dP' \hat{T}(P, P') \left[\int dP'' \hat{C}_s(P', P'') \hat{M}_2(P'') W''^2 + \right. \\
&\left. \sum_{n=1}^{\infty} \hat{q}_n(P') \sum_{i=1}^n \int dP''_{(i)} \hat{C}_n(P', P''_{(i)}) \hat{M}_2(P''_{(i)}) (W''_{n(i)})^2 \right]
\end{aligned} \tag{C.26}$$

If all the outgoing fission particles are emitted with the same weight:

$$\begin{aligned}
W^2 \hat{M}_2(P) &= \int dP' \hat{T}(P, P') (\hat{f}(P, P'))^2 (W')^2 \\
&+ 2 \int dP' \hat{T}(P, P') \hat{f}(P, P') W' \left[\int dP'' \hat{C}_s(P', P'') \hat{M}_1(P'') W'' + \right. \\
&\left. \sum_{n=1}^{\infty} \hat{q}_n(P') n \int dP'' \hat{C}_n(P', P'') \hat{M}_1(P'') W_n'' \right] \\
&+ \int dP' \hat{T}(P, P') \left[2 \int dP'' \hat{C}_s(P', P'') \hat{M}_1(P'') W'' \sum_{n=1}^{\infty} \hat{q}_n(P') n \int dP'' \hat{C}_n(P', P'') \hat{M}_1(P'') W_n'' \right. \\
&\left. + \sum_{n=1}^{\infty} \hat{q}_n(P') n(n-1) \left(\int dP''_{(k)} \hat{C}_n(P', P'') \hat{M}_1(P'') W_n'' \right)^2 \right] \\
&+ \int dP' \hat{T}(P, P') \left[\int dP'' \hat{C}_s(P', P'') \hat{M}_2(P'') W''^2 + \right. \\
&\left. \sum_{n=1}^{\infty} \hat{q}_n(P') n \int dP'' \hat{C}_n(P', P'') \hat{M}_2(P'') (W_n'')^2 \right]
\end{aligned} \tag{C.27}$$

$$\begin{aligned}
W^2 \hat{M}_2(P) &= \int dP' \hat{T}(P, P') (\hat{f}(P, P'))^2 (W')^2 \\
&+ 2 \int dP' \hat{T}(P, P') \hat{f}(P, P') W' \left[\int dP'' \hat{C}_s(P', P'') \hat{M}_1(P'') W'' \right] \\
&+ 2 \int dP' \hat{T}(P, P') \hat{f}(P, P') W' \left[\sum_{n=1}^{\infty} \hat{q}_n(P') n \int dP'' \hat{C}_n(P', P'') \hat{M}_1(P'') W_n'' \right] \\
&+ \int dP' \hat{T}(P, P') \left[\int dP'' \hat{C}_s(P', P'') \hat{M}_2(P'') W''^2 \right] \\
&+ \int dP' \hat{T}(P, P') \left[\sum_{n=1}^{\infty} \hat{q}_n(P') n \int dP'' \hat{C}_n(P', P'') \hat{M}_2(P'') (W_n'')^2 \right] \\
&+ \int dP' \hat{T}(P, P') \left[2 \int dP'' \hat{C}_s(P', P'') \hat{M}_1(P'') W'' \sum_{n=1}^{\infty} \hat{q}_n(P') n \int dP'' \hat{C}_n(P', P'') \hat{M}_1(P'') W_n'' \right. \\
&\left. + \int dP' \hat{T}(P, P') \left[\sum_{n=1}^{\infty} \hat{q}_n(P') n(n-1) \left(\int dP'' \hat{C}_n(P', P'') \hat{M}_1(P'') W_n'' \right)^2 \right] \right]
\end{aligned} \tag{C.28}$$

To be compared with the original expression for the second order moment of a non-analog game (the one derived under the hypothesis that scattering and fission are mutually exclusives), which is:

$$\begin{aligned}
W^2 \hat{\mathbb{M}}_2(P) &= \int dP' \hat{T}(P, P') \hat{c}_a(P') \left[W' \hat{f}(P, P') + W^a \hat{f}_a(P') \right]^2 \\
&+ \sum_{r=0}^2 \binom{2}{r} \int dP' \hat{T}(P, P') \hat{c}_s(P') \int dP'' \hat{C}_s(P', P'') \\
&\left[W' \hat{f}(P, P') + W'' \hat{f}_s(P', P'') \right]^{2-r} (W'')^r \hat{M}_r(P'') \\
&+ \sum_{r=0}^2 \binom{2}{r} \int dP' \hat{T}(P, P') \hat{c}_f(P') \sum_{n=1}^{\infty} n \hat{q}_n(P') \\
&\int dP'' \hat{C}_n(P', P'') \left[W' \hat{f}(P, P') + W''_n \hat{f}_n(P', P'') \right]^{2-r} (W''_n)^r \hat{M}_r(P'') \\
&+ \int dP' \hat{T}(P, P') \hat{c}_f(P') \sum_{n=1}^{\infty} n(n-1) \hat{q}_n(P') \left\{ \int dP'' \hat{C}_n(P', P'') W''_n \left[\hat{f}_n(P', P'') + \hat{M}_1(P'') \right] \right\}^2 \\
&- \int dP' \hat{T}(P, P') \hat{c}_f(P') \sum_{n=1}^{\infty} (n-1) \hat{q}_n(P') (W')^2 (\hat{f}(P, P'))^2
\end{aligned} \tag{C.29}$$

A slight reworking will be done on the previous equation; putting $\hat{f}_a(P') = \hat{f}_s(P', P'') = \hat{f}_n(P', P'') = 0$ and $W = 1$:

$$\begin{aligned}
\hat{\mathbb{M}}_2(P) &= \int dP' \hat{T}(P, P') \hat{c}_a(P') \left[W' \hat{f}(P, P') \right]^2 \\
&+ \sum_{r=0}^2 \binom{2}{r} \int dP' \hat{T}(P, P') \hat{c}_s(P') \int dP'' \hat{C}_s(P', P'') \left[W' \hat{f}(P, P') \right]^{2-r} (W'')^r \hat{M}_r(P'') \\
&+ \sum_{r=0}^2 \binom{2}{r} \int dP' \hat{T}(P, P') \hat{c}_f(P') \sum_{n=1}^{\infty} n \hat{q}_n(P') \int dP'' \hat{C}_n(P', P'') \left[W' \hat{f}(P, P') \right]^{2-r} (W''_n)^r \hat{M}_r(P'') \\
&+ \int dP' \hat{T}(P, P') \hat{c}_f(P') \sum_{n=1}^{\infty} n(n-1) \hat{q}_n(P') \left\{ \int dP'' \hat{C}_n(P', P'') W''_n \left[\hat{M}_1(P'') \right] \right\}^2 \\
&- \int dP' \hat{T}(P, P') \hat{c}_f(P') \sum_{n=1}^{\infty} (n-1) \hat{q}_n(P') (W')^2 (\hat{f}(P, P'))^2
\end{aligned} \tag{C.30}$$

Explicating now the binomial coefficients and the sum over r :

$$\begin{aligned}
\hat{\mathbb{M}}_2(P) &= \int dP' \hat{T}(P, P') \hat{c}_a(P') \left[W' \hat{f}(P, P') \right]^2 \\
&+ 1 \cdot \int dP' \hat{T}(P, P') \hat{c}_s(P') \int dP'' \hat{C}_s(P', P'') \left[W' \hat{f}(P, P') \right]^2 \\
&+ 2 \cdot \int dP' \hat{T}(P, P') \hat{c}_s(P') \int dP'' \hat{C}_s(P', P'') \left[W' \hat{f}(P, P') \right] (W'') \hat{M}_1(P'') \\
&+ 1 \cdot \int dP' \hat{T}(P, P') \hat{c}_s(P') \int dP'' \hat{C}_s(P', P'') (W'')^2 \hat{M}_2(P'') \\
&+ 1 \cdot \int dP' \hat{T}(P, P') \hat{c}_f(P') \sum_{n=1}^{\infty} n \hat{q}_n(P') \int dP'' \hat{C}_n(P', P'') \left[W' \hat{f}(P, P') \right]^2 \\
&+ 2 \cdot \int dP' \hat{T}(P, P') \hat{c}_f(P') \sum_{n=1}^{\infty} n \hat{q}_n(P') \int dP'' \hat{C}_n(P', P'') \left[W' \hat{f}(P, P') \right] (W'_n) \hat{M}_1(P'') \\
&+ 1 \cdot \int dP' \hat{T}(P, P') \hat{c}_f(P') \sum_{n=1}^{\infty} n \hat{q}_n(P') \int dP'' \hat{C}_n(P', P'') (W'_n)^2 \hat{M}_2(P'') \\
&+ \int dP' \hat{T}(P, P') \hat{c}_f(P') \sum_{n=1}^{\infty} n(n-1) \hat{q}_n(P') \left\{ \int dP'' \hat{C}_n(P', P'') W'_n \left[\hat{M}_1(P'') \right] \right\}^2 \\
&- \int dP' \hat{T}(P, P') \hat{c}_f(P') \sum_{n=1}^{\infty} (n-1) \hat{q}_n(P') (W')^2 (\hat{f}(P, P'))^2
\end{aligned} \tag{C.31}$$

Grouping together the terms with $\left[W' \hat{f}(P, P') \right]^2$:

$$\begin{aligned}
\hat{\mathbb{M}}_2(P) &= \int dP' \hat{T}(P, P') \left[W' \hat{f}(P, P') \right]^2 \\
&\cdot \left[\hat{c}_a(P') + \hat{c}_s(P') \int dP'' \hat{C}_s(P', P'') + \right. \\
&\hat{c}_f(P') \sum_{n=1}^{\infty} n \hat{q}_n(P') \int dP'' \hat{C}_n(P', P'') - \hat{c}_f(P') \sum_{n=1}^{\infty} (n-1) \hat{q}_n(P') \left. \right] \\
&+ 2 \cdot \int dP' \hat{T}(P, P') \hat{c}_s(P') \int dP'' \hat{C}_s(P', P'') \left[W' \hat{f}(P, P') \right] (W'') \hat{M}_1(P'') \\
&+ 1 \cdot \int dP' \hat{T}(P, P') \hat{c}_s(P') \int dP'' \hat{C}_s(P', P'') (W'')^2 \hat{M}_2(P'') \\
&+ 2 \cdot \int dP' \hat{T}(P, P') \hat{c}_f(P') \sum_{n=1}^{\infty} n \hat{q}_n(P') \int dP'' \hat{C}_n(P', P'') \left[W' \hat{f}(P, P') \right] (W'_n) \hat{M}_1(P'') \\
&+ 1 \cdot \int dP' \hat{T}(P, P') \hat{c}_f(P') \sum_{n=1}^{\infty} n \hat{q}_n(P') \int dP'' \hat{C}_n(P', P'') (W'_n)^2 \hat{M}_2(P'') \\
&+ \int dP' \hat{T}(P, P') \hat{c}_f(P') \sum_{n=1}^{\infty} n(n-1) \hat{q}_n(P') \left\{ \int dP'' \hat{C}_n(P', P'') W'_n \left[\hat{M}_1(P'') \right] \right\}^2
\end{aligned} \tag{C.32}$$

Knowing also the fact that $\int dP'' \hat{C}_i(P', P'') = 1$:

$$\begin{aligned}
\hat{\mathbb{M}}_2(P) &= \int dP' \hat{T}(P, P') \left[W' \hat{f}(P, P') \right]^2 \cdot \left[\hat{c}_a(P') + \hat{c}_s(P') + \hat{c}_f(P') \right] \\
&+ 2 \cdot \int dP' \hat{T}(P, P') \hat{c}_s(P') \int dP'' \hat{C}_s(P', P'') \left[W' \hat{f}(P, P') \right] (W'') \hat{M}_1(P'') \\
&+ 1 \cdot \int dP' \hat{T}(P, P') \hat{c}_s(P') \int dP'' \hat{C}_s(P', P'') (W'')^2 \hat{M}_2(P'') \\
&+ 2 \cdot \int dP' \hat{T}(P, P') \hat{c}_f(P') \sum_{n=1}^{\infty} n \hat{q}_n(P') \int dP'' \hat{C}_n(P', P'') \left[W' \hat{f}(P, P') \right] (W''_n) \hat{M}_1(P'') \\
&+ 1 \cdot \int dP' \hat{T}(P, P') \hat{c}_f(P') \sum_{n=1}^{\infty} n \hat{q}_n(P') \int dP'' \hat{C}_n(P', P'') (W''_n)^2 \hat{M}_2(P'') \\
&+ \int dP' \hat{T}(P, P') \hat{c}_f(P') \sum_{n=1}^{\infty} n(n-1) \hat{q}_n(P') \left\{ \int dP'' \hat{C}_n(P', P'') W''_n \left[\hat{M}_1(P'') \right] \right\}^2
\end{aligned} \tag{C.33}$$

After all of this, it is possible to write the original equation in a way more similar to the one of the equation founded previously for the forced fission scheme:

$$\begin{aligned}
\hat{\mathbb{M}}_2(P) &= \int dP' \hat{T}(P, P') \left[W' \hat{f}(P, P') \right]^2 \\
&+ \int dP' \hat{T}(P, P') \hat{c}_s(P') \int dP'' \hat{C}_s(P', P'') (W'')^2 \hat{M}_2(P'') \\
&+ \int dP' \hat{T}(P, P') \hat{c}_f(P') \sum_{n=1}^{\infty} n \hat{q}_n(P') \int dP'' \hat{C}_n(P', P'') (W''_n)^2 \hat{M}_2(P'') \\
&+ 2 \int dP' \hat{T}(P, P') \left\{ \left[\hat{c}_s(P') \int dP'' \hat{C}_s(P', P'') (W'') \hat{M}_1(P'') \right. \right. \\
&+ \left. \left. \hat{c}_f(P') \sum_{n=1}^{\infty} n \hat{q}_n(P') \int dP'' \hat{C}_n(P', P'') (W''_n) \hat{M}_1(P'') \right] W' \hat{f}(P, P') \right\} \\
&+ \int dP' \hat{T}(P, P') \hat{c}_f(P') \sum_{n=1}^{\infty} n(n-1) \hat{q}_n(P') \left\{ \int dP'' \hat{C}_n(P', P'') W''_n \left[\hat{M}_1(P'') \right] \right\}^2
\end{aligned} \tag{C.34}$$

The equation of the second order moment for the forced fission scheme was instead:

$$\begin{aligned}
\hat{M}_2(P) = & \int dP' \hat{T}(P, P') (\hat{f}(P, P'))^2 (W')^2 \\
& + \int dP' \hat{T}(P, P') \left[\int dP'' \hat{C}_s(P', P'') \hat{M}_2(P'') W''^2 \right] \\
& + \int dP' \hat{T}(P, P') \left[\sum_{n=1}^{\infty} \hat{q}_n(P') n \int dP'' \hat{C}_n(P', P'') \hat{M}_2(P'') (W''_n)^2 \right] \\
& + 2 \int dP' \hat{T}(P, P') \hat{f}(P, P') W' \left[\int dP'' \hat{C}_s(P', P'') \hat{M}_1(P'') W'' \right. \\
& \left. + \sum_{n=1}^{\infty} \hat{q}_n(P') n \int dP'' \hat{C}_n(P', P'') \hat{M}_1(P'') W''_n \right] \\
& + \int dP' \hat{T}(P, P') \left[2 \int dP'' \hat{C}_s(P', P'') \hat{M}_1(P'') W'' \sum_{n=1}^{\infty} \hat{q}_n(P') n \int dP'' \hat{C}_n(P', P'') \hat{M}_1(P'') W''_n \right. \\
& \left. + \int dP' \hat{T}(P, P') \left[\sum_{n=1}^{\infty} \hat{q}_n(P') n(n-1) \left(\int dP''_{(k)} \hat{C}_n(P', P'') \hat{M}_1(P'') W''_n \right)^2 \right] \right]
\end{aligned} \tag{C.35}$$

It is possible to note the following:

- No multiplicative terms $\hat{c}_s(P')$ and $\hat{c}_f(P')$ in front of every scattering and fission post collision density, which are present in the "analog" version, appear in the "forced fission" version.
- Different definition of the weight correction W'' and W''_n .
- One more term (the fifth one of C.35) which symbolize the interference between scattering particle and fission particle/s appears in the forced fission version (it is similar in structure to term which is the interference between fission particles)

Using the just derived expressions of the first order moment (C.15 and C.16) and of the second order moment (C.35) it is possible to impose:

$$\frac{\hat{M}_2(P)}{\hat{M}_1(P)} = \hat{M}_1(P) \tag{C.36}$$

Or, knowing that the first order moment needs to be preserved, regardless of the game:

$$\frac{\hat{M}_2(P)}{\hat{M}_1(P)} = M_1(P) \tag{C.37}$$

Using the original analog game instead of the non-analog starting game will in fact help with the derivation.

From now on the "hat" symbol will be used to refer to the non-analog starting game (forced fission game), and the "hat" and "asterisk" symbol to the non-analog zero-variance game (zero variance forced fission game), while if no symbols are present it will indicate the original game (purely analog game).

The first order moment can be rewritten as:

$$M_1(P) = \int dP' T(P, P') f(P, P') + \int dP' T(P, P') \sum_{n=1}^{\infty} n c_n(P') \int dP'' C_n(P', P'') M_1(P'') \quad (\text{C.38})$$

Where for the case of $n = 1$:

$$\begin{aligned} c_1(P') &= c_s(P') + c_f(P') q_1(P') \\ C_1(P', P'') &= \frac{c_s(P') C_s(P', P'') + c_f(P') q_1(P') C_1(P', P'')}{c_1(P')} \end{aligned} \quad (\text{C.39})$$

Then, by defining:

$$\bar{m}_n(P') = \int dP'' C_n(P', P'') M_1(P'') \quad (\text{C.40})$$

The first order moment is:

$$\begin{aligned} M_1(P) &= \int dP' T(P, P') \left\{ f(P, P') + \sum_{n=1}^{\infty} n c_n(P') \left[1 - H(P, P') H_n(P') \right] \bar{m}_n(P') \right\} \\ &+ \int dP' T(P, P') H(P, P') \sum_{n=1}^{\infty} n c_n(P') H_n(P') \bar{m}_n(P') \end{aligned} \quad (\text{C.41})$$

Finally the ratio to be estimated is:

$$\begin{aligned} \frac{\hat{M}_2^*(P)}{M_1(P)} &= \int dP' \hat{T}^*(P, P') \left\{ (\hat{f}(P, P'))^2 (W'^*)^2 + \left[\int dP'' \hat{C}_s^*(P', P'') \hat{M}_2^*(P'') (W''^*)^2 \right] \right. \\ &+ \left[\sum_{n=1}^{\infty} \hat{q}_n^*(P') n \int dP'' \hat{C}_n^*(P', P'') \hat{M}_2^*(P'') ((W_n'')^*)^2 \right] \\ &+ 2 \hat{f}(P, P') W'^* \left[\int dP'' \hat{C}_s^*(P', P'') M_1(P'') W''^* + \sum_{n=1}^{\infty} \hat{q}_n^*(P') n \int dP'' \hat{C}_n^*(P', P'') M_1(P'') (W_n'')^* \right] \\ &+ \left[2 \int dP'' \hat{C}_s^*(P', P'') M_1(P'') W''^* \sum_{n=1}^{\infty} \hat{q}_n^*(P') n \int dP'' \hat{C}_n^*(P', P'') M_1(P'') (W_n'')^* \right] \\ &+ \left. \left[\sum_{n=1}^{\infty} \hat{q}_n^*(P') n(n-1) \left(\int dP'' \hat{C}_n^*(P', P'') M_1(P'') (W_n'')^* \right)^2 \right] \right\} / M_1(P) \end{aligned} \quad (\text{C.42})$$

With weight generation rules defined by:

$$\begin{aligned} W'^* &= \frac{T(P, P')}{\hat{T}^*(P, P')} \\ W''^* &= W'^* \frac{c_s(P') C_s(P', P'')}{\hat{C}_s^*(P', P'')} \\ (W_n'')^* &= W'^* \frac{c_f(P') q_n(P') C_n(P', P'')}{\hat{q}_n^*(P') \hat{C}_n^*(P', P'')} \end{aligned} \quad (\text{C.43})$$

The ratio can be split into:

$$\begin{aligned} \frac{\hat{M}_2^*(P)}{M_1(P)} &= \int dP' \hat{T}^*(P, P') \left\{ X_1 + X_2 + X_3 + X_4 \right\} / M_1(P) \\ &+ \int dP' \hat{T}^*(P, P') \left\{ X_5 + X_6 \right\} / M_1(P) \end{aligned} \quad (\text{C.44})$$

Where the second term is:

$$\begin{aligned} \left\{ X_5 + X_6 \right\} / M_1(P) &= \left\{ \left[\int dP'' \hat{C}_s^*(P', P'') \hat{M}_2^*(P'') (W''^*)^2 \right] \right\} / M_1(P) \\ &+ \left\{ \left[\sum_{n=1}^{\infty} \hat{q}_n^*(P') n \int dP'' \hat{C}_n^*(P', P'') \hat{M}_2^*(P'') ((W''_n)^*)^2 \right] \right\} / M_1(P) \end{aligned} \quad (\text{C.45})$$

$$\begin{aligned} \left\{ X_5 + X_6 \right\} / M_1(P) &= \int dP'' \hat{C}_s^*(P', P'') \hat{M}_2^*(P'') (W''^*)^2 \frac{\Theta(P') M_1(P'')}{\Theta(P') M_1(P'')} \frac{1}{M_1(P)} \\ &+ \sum_{n=1}^{\infty} \hat{q}_n^*(P') n \int dP'' \hat{C}_n^*(P', P'') \hat{M}_2^*(P'') ((W''_n)^*)^2 \frac{\Theta(P') M_1(P'')}{\Theta(P') M_1(P'')} \frac{1}{M_1(P)} \end{aligned} \quad (\text{C.46})$$

$$\begin{aligned} \left\{ X_5 + X_6 \right\} / M_1(P) &= \frac{\Theta(P')}{M_1(P)} \left\{ \int dP'' \hat{C}_s^*(P', P'') \frac{M_1(P'')}{\Theta(P')} (W''^*)^2 \left[\frac{\hat{M}_2^*(P'')}{M_1(P'')} \right] \right. \\ &+ \left. \sum_{n=1}^{\infty} \hat{q}_n^*(P') n \int dP'' \hat{C}_n^*(P', P'') \frac{M_1(P'')}{\Theta(P')} ((W''_n)^*)^2 \left[\frac{\hat{M}_2^*(P'')}{M_1(P'')} \right] \right\} \end{aligned} \quad (\text{C.47})$$

$$\begin{aligned} \left\{ X_5 + X_6 \right\} / M_1(P) &= \frac{\Theta(P')}{M_1(P)} \left\{ \int dP'' \frac{M_1(P'')}{\Theta(P')} \left[\frac{\hat{M}_2^*(P'')}{M_1(P'')} \right] \right. \\ &\cdot \left[\hat{C}_s^*(P', P'') (W''^*)^2 + \sum_{n=1}^{\infty} \hat{q}_n^*(P') n \hat{C}_n^*(P', P'') ((W''_n)^*)^2 \right] \left. \right\} \end{aligned} \quad (\text{C.48})$$

So:

$$\begin{aligned} \int dP'' \hat{T}^*(P', P'') \left\{ X_5 + X_6 \right\} / M_1(P) &= \int dP'' \hat{T}^*(P', P'') \frac{\Theta(P')}{M_1(P)} \left\{ \int dP'' \frac{M_1(P'')}{\Theta(P')} \left[\frac{\hat{M}_2^*(P'')}{M_1(P'')} \right] \right. \\ &\cdot \left[\hat{C}_s^*(P', P'') (W''^*)^2 + \sum_{n=1}^{\infty} \hat{q}_n^*(P') n \hat{C}_n^*(P', P'') ((W''_n)^*)^2 \right] \left. \right\} \end{aligned} \quad (\text{C.49})$$

Where $\Theta(P')$ is for known arbitrary function. Now it is required to compare:

$$\int dP' T(P, P') H(P, P') \sum_{n=1}^{\infty} n c_n(P') H_n(P') \bar{m}_n(P') \quad (\text{C.50})$$

and:

$$\int dP' \hat{T}^*(P', P'') \frac{\Theta(P')}{M_1(P)} \left\{ \int dP'' \frac{M_1(P'')}{\Theta(P')} \left[\frac{\hat{M}_2^*(P'')}{M_1(P'')} \right] \cdot \left[\hat{C}_s^*(P', P'') (W''^*)^2 + \sum_{n=1}^{\infty} \hat{q}_n^*(P') n \hat{C}_n^*(P', P'') ((W_n'')^*)^2 \right] \right\} \quad (\text{C.51})$$

Reorganizing the two terms a little, for the first one the result is:

$$\int dP' \int dP'' M_1(P'') \left\{ T(P, P') H(P, P') \sum_{n=1}^{\infty} n H_n(P') c_n(P') C_n(P', P'') \right\} \quad (\text{C.52})$$

And expanding the term for $n = 1$:

$$\rightarrow H_1(P') c_1(P') C_1(P', P'') = H_1(P') \left(c_s(P') C_s(P', P'') + c_f(P') q_1(P') C_1(P', P'') \right) \quad (\text{C.53})$$

The final first term to be compared is then:

$$\int dP' \int dP'' M_1(P'') \left\{ T(P, P') H(P, P') \left[H_1(P') c_s(P') C_s(P', P'') + \sum_{n=1}^{\infty} n c_f(P') q_n(P') H_n(P') C_n(P', P'') \right] \right\} \quad (\text{C.54})$$

While the second one after some manipulation becomes:

$$\int dP' \int dP'' \left[\frac{\hat{M}_2^*(P'')}{M_1(P'')} \right] \left\{ \hat{T}^*(P', P'') \frac{\Theta(P')}{M_1(P)} \frac{M_1(P'')}{\Theta(P')} \cdot \left[\hat{C}_s^*(P', P'') (W''^*)^2 + \sum_{n=1}^{\infty} \hat{q}_n^*(P') n \hat{C}_n^*(P', P'') ((W_n'')^*)^2 \right] \right\} \quad (\text{C.55})$$

And the two terms inside the curly brackets needs to be same. Substituting the weight generation rules for W''^* and $(W_n'')^*$ into the last equation:

$$\dots = \left\{ \hat{T}^*(P', P'') \frac{\Theta(P')}{M_1(P)} \frac{M_1(P'')}{\Theta(P')} \cdot \left[\hat{C}_s^*(P', P'') \left(W'^* \frac{c_s(P') C_s(P', P'')}{\hat{C}_s^*(P', P'')} \right)^2 + \sum_{n=1}^{\infty} \hat{q}_n^*(P') n \hat{C}_n^*(P', P'') \left(W'^* \frac{c_f(P') q_n(P') C_n(P', P'')}{\hat{q}_n^*(P') \hat{C}_n^*(P', P'')} \right)^2 \right] \right\} \quad (\text{C.56})$$

$$\dots = \left\{ \hat{T}^*(P', P'') \frac{\Theta(P')}{M_1(P)} \frac{M_1(P'')}{\Theta(P')} \left(\frac{T(P, P')}{\hat{T}^*(P, P')} \right)^2 \cdot \left[\hat{C}_s^*(P', P'') \left(\frac{c_s(P') C_s(P', P'')}{\hat{C}_s^*(P', P'')} \right)^2 + \sum_{n=1}^{\infty} \hat{q}_n^*(P') n \hat{C}_n^*(P', P'') \left(\frac{c_f(P') q_n(P') C_n(P', P'')}{\hat{q}_n^*(P') \hat{C}_n^*(P', P'')} \right)^2 \right] \right\} \quad (\text{C.57})$$

$$\begin{aligned} \dots &= \left\{ \frac{\Theta(P')}{M_1(P)} \frac{M_1(P'')}{\Theta(P')} \frac{(T(P, P'))^2}{\hat{T}^*(P, P')} \right. \\ &\quad \cdot \left. \left[\frac{(c_s(P')C_s(P', P''))^2}{\hat{C}_s^*(P', P'')} + \sum_{n=1}^{\infty} n \frac{(c_f(P')q_n(P')C_n(P', P''))^2}{\hat{q}_n^*(P')\hat{C}_n^*(P', P'')} \right] \right\} \end{aligned} \quad (\text{C.58})$$

$$\begin{aligned} \dots &= \left\{ T(P, P') \cdot \frac{\Theta(P')}{M_1(P)} \frac{T(P, P')}{\hat{T}^*(P, P')} \right. \\ &\quad \cdot \frac{M_1(P'')}{\Theta(P')} \cdot \left[c_s(P')C_s(P', P'') \frac{c_s(P')C_s(P', P'')}{\hat{C}_s^*(P', P'')} \right. \\ &\quad \left. + \sum_{n=1}^{\infty} n c_f(P')q_n(P')C_n(P', P'') \frac{c_f(P')q_n(P')C_n(P', P'')}{\hat{q}_n^*(P')\hat{C}_n^*(P', P'')} \right] \left. \right\} \end{aligned} \quad (\text{C.59})$$

Then imposing to the equality of C.54 and C.59, the first result obtained is:

$$\frac{\Theta(P')}{M_1(P)} \frac{T(P, P')}{\hat{T}^*(P, P')} = H(P, P') \quad (\text{C.60})$$

Or:

$$\hat{T}^*(P, P') = \frac{\Theta(P')}{M_1(P)} \frac{T(P, P')}{H(P, P')} \quad (\text{C.61})$$

Which is the same result found by Lux for the zero-variance flight kernel [1]. Still, to finish first equality it is also necessary to impose the equivalence between the second line of C.59 and the collision part of the corresponding term. In particular:

$$\begin{cases} H_1(P') = \frac{M_1(P'')}{\Theta(P')} \frac{c_s(P')C_s(P', P'')}{\hat{C}_{s^*}(P', P'')} \rightarrow \hat{C}_s^*(P', P'') = \frac{M_1(P'')}{\Theta(P')} \frac{c_s(P')C_s(P', P'')}{H_1(P')} \\ H_n(P') = \frac{M_1(P'')}{\Theta(P')} \frac{c_f(P')q_n(P')C_n(P', P'')}{\hat{q}_n^*(P')\hat{C}_n^*(P', P'')} \rightarrow \hat{q}_n^*(P')\hat{C}_n^*(P', P'') = \frac{M_1(P'')}{\Theta(P')} \frac{c_f(P')q_n(P')C_n(P', P'')}{H_n(P')} \end{cases} \quad (\text{C.62})$$

Integrating over dP'' the left and right side of the equations will result in:

$$\begin{cases} c_s(P')\bar{m}_s(P') = \Theta(P')H_1(P') \\ c_f(P')q_n(P')\bar{m}_n(P') = \hat{q}_n^*(P')\Theta(P')H_n(P') \end{cases} \quad (\text{C.63})$$

All of this for $\Theta(P')$, $H(P, P')$, $H_n(P')$ arbitrary functions.

The constraint is on those function can be for example the normalization condition on $\hat{T}^*(P, P')$, so:

$$\begin{aligned} \int dP' \frac{\Theta(P')}{M_1(P)} \frac{T(P, P')}{H(P, P')} &= 1 \\ \int dP' T(P, P') \frac{\Theta(P')}{H(P, P')} &= M_1(P) \end{aligned} \quad (\text{C.64})$$

Comparing this last expression with the first order moment:

$$\frac{\Theta(P')}{H(P, P')} = f(P, P') + \overline{M}_1(P') \quad (\text{C.65})$$

Where:

$$\overline{M}_1(P') = \int dP'' C(P', P'') M_1(P'') \quad (\text{C.66})$$

So, from the condition on X_5 and X_6 it is possible to derive the expression for the zero-variance flight kernel in a closed form, such as:

$$\hat{T}^*(P, P') = T(P, P') \frac{f(P, P') + \overline{M}_1(P')}{M_1(P)} \quad (\text{C.67})$$

The equality of the others terms of the ratio $\hat{M}_2^*(P) / M_1(P)$ is still missing; in particular the equality between:

$$\int dP' \hat{T}^*(P, P') \left\{ X_1 + X_2 + X_3 + X_4 \right\} / M_1(P) \quad (\text{C.68})$$

and

$$\int dP' T(P, P') \left\{ f(P, P') + \sum_{n=1}^{\infty} n c_n(P') \left[1 - H(P, P') H_n(P') \right] \overline{m}_n(P') \right\} \quad (\text{C.69})$$

Trying to write the first of these two terms in a different way by substituting the weight generation rules:

$$\begin{aligned} \int dP' \hat{T}^*(P, P') \left\{ X_1 \right\} / M_1(P) &= \int dP' \hat{T}^*(P, P') (\hat{f}(P, P'))^2 (W'^*)^2 / M_1(P) \\ &= \int dP' \hat{T}^*(P, P') (\hat{f}(P, P'))^2 \left(\frac{T(P, P')}{\hat{T}^*(P, P')} \right)^2 / M_1(P) \\ &= \int dP' T(P, P') (f(P, P'))^2 \frac{T(P, P')}{\hat{T}^*(P, P') M_1(P)} \\ &= \int dP' T(P, P') f(P, P') \frac{f(P, P') H(P, P')}{\Theta(P')} \end{aligned} \quad (\text{C.70})$$

$$\begin{aligned}
\int dP' \hat{T}^*(P, P') \left\{ X_2 \right\} / M_1(P) &= \int dP' \hat{T}^*(P, P') 2\hat{f}(P, P') W'^* \left[\int dP'' \hat{C}_s^*(P', P'') M_1(P'') W''^* \right. \\
&\quad \left. + \sum_{n=1}^{\infty} \hat{q}_n^*(P') n \int dP'' \hat{C}_n^*(P', P'') M_1(P'') (W''_n)^* \right] / M_1(P) \\
&= 2 \int dP' \hat{T}^*(P, P') f(P, P') W'^* \cdot \left[\int dP'' \hat{C}_s^*(P', P'') M_1(P'') W'^* \frac{c_s(P') C_s(P', P'')}{\hat{C}_s^*(P', P'')} \right. \\
&\quad \left. + \sum_{n=1}^{\infty} \hat{q}_n^*(P') n \int dP'' \hat{C}_n^*(P', P'') M_1(P'') W'^* \frac{c_f(P') q_n(P') C_n(P', P'')}{\hat{q}_n^*(P') \hat{C}_n^*(P', P'')} \right] / M_1(P) \\
&= 2 \int dP' \hat{T}^*(P, P') f(P, P') \frac{(W'^*)^2}{M_1(P)} \cdot \left[c_s(P') \int dP'' C_s(P', P'') M_1(P'') \right. \\
&\quad \left. + \sum_{n=1}^{\infty} c_f(P') n q_n(P') \int dP'' C_n(P', P'') M_1(P'') \right] \\
&= 2 \int dP' T(P, P') f(P, P') \frac{H(P, P')}{\Theta(P')} \cdot \sum_{n=1}^{\infty} n c_n(P') \bar{m}_n(P')
\end{aligned} \tag{C.71}$$

$$\begin{aligned}
\int dP' \hat{T}^*(P, P') \left\{ X_3 \right\} / M_1(P) &= \int dP' \hat{T}^*(P, P') \left[\sum_{n=1}^{\infty} \hat{q}_n^*(P') n(n-1) \left(\int dP'' \hat{C}_n^*(P', P'') M_1(P'') W''_n^* \right)^2 \right] / M_1(P) \\
&= \int dP' \hat{T}^*(P, P') \left[\sum_{n=1}^{\infty} \hat{q}_n^*(P') n(n-1) \right. \\
&\quad \left. \cdot \left(\int dP'' \hat{C}_n^*(P', P'') M_1(P'') W'^* \frac{c_f(P') q_n(P') C_n(P', P'')}{\hat{q}_n^*(P') \hat{C}_n^*(P', P'')} \right)^2 \right] / M_1(P) \\
&= \int dP' \hat{T}^*(P, P') \frac{(W'^*)^2}{M_1(P)} \left[\sum_{n=1}^{\infty} \hat{q}_n^*(P') n(n-1) \cdot \left(\int dP'' C_n(P', P'') M_1(P'') \frac{c_f(P') q_n(P')}{\hat{q}_n^*(P')} \right)^2 \right] \\
&= \int dP' T(P, P') \frac{H(P, P')}{\Theta(P')} \left[\sum_{n=1}^{\infty} \hat{q}_n^*(P') n(n-1) \left(\frac{c_f(P') q_n(P')}{\hat{q}_n^*(P')} \right)^2 \cdot (\bar{m}_n(P'))^2 \right] \\
&= \int dP' T(P, P') \frac{H(P, P')}{\Theta(P')} \left[\sum_{n=1}^{\infty} c_f(P') q_n(P') n(n-1) (\bar{m}_n(P'))^2 \left(\frac{c_f(P') q_n(P')}{\hat{q}_n^*(P')} \right) \right]
\end{aligned} \tag{C.72}$$

$$\begin{aligned}
\int dP' \hat{T}^*(P, P') \left\{ X_4 \right\} / M_1(P) &= \int dP' \hat{T}^*(P, P') \left[2 \int dP'' \hat{C}_s^*(P', P'') M_1(P'') W'^* \right. \\
&\quad \cdot \left. \sum_{n=1}^{\infty} \hat{q}_n^*(P') n \int dP'' \hat{C}_n^*(P', P'') M_1(P'') (W_n'')^* \right] / M_1(P) \\
&= 2 \int dP' \hat{T}^*(P, P') \left[\int dP'' \hat{C}_s^*(P', P'') M_1(P'') W'^* \frac{c_s(P') C_s(P', P'')}{\hat{C}_s^*(P', P'')} \right. \\
&\quad \cdot \left. \sum_{n=1}^{\infty} \hat{q}_n^*(P') n \int dP'' \hat{C}_n^*(P', P'') M_1(P'') W'^* \frac{c_f(P') q_n(P') C_n(P', P'')}{\hat{q}_n^*(P') \hat{C}_n^*(P', P'')} \right] / M_1(P) \\
&= 2 \int dP' \hat{T}^*(P, P') \frac{(W'^*)^2}{M_1(P)} \left[c_s(P') \int dP'' C_s(P', P'') M_1(P'') \right. \\
&\quad \cdot \left. \sum_{n=1}^{\infty} c_f(P') n q_n(P') \int dP'' C_n(P', P'') M_1(P'') \right] \\
&= 2 \int dP' T(P, P') \frac{H(P, P')}{\Theta(P')} \left[c_s(P') \bar{m}_s(P') \cdot \sum_{n=1}^{\infty} c_f(P') n q_n(P') \bar{m}_n(P') \right]
\end{aligned} \tag{C.73}$$

So:

$$\begin{aligned}
\int dP' \hat{T}^*(P, P') \left\{ X_1 + X_2 + X_3 + X_4 \right\} / M_1(P) &= \int dP' T(P, P') \frac{H(P, P')}{\Theta(P')} \left\{ (f(P, P'))^2 \right. \\
&\quad + 2f(P, P') \sum_{n=1}^{\infty} n c_n(P') \bar{m}_n(P') \\
&\quad + \sum_{n=1}^{\infty} n(n-1) c_f(P') q_n(P') (\bar{m}_n(P'))^2 \frac{c_f(P') q_n(P')}{\hat{q}_n^*(P')} \\
&\quad \left. + 2 \left[c_s(P') \bar{m}_s(P') \cdot \sum_{n=1}^{\infty} c_f(P') n q_n(P') \bar{m}_n(P') \right] \right\}
\end{aligned} \tag{C.74}$$

Taking the last two terms it is possible to write:

$$\dots = \sum_{n=1}^{\infty} c_f(P') n q_n(P') \bar{m}_n(P') \left[(n-1) \bar{m}_n(P') \frac{c_f(P') q_n(P')}{\hat{q}_n^*(P')} + 2c_s(P') \bar{m}_s(P') \right] \tag{C.75}$$

Once again, all of this needs to be compared with:

$$\int dP' T(P, P') \left\{ f(P, P') + \sum_{n=1}^{\infty} n c_n(P') \left[1 - H(P, P') H_n(P') \right] \bar{m}_n(P') \right\} \tag{C.76}$$

At the end, the equality which needs to be satisfied is:

$$\begin{aligned}
& \frac{H(P, P')}{\Theta(P')} \left\{ (f(P, P'))^2 + 2f(P, P') \sum_{n=1}^{\infty} n c_n(P') \bar{m}_n(P') \right. \\
& \left. + \sum_{n=1}^{\infty} c_f(P') n q_n(P') \bar{m}_n(P') \left[(n-1) \bar{m}_n(P') \frac{c_f(P') q_n(P')}{\hat{q}_n^*(P')} + 2c_s(P') \bar{m}_s(P') \right] \right\} \quad (\text{C.77}) \\
& = \\
& \left\{ f(P, P') + \sum_{n=1}^{\infty} n c_n(P') \left[1 - H(P, P') H_n(P') \right] \bar{m}_n(P') \right\}
\end{aligned}$$

$$\begin{aligned}
& f(P, P') \left\{ \frac{H(P, P')}{\Theta(P')} \left[(f(P, P')) + \sum_{n=1}^{\infty} n c_n(P') \bar{m}_n(P') \right] \right\} \\
& + \frac{H(P, P')}{\Theta(P')} \left\{ f(P, P') \sum_{n=1}^{\infty} n c_n(P') \bar{m}_n(P') + \sum_{n=1}^{\infty} c_f(P') n q_n(P') \bar{m}_n(P') \right. \\
& \left. \left[(n-1) \bar{m}_n(P') \frac{c_f(P') q_n(P')}{\hat{q}_n^*(P')} + 2c_s(P') \bar{m}_s(P') \right] \right\} \quad (\text{C.78}) \\
& = \\
& \left\{ f(P, P') + \sum_{n=1}^{\infty} n c_n(P') \left[1 - H(P, P') H_n(P') \right] \bar{m}_n(P') \right\}
\end{aligned}$$

Substituting $\sum_{n=1}^{\infty} n c_n(P') \bar{m}_n(P')$ in the first and second line with $\bar{M}_1(P')$:

$$\begin{aligned}
& f(P, P') \left\{ \frac{H(P, P')}{\Theta(P')} \left[(f(P, P')) + \bar{M}_1(P') \right] \right\} \\
& + \frac{H(P, P')}{\Theta(P')} \left\{ f(P, P') \bar{M}_1(P') + \sum_{n=1}^{\infty} c_f(P') n q_n(P') \bar{m}_n(P') \left[(n-1) \bar{m}_n(P') \frac{c_f(P') q_n(P')}{\hat{q}_n^*(P')} + 2c_s(P') \bar{m}_s(P') \right] \right\} \\
& = \\
& \left\{ f(P, P') + \sum_{n=1}^{\infty} n c_n(P') \left[1 - H(P, P') H_n(P') \right] \bar{m}_n(P') \right\} \quad (\text{C.79})
\end{aligned}$$

Knowing that $\frac{\Theta(P')}{H(P, P')} = f(P, P') + \bar{M}_1(P')$, it is possible to eliminate the equal terms $f(P, P')$ on both sides:

$$\begin{aligned}
& \frac{H(P, P')}{\Theta(P')} \left\{ f(P, P') \sum_{n=1}^{\infty} n c_n(P') \bar{m}_n(P') + \sum_{n=1}^{\infty} c_f(P') n q_n(P') \bar{m}_n(P') \left[\right. \right. \\
& \left. \left. (n-1) \bar{m}_n(P') \frac{c_f(P') q_n(P')}{\hat{q}_n^*(P')} + 2c_s(P') \bar{m}_s(P') \right] \right\} \\
& = \\
& \left\{ \sum_{n=1}^{\infty} n c_n(P') \left[1 - H(P, P') H_n(P') \right] \bar{m}_n(P') \right\}
\end{aligned} \tag{C.80}$$

Which is a different equation compared to the one found by Lux, since the hypothesis were different. Explicating the term for $n = 1$ into its fission and scattering part:

$$\begin{aligned}
& \frac{H(P, P')}{\Theta(P')} \left\{ f(P, P') \left[c_s(P') \bar{m}_s(P') \right] + f(P, P') \left[\sum_{n=1}^{\infty} c_f(P') n q_n(P') \bar{m}_n(P') \right] \right. \\
& + \sum_{n=1}^{\infty} c_f(P') n q_n(P') \bar{m}_n(P') \left[(n-1) \bar{m}_n(P') \frac{c_f(P') q_n(P')}{\hat{q}_n^*(P')} \right] \\
& \left. + \sum_{n=1}^{\infty} c_f(P') n q_n(P') \bar{m}_n(P') \left[2c_s(P') \bar{m}_s(P') \right] \right\} \\
& = \\
& c_s(P') \bar{m}_s(P') + \sum_{n=1}^{\infty} c_f(P') n q_n(P') \bar{m}_n(P') \\
& - c_s(P') \bar{m}_s(P') H(P, P') H_1(P') - \sum_{n=1}^{\infty} c_f(P') n q_n(P') H(P, P') H_n(P') \bar{m}_n(P')
\end{aligned} \tag{C.81}$$

$$\begin{aligned}
& \left[c_s(P') \bar{m}_s(P') \right] \cdot \left\{ \frac{H(P, P')}{\Theta(P')} \left[f(P, P') + \sum_{n=1}^{\infty} c_f(P') n q_n(P') \bar{m}_n(P') \right] \right\} \\
& + \sum_{n=1}^{\infty} \left[c_f(P') n q_n(P') \bar{m}_n(P') \right] \cdot \left\{ \frac{H(P, P')}{\Theta(P')} \left[f(P, P') + (n-1) \bar{m}_n(P') \frac{c_f(P') q_n(P')}{\hat{q}_n^*(P')} + c_s(P') \bar{m}_s(P') \right] \right\} \\
& = \\
& \left[c_s(P') \bar{m}_s(P') \right] \cdot \left\{ 1 - H(P, P') H_1(P') \right\} \\
& + \sum_{n=1}^{\infty} \left[c_f(P') n q_n(P') \bar{m}_n(P') \right] \cdot \left\{ 1 - H(P, P') H_n(P') \right\}
\end{aligned} \tag{C.82}$$

It is possible to substitute the $\hat{q}_n^*(P')$ and obtain:

$$\begin{aligned}
& \left[c_s(P') \bar{m}_s(P') \right] \cdot \left\{ \frac{H(P, P')}{\Theta(P')} \left[f(P, P') + \sum_{n=1}^{\infty} c_f(P') n q_n(P') \bar{m}_n(P') \right] \right\} \\
& + \sum_{n=1}^{\infty} \left[c_f(P') n q_n(P') \bar{m}_n(P') \right] \cdot \left\{ \frac{H(P, P')}{\Theta(P')} \left[f(P, P') + (n-1)\Theta(P')H_n(P') + c_s(P') \bar{m}_s(P') \right] \right\} \\
& = \\
& \left[c_s(P') \bar{m}_s(P') \right] \cdot \left\{ 1 - H(P, P')H_1(P') \right\} \\
& + \sum_{n=1}^{\infty} \left[c_f(P') n q_n(P') \bar{m}_n(P') \right] \cdot \left\{ 1 - H(P, P')H_n(P') \right\}
\end{aligned} \tag{C.83}$$

For the second term of each side:

$$\begin{aligned}
& \frac{H(P, P')}{\Theta(P')} \left[f(P, P') + (n-1)\Theta(P')H_n(P') + c_s(P') \bar{m}_s(P') \right] = 1 - H(P, P')H_n(P') \\
& \frac{H(P, P')}{\Theta(P')} \left[f(P, P') + n\Theta(P')H_n(P') + c_s(P') \bar{m}_s(P') \right] = 1 \\
& \left[f(P, P') + nc_f(P') \frac{q_n(P')}{\hat{q}_n^*(P')} \bar{m}_n(P') + c_s(P') \bar{m}_s(P') \right] = \frac{\Theta(P')}{H(P, P')}
\end{aligned} \tag{C.84}$$

$$\begin{aligned}
& f(P, P') + nc_f(P') \frac{q_n(P')}{\hat{q}_n^*(P')} \bar{m}_n(P') + c_s(P') \bar{m}_s(P') = f(P, P') + \bar{M}_1(P') \\
& nc_f(P') \frac{q_n(P')}{\hat{q}_n^*(P')} \bar{m}_n(P') + c_s(P') \bar{m}_s(P') = \bar{M}_1(P') \\
& nc_f(P') \frac{q_n(P')}{\hat{q}_n^*(P')} \bar{m}_n(P') = \bar{M}_1(P') - c_s(P') \bar{m}_s(P')
\end{aligned} \tag{C.85}$$

$$\hat{q}_n^*(P') = \frac{nc_f(P')q_n(P')\bar{m}_n(P')}{\bar{M}_1(P') - c_s(P')\bar{m}_s(P')} \tag{C.86}$$

Which is a second result, once again different from the one derived from an analog zero-variance game. Regarding the first terms of each side of equation C.83:

$$\begin{aligned}
\frac{H(P, P')}{\Theta(P')} \left[f(P, P') + \sum_{n=1}^{\infty} c_f(P') n q_n(P') \bar{m}_n(P') \right] &= 1 - H(P, P') H_1(P') \\
\frac{H(P, P')}{\Theta(P')} \left[f(P, P') + \sum_{n=1}^{\infty} c_f(P') n q_n(P') \bar{m}_n(P') + c_s(P') \bar{m}_s(P') - c_s(P') \bar{m}_s(P') \right] &= 1 - H(P, P') H_1(P') \\
\frac{H(P, P')}{\Theta(P')} \left[f(P, P') + \bar{M}_1(P') - c_s(P') \bar{m}_s(P') \right] &= 1 - H(P, P') H_1(P') \\
f(P, P') + \bar{M}_1(P') - c_s(P') \bar{m}_s(P') &= \frac{\Theta(P')}{H(P, P')} - H(P, P') H_1(P') \cdot \frac{\Theta(P')}{H(P, P')} \\
- c_s(P') \bar{m}_s(P') &= -H_1(P') \Theta(P')
\end{aligned} \tag{C.87}$$

Which is true in view of a previous equation. Then the post-collision densities are finally:

$$\hat{C}_s^*(P') = \frac{C_s(P', P'') M_1(P'')}{\bar{m}_s(P')} \tag{C.88}$$

$$\hat{C}_n^*(P') = \frac{C_n(P', P'') M_1(P'')}{\bar{m}_n(P')} \tag{C.89}$$

If $\hat{C}_n(P', P'')$ does not depend on n , $\hat{q}_n^*(P')$ could be rewritten as:

$$\begin{aligned}
\hat{q}_n^*(P') &= \frac{nc_f(P') q_n(P') \bar{m}_n(P')}{\bar{M}_1(P') - c_s(P') \bar{m}_s(P')} \\
&= \frac{nc_f(P') q_n(P') \int dP'' C_f(P', P'') M_1(P'')}{\sum_{n=1}^{\infty} nc_f(P') q_n(P') \int dP'' C_f(P', P'') M_1(P'')} \\
&= \frac{nq_n(P')}{\sum_{n=1}^{\infty} nq_n(P')} = \frac{nq_n(P')}{\nu_f(P')}
\end{aligned} \tag{C.90}$$

Where no reaction channel probability is present. But also:

$$\begin{aligned}
\hat{q}_n^*(P') &= \frac{nc_f(P') q_n(P') \int dP'' C_f(P', P'') M_1(P'')}{\int dP'' C(P', P'') M_1(P'') - c_s(P') \int dP'' C_s(P', P'') M_1(P'')} \\
&= \frac{nc_f(P') q_n(P') \int dP'' C_f(P', P'') M_1(P'')}{\int dP'' C(P', P'') M_1(P'')} \cdot \left(1 - \frac{c_s(P') \int dP'' C_s(P', P'') M_1(P'')}{\int dP'' C(P', P'') M_1(P'')} \right)^{-1}
\end{aligned} \tag{C.91}$$

The expressions for the biased probabilities for the zero variance game derived from an analog game can be derived as:

$$\hat{c}_f(P') \hat{q}_n(P') = \frac{nc_f(P') q_n(P') \int dP'' C_f(P', P'') M_1(P'')}{\int dP'' C(P', P'') M_1(P'')} \tag{C.92}$$

$$\hat{c}_s(P') = \frac{c_s(P') \int dP'' C_s(P', P'') M_1(P'')}{\int dP'' C(P', P'') M_1(P'')} \quad (\text{C.93})$$

So:

$$\hat{q}_n^*(P') = \frac{\hat{c}_f(P') \hat{q}_n(P')}{1 - \hat{c}_s(P')} \rightarrow \frac{\hat{q}_n^*(P')}{\hat{q}_n(P')} = \frac{\hat{c}_f(P')}{1 - \hat{c}_s(P')} \quad (\text{C.94})$$

But since $\hat{c}_f(P') + \hat{c}_s(P') + \hat{c}_a(P') = 1$ and $\hat{c}_a(P') = 0$, then:

$$\frac{\hat{q}_n^*(P')}{\hat{q}_n(P')} = 1 \quad (\text{C.95})$$

Bibliography

- [1] I. Lux, *Monte Carlo Particle Transport Methods: Neutron and Photon Calculations*. Boca Raton: Taylor Francis, May 2018, ISBN: 9781351074834.
- [2] J. E. Hoogenboom, “Zero-variance Monte Carlo schemes revisited,” *Nuclear Science and Engineering*, vol. 160, no. 1, pp. 1–22, 2008.
- [3] T. E. Booth and E. D. Cashwell, “Analysis of error in Monte Carlo transport calculations,” *Nuclear Science and Engineering*, vol. 71, no. 2, pp. 128–142, 1979.
- [4] M. Falabino, *Test and optimization of variance reduction methods in shielding problems with multiplicative media*, Jul. 2019. [Online]. Available: <https://webthesis.biblio.polito.it/11320/>.
- [5] Boston University, *The neutron transport equation*, <https://sites.bu.edu/cliveg/files/2021/09/transport-equation-derivation.pdf>, Accessed: 2024-11-13, 2021.
- [6] E. E. Lewis and W. F. Miller, *Computational methods of neutron transport*. Wiley-Interscience, Jan. 1984, ISBN: 9780471092452. [Online]. Available: <https://www.osti.gov/biblio/5538794>.
- [7] J. L. Devore, *Probability and Statistics for Engineering and the Sciences: International Metric Edition*. Mason, OH: Cengage, 2016.
- [8] K. Fröhlicher, “Amélioration des simulations Monte Carlo en physique des réacteurs par échantillonnage adaptatif des histoires de neutrons,” English, NNT : 2023UP-ASP011, Thesis in Statistical Mechanics, Université Paris-Saclay, 2023.
- [9] P. Saidi, M. Sadeghi, and C. Tenreiro, “Variance reduction of Monte Carlo simulation in nuclear engineering field,” Mar. 2013.
- [10] V. Vitali, “Monte Carlo analysis of heterogeneity and core decoupling effects on reactor kinetics: Application to the eole critical facility,” English, NNT : 2020UPASP045, Thesis in Nuclear Theory, Université Paris-Saclay, 2020.
- [11] T. Bonnet, H. Belanger, D. Mancusi, and A. Zoia, “The effect of branchless collisions and population control on correlations in Monte Carlo power iteration,” *Nuclear Science and Engineering*, vol. 198, pp. 1–28, Feb. 2024.
- [12] B. L. Sjenitzer, “The dynamic Monte Carlo method for transient analysis of nuclear reactors,” Ph.D. dissertation, Delft University of Technology, 2013, ISBN: 9789088916571.
- [13] S. Christoforou, “A zero-variance based scheme for Monte Carlo criticality simulations,” Ph.D. dissertation, Delft University of Technology, 2010, ISBN: 9789609322478.
- [14] I. Lux, “Variance and efficiency in Monte Carlo transport calculations,” *Computer Physics Communications*, vol. 20, no. 1, pp. 119–125, 1980, ISSN: 0010-4655. [Online]. Available: <https://www.sciencedirect.com/science/article/pii/0010465580901174>.

- [15] D. Legrady, M. Halasz, J. Kophazi, B. Molnar, and G. Tolnai, “Population-based variance reduction for dynamic Monte Carlo,” *Annals of Nuclear Energy*, vol. 149, p. 107752, 2020.
- [16] Z. I. Botev and D. P. Kroese, “Efficient Monte Carlo simulation via the generalized splitting method,” *Statistics and Computing*, vol. 22, pp. 1–16, 2012.
- [17] S. Chen, Y. Yang, M. Morales, and S. Zhang, “Algorithm for branching and population control in correlated sampling,” *Physical Review Research*, vol. 5, no. 4, p. 043169, 2023.
- [18] I. N. Medvedev and G. A. Mikhailov, “Study of weighted Monte Carlo algorithms with branching,” *Computational Mathematics and Mathematical Physics*, vol. 49, pp. 428–438, 2009.
- [19] A. Mancusi Davide Zoia, “Zero-variance schemes for kinetic Monte Carlo simulations,” *Eur. Phys. J. Plus*, vol. 135, no. 5, p. 401, 2020. [Online]. Available: <https://doi.org/10.1140/epjp/s13360-020-00387-8>.